

JPL D-27667

SPITZER SPACE TELESCOPE

Focal Plane Survey Final Report

David S. Bayard
Bryan H. Kang
Paul B. Brugarolas
Dhemitrios Boussalis

July 8, 2004



Jet Propulsion Laboratory
California Institute of Technology

Copyright © 2004 California Institute of Technology. Government sponsorship acknowledged.

SPITZER SPACE TELESCOPE

Focal Plane Survey Final Report

D.S. Bayard, B.H. Kang, P.B. Brugarolas and D. Boussalis

Autonomy and Control Section (345)
Jet Propulsion Laboratory
California Institute of Technology
4800 Oak Grove Drive
Pasadena, CA 91109

Contents

| | |
|---|-----------|
| 1 EXECUTIVE SUMMARY | 4 |
| 2 INTRODUCTION | 6 |
| 3 OVERVIEW | 9 |
| 3.1 Instrument Pointing Frame (IPF) Kalman Filter | 9 |
| 3.2 Details of IPF Kalman Filter | 9 |
| 3.3 Experiment Design Procedure | 10 |
| 3.4 Calibration Procedure | 12 |
| 3.5 Mission Timeline of Calibration Runs | 13 |
| 4 FRAMES AND COORDINATE SYSTEMS | 14 |
| 4.1 Pointing-Relevant Frames | 14 |
| 4.2 Standard Coordinates | 16 |
| 4.3 Oriented Angular Pixel (OAP) Coordinates | 17 |
| 4.4 Mapping OAP to Standard Coordinates | 17 |
| 4.5 Calibration Equation | 18 |
| 5 IPF FILTER PARAMETERS | 19 |
| 5.1 Full State Description | 19 |
| 5.2 Optical Distortion Parameters | 21 |
| 5.3 Scan Mirror Rotation Parameters | 21 |
| 5.4 Telescope Frame Parameters | 21 |
| 5.5 Thermomechanical Drift Parameters | 22 |
| 5.6 Attitude and Gyro Parameters | 22 |
| 5.7 IPF Parameter Mask | 23 |
| 6 TOP LEVEL SUMMARY | 24 |
| 6.1 Focal Plane Survey Results | 24 |
| 6.2 Comparison to Pre-Flight Estimates | 27 |
| 7 FOCAL PLANE SURVEYS | 29 |
| 7.1 Pre-Coarse Surveys | 29 |
| 7.2 Coarse Surveys | 30 |

| | | |
|-----------|--|-----------|
| 7.3 | Fine Surveys | 31 |
| 8 | DETAILED EXAMPLES | 32 |
| 8.1 | Example 1: IRS Red Peak-Up Array (frame 018) | 33 |
| 8.2 | Example 2: IRS Short-Lo Slit (frame 028) | 41 |
| 8.3 | Example 3: IRAC 3.6 um Array (frame 068) | 49 |
| 8.4 | Example 4: MIPS 24 um Array (frame 095) | 57 |
| 9 | INDIVIDUAL RUN SUMMARIES | 67 |
| 9.1 | IPF EXECUTION SUMMARY OF ID701018 | 68 |
| 9.2 | IPF EXECUTION SUMMARY OF ID701019 | 69 |
| 9.3 | IPF EXECUTION SUMMARY OF ID701022 | 70 |
| 9.4 | IPF EXECUTION SUMMARY OF ID701023 | 71 |
| 9.5 | IPF EXECUTION SUMMARY OF ID502028 | 72 |
| 9.6 | IPF EXECUTION SUMMARY OF ID502034 | 73 |
| 9.7 | IPF EXECUTION SUMMARY OF ID502040 | 74 |
| 9.8 | IPF EXECUTION SUMMARY OF ID501046 | 75 |
| 9.9 | IPF EXECUTION SUMMARY OF ID502052 | 76 |
| 9.10 | IPF EXECUTION SUMMARY OF ID501058 | 77 |
| 9.11 | IPF EXECUTION SUMMARY OF ID502068 | 78 |
| 9.12 | IPF EXECUTION SUMMARY OF ID502069 | 79 |
| 9.13 | IPF EXECUTION SUMMARY OF ID502075 | 80 |
| 9.14 | IPF EXECUTION SUMMARY OF ID502076 | 81 |
| 9.15 | IPF EXECUTION SUMMARY OF ID703087 | 82 |
| 9.16 | IPF EXECUTION SUMMARY OF ID602095 | 83 |
| 9.17 | IPF EXECUTION SUMMARY OF ID704107 | 84 |
| 9.18 | IPF EXECUTION SUMMARY OF ID702118 | 85 |
| 9.19 | IPF EXECUTION SUMMARY OF ID703121 | 86 |
| 10 | LESSONS LEARNED | 87 |
| 10.1 | General | 87 |
| 10.2 | Model Fidelity | 89 |
| 11 | CONCLUSIONS | 90 |

1 EXECUTIVE SUMMARY

This final report summarizes the results and accuracies of the Spitzer Space Telescope focal plane survey. Accuracies achieved are compared to the focal plane survey calibration requirements put forth in the SIRTf IOC-SV Mission Plan [14] and pre-flight predictions made in [2]. The results of this focal plane survey are presently being used to support in-flight precision pointing, precision incremental offsets, IRS peakup array calibration, and ground pointing reconstruction.

The Spitzer Space Telescope was launched on August 25, 2003. The focal plane survey was performed during the first four-month period spanning September through December 2003. An additional round of Fine survey runs for the MIPS instrument was performed the last week of April 2004. All focal plane calibration data sets were analyzed using a high-order 37-state Instrument Pointing Frame (IPF) Kalman filter. This novel high-order estimator approach to calibration allowed the estimation of engineering and science parameters simultaneously in the same filter formulation, and proved to be a very efficient and accurate method for implementing the focal plane survey.

The main conclusion of this study is that all focal plane calibration requirements have been met with the survey strategy as implemented. Margins range from 4 percent for the IRS Long-Lo slit (frame 046) which has a tight 0.28" requirement, to 89 percent for the MIPS 70 um array (frame 107) which has a more generous 2.6" requirement. These post-flight results closely match pre-flight predictions.

An unexpected event was the discovery of a non-repeatability in the MIPS scan mirror on the order of 1 arcsecond. Although the accuracy of the focal plane calibration for the MIPS 24 um array is 0.09 arcseconds (with a requirement of 0.14 arcseconds), the pointing accuracy will ultimately be limited by this 1-arcsec non-repeatability. This mostly impacts the MIPS 24 um array since the other MIPS arrays do not have as tight requirements. It is also noted that the scan mirror non-repeatability seems to be a long-term effect in the sense that variations are predominantly seen from campaign to campaign rather than within any single campaign.

To lessen the effect of non-repeatability on pointing accuracy, the MIPS team recently redefined the MIPS 24 um Prime and Inferred frames to be an average of results from two separate IPF calibrations. This was intended to place the frames near their "center of repeatability", so that the resulting frames should be repeatable to approximately 0.5 arcsec.

For pointing purposes, the most critical calibrations are for the IRS Peakup sweet spots and short wavelength slit centers (frames 019, 023, 052, 028, 034). Results show that these frames are meeting their 0.14" requirements with an expected accuracy of approximately 0.09", which corresponds to a 36 percent margin.

SUMMARIZING STATISTICS

- All focal plane survey requirements satisfied
- Total of 76 official calibration data sets processed
 - 19 Pre-Coarse
 - 29 Coarse
 - 28 Fine
- Total of 56 Pointing Frames calibrated
- > 1500 parameters estimated
- 4-6 hours processing time per data set
- Largest run: 1338 centroids (IRAC 3.6 um array)
- Largest correction: 2.04 arcmin (MIPS 70 um narrow)
- Typical correction: 15.0 arcsec
- Survey Accuracy (typical): 0.09 arcsec

2 INTRODUCTION

This is the final report describing the focal plane survey for the Spitzer Space Telescope. The main purpose of the final report is to summarize the accuracies attained and to compare them against the focal plane survey calibration requirements put forth in the SIRTf IOC-SV Mission Plan [14], and to the pre-flight error predictions put forth in an earlier covariance analysis study [2]. All reported errors are based on using the full fidelity of the 37 state Instrument Pointing Frame (IPF) Kalman filter to provide a reliable and accurate error analysis. The KF covariances were scaled by a correction factor dependent on the magnitude of the observed residuals.

The planned focal plane survey strategies were first developed based on a simple spread-sheet error analysis [14], and then subsequently confirmed with a more detailed end-to-end covariance analysis [2]. The latter analysis verified that the planned experiments were sufficiently informative about the desired calibration parameters, and were repeated a sufficiently large number of times so that requirements could be met by optimally processing the obtained data.

The 19 Prime frames in the telescope focal plane are depicted in Figure 2.1. Each Prime Frame is calibrated with a dedicated focal plane survey effort. Also shown are the Brown angle conventions, which are used for reporting all calibrated frame locations. The Brown angles correspond to a 3,2,1 Euler angle sequence, but with a nonstandard sign convention adopted by R.J. Brown in [8].

The Spitzer focal plane surveys can be split into three categories: Pre-Coarse, Coarse, and Fine. The Pre-Coarse and Coarse focal plane surveys served as useful precursors to the Fine surveys, allowing successive pointing refinements while the telescope was still cooling and before final focus adjustments were made. While such precursor surveys are described herein, this final report will focus on the Fine Surveys, since they must meet the most stringent calibration requirements relevant to the normal mission. All runs described in this report have been delivered to DOM (that stands for “Distributed Object Manager” and is Spitzer’s main mission database), and are part of the official mission archive.

A complete set of IPF reports for all delivered calibration runs can be found at the URL:

https://sirtfweb/pub/IPF_focal_plane_survey

For convenience, the IPF reports for the most up-to-date Fine surveys are included as Appendices to the present final report (Appendix A: IRS; Appendix B: IRAC; Appendix C: MIPS).

The main conclusion of this study is that all focal plane calibration requirements have been met with the survey strategy as implemented. Margins range from 4 percent for the IRS Long-Lo slit (frame 046) which has a tight 0.28” requirement, to 89 percent for the MIPS 70 um array (frame 107) which has a more generous 2.6” requirement. Overall, these post-flight results closely match pre-flight predictions.

For pointing purposes, the most critical calibrations are for the IRS Peakup sweet spots and short wavelength slit centers (frames 019, 023, 052, 028, 034). Results show that these frames are meeting their 0.14” requirements with an expected accuracy of approximately 0.09”, which corresponds to a 36 percent margin.

The MIPS instrument presented some unexpected challenges for focal plane survey during

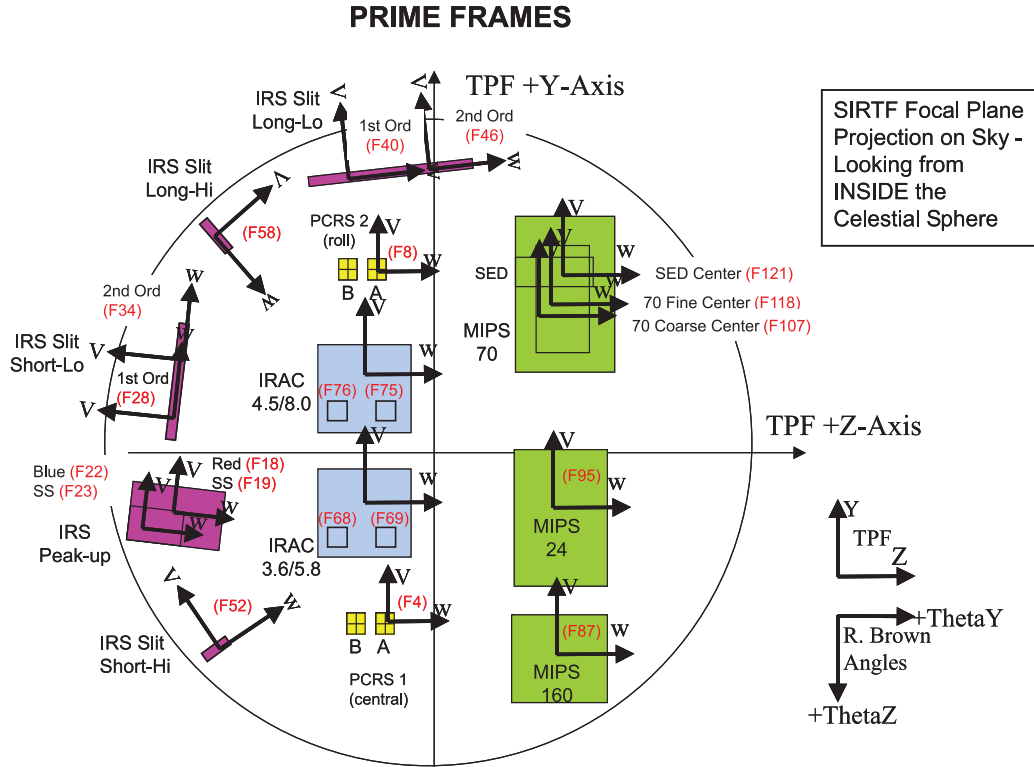


Figure 2.1: Prime Frames in Focal Plane

the IOC/SV period:

- The scan mirror was found to be significantly shifted compared to pre-flight predictions, by as much as 2 arcminutes in the scan direction. This limited the number of sources which fell on the 70 micron arrays (wide and narrow) in the early survey attempts.
- The 70 micron arrays (wide and narrow) and SED suffered from significant degradation in centroiding accuracy over half of the array. Good centroids were effectively provided on only half of the array which did not allow a good separation of plate scale parameters from alignment parameters in the calibration process.
- The 160 um initially suffered from stray-light problems.
- For the 24 um array, IPF results indicate a lack of scan-mirror repeatability on the order of 1". This is seen by comparing runs ID502095 and ID602095, whose estimates of the Brown angles for the Prime frame (095) differs in the Theta-Z direction (i.e., the scan mirror direction) by more than 1". Such a difference is not explainable by the calibration accuracy which should be good to .0884" for each run taken by itself.

The MIPS team studied the scan mirror non-repeatability in more detail and found it to be a real phenomena. Interestingly, the MIPS team found that while the scan mirror non-repeatability can occur from campaign to campaign, it generally does not occur within a

single campaign. This is consistent with the IPF results where the non-repeatability was seen between runs ID502095 and ID602095, that were taken in separate campaigns.

Because of these difficulties, all of the MIPS arrays (except for the 24 μm array) were recalibrated during the last week of April 2004. The experiment designs were modified based on the lessons learned during IOC/SV. Specifically, the stray light problem for the 160 μm array was avoided by using a Seyfert galaxy as the source; and the bad half of the 70 μm arrays and SED were avoided by concentrating centroids on the good side of the arrays. All Post-IOC/SV MIPS calibrations are included in this document.

To lessen the influence of scan mirror non-repeatability on pointing accuracy, the MIPS team recently redefined the MIPS 24 μm Prime and Inferred frames to be an average of the frame estimates obtained from the two separate calibrations, ID502095 and ID602095.

An overview of the IPF Kalman filter, experiment design, calibration procedure, and mission calibration timeline is given in Section 3. The focal plane parametrization discussed in Section 4 and the Kalman filter parameters are discussed in Section 5. The main results of the report are given in Section 6 which provides a top level summary of the focal plane survey, and a comparison with pre-flight accuracy predictions. All Pre-Coarse, Coarse, and Fine survey runs are summarized in Section 7. Four specific examples are highlighted in Section 8. More complete information associated with all the Fine surveys is given in the Run Summaries of Section 9. Lessons learned are given in Section 10, and Conclusions are postponed until Section 11.

IPF reports of all the latest calibration runs are given in the Appendices (see Appendix A for IRS, Appendix B for IRAC, and Appendix C for MIPS). The Appendices include centroid plots and estimated parameter values and accuracies for optical distortions, scan mirror parameters, systematic pointing errors, etc. The Appendices also include Pre-Coarse survey data for IRAC used for comparing plate scales and optical distortion parameters with other approaches.

3 OVERVIEW

3.1 Instrument Pointing Frame (IPF) Kalman Filter

The Spitzer calibration approach is based on using a high-order Kalman filter that combines both engineering parameters and science parameters into a single filter formulation. In this approach, engineering parameters such as pointing alignments, thermomechanical drift and gyro drifts are estimated along with science parameters such as plate scales and optical distortions.

The high-order estimator is denoted as the Instrument Pointing Frame (IPF) Kalman filter. This integrated approach to the problem has the advantage of being able to correct engineering and science errors without issues of interference discussed in [13], and without requiring iteration between separate teams of engineering and science analysts. The IPF Kalman filter has been adopted by the Spitzer mission as main estimation approach to support all focal plane survey efforts, and is the baseline method for providing calibration updates to the on-board frame table. Because of its high order, the Kalman filter had to be designed carefully using special scalings, a modern array square-root filtering approach, and advanced numerical techniques. The resulting focal plane survey approach is very general, being applicable to a wide range of science instruments such as imaging cameras, spectroscopy slits, and scanning-type arrays.

The paper will discuss results obtained from running the IPF Kalman filter on 76 different data sets. The data sets include focal plane survey data for all of Spitzer’s science instruments, i.e., MIPS, IRAC, and the IRS (both Pickup Arrays and Spectroscopy slits). The IPF filter supported updating 128 instrument pointing frames in the in-flight frame table, and over 1500 focal plane parameters characterizing alignments, plate scales, and optical distortions.

3.2 Details of IPF Kalman Filter

The IPF Kalman filter is a high-order square-root iterated linearized Kalman filter which is parametrized for calibrating the Spitzer’s telescope focal plane and aligning the science instrument arrays with respect to the telescope boresight. The Spitzer’s most stringent calibration requirements are set at 0.14 arcseconds, 1-sigma, radial. In order to achieve this level of accuracy, the filter utilizes 37 states to estimate desired alignments while also correcting for expected systematic errors due to: (1) optical distortions, (2) scanning mirror scale-factor and misalignment, (3) frame alignment variation due to thermomechanically induced drift, and (4) gyro bias and bias-drift in all axes. The gyro scale factor and alignment parameters are not included because they are calibrated separately using a dedicated in-flight gyro calibration filter. The estimated pointing frames and calibration parameters support on-board precision pointing capability, in addition to end-to-end “pixels on the sky” ground pointing reconstruction efforts.

An additional feature of the IPF filter is its use of polynomials to characterize time-dependent behaviours. The gyro drift and thermomechanically induced alignment drift are characterized as a polynomial function of time. Since polynomial coefficients are constant, this design retains the global re-linearization of the Kalman filter (an advantage of the calibration approach taken in the TOPEX mission), while still accommodating time-varying behaviours. A similar polynomial

approach was used by the authors in NASA’s recent SRTM mission with very good results [21].

In order to meet calibration requirements, the IPF Kalman filter has several novel and important features. These features include (1) A gyro pre-processor which allows gyro sensitivities to be pre-computed and stored beforehand. This eliminates the need for repeated and time-consuming gyro sensitivity propagation during each filter cycle; (2) A parameter “masking” capability which allows the user to restrict estimation to an arbitrary subset of the total number of parameters. This provides a flexible parametrization which can be used to match different levels of model fidelity to the various science array types; (3) A formulation based on a square-root iterated linearized Kalman filter to provide high accuracy and robust numerical conditioning; (4) The flexibility to sequentially update prior estimates based on multiple data sets taken on separate days of the mission (i.e., a “multi-run” tool); (5) A sandwich-based experiment design which provides observability of all desired parameters by starting and ending on the same reference sensor, and which allows the same Kalman filter to be used for a multitude of different array types (cameras, spectroscopy slits, scanning instruments); (6) The ability to integrate both visible and infra-red sources in the same calibration data set; (7) The ability to process partial centroids which only contain information along a single axis of the array (i.e., “slit mode”). This occurs, for example, when calibrating the entrance aperture of a spectroscopy slit by first scanning a source across the narrow slit width, and then subsequently along its length; (8) Operation in one of several possible “lite” modes to allow a trade-off between accuracy and robustness. For example, a completely gyroless mode can be invoked for small and/or incomplete data sets.

3.3 Experiment Design Procedure

The calibration of the focal plane is performed using a series of experiments denoted as “Sandwich” maneuvers. A generic sandwich maneuver is shown in Figure 3.1 and consists of the following sequence of steps.

1. Locate a target star on the first PCRS detector, PCRS 1, and take one or more centroid measurements.
2. Move the target star to PCRS 2, and take one or more centroid measurements
3. Move the target star to several positions on the desired science instrument array, and take a centroid measurement at each location (for example, a 3x3 grid pattern)
4. Return to the PCRS 1 detector, and take one or more centroid measurements.

The centroids taken on the science array are arbitrary, but must result in a time-tagged list of centroids (with both x and y coordinates). This approach is very general, allowing for grid patterns, dither patterns, simultaneous star clusters, etc. For the MIPS instrument, the time-tagged list of centroids includes additional information about the commanded scan mirror offsets, so that the scan mirror can be calibrated with respect to scale factor and alignment (i.e., along track and cross-track type errors). For IRS spectroscopy slits, the centroids are “faked” in

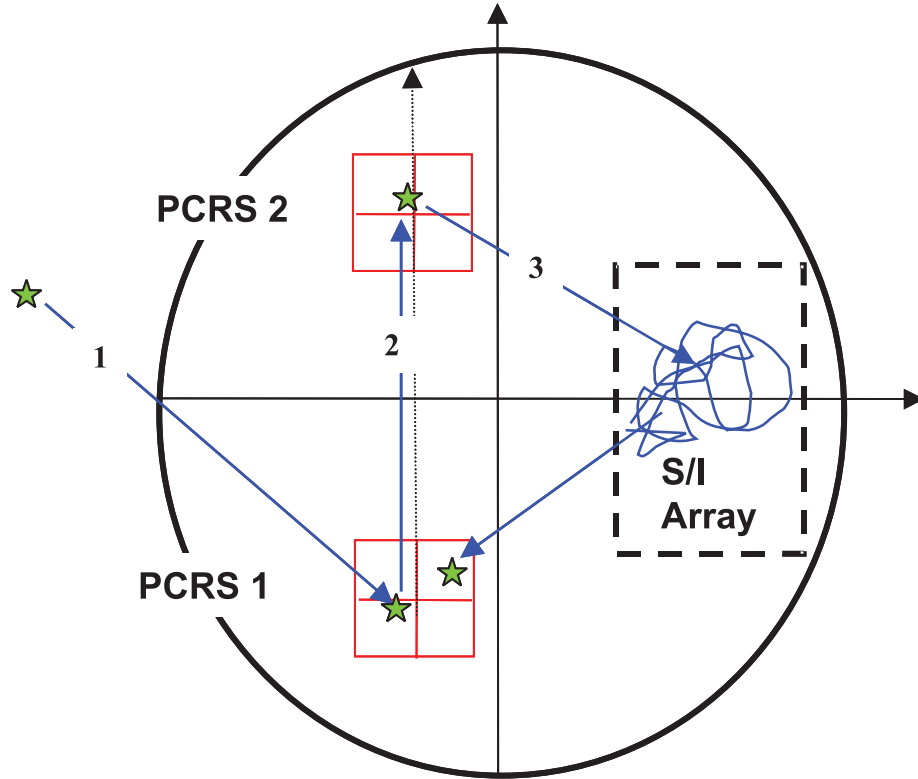


Figure 3.1: Sandwich Maneuver for Calibration Experiment Design

the sense that the source is scanned across the slit and the centroid is reported at the center of the slit at the time instant of maximum flux.

The Telescope pointing frame (TPF) is defined in terms of the location of the two PCRS boresight unit vectors (i.e., reference frame defined by measurements). By transitioning between the two PCRS and the science array, the sandwich maneuver is informative about the location of the IPF with respect to the TPF (i.e., the alignment matrix T in Figure 4.1), and the TPF with respect to the body frame (i.e., the alignment matrix R in Figure 4.1). Also, by beginning and ending on the same PCRS, the sandwich maneuver is informative about accumulated attitude error due to gyro drift, which can be calibrated out accordingly. The sandwich maneuvers are repeated a statistical number of times to ensure that the random errors can be adequately reduced by smoothing the data.

3.4 Calibration Procedure

Each of the science instrument teams designed their planned survey manuevers, including the number of repeats used for their Fine survey calibration strategy. The cognizant science team leads for this effort were:

- Jocelyn Keene - MIPS arrays
- Peter Eisenhardt - IRAC arrays
- Carl Grillmair - IRS slits
- Keven Uchida - IRS pickup arrays

For each of the Prime Frames, the following procedure was followed:

- Pointing command sequences associated with a particular Prime frame calibration were generated and put on-board.
- The pointing command sequences were executed, generating PCRS centroids, science instrument images, and attitude history data. All relevant data was downlinked via telemetry.
- The science images were centroided by the instrument teams (at the Spitzer Science Center), and formatted into a CA-file structure; the PCRS centroids were extracted and formatted (by Lockheed-Martin, Denver) into a CB-file structure; and the attitude history data was formatted by JPL/MIPL into an AA-file structure. The desired offset frame locations (relative to the Prime frames) are specified in in the offset FF-file.
- The CA,CB, and AA files were used as inputs to the Instrument Pointing Frame (IPF) Kalman filter [3][9][4] which generated the required calibration products in the form of IF, LG and TR files.

The relevant software interface documents are given as follows: CA and CS file [16], FF-file [17], CB file [18], AA and AS file [19] and the IPF output file [20].

Since the IPF filter is a fully operational Kalman filter, it generates both mean and covariance information. The covariance information is meaningful for providing a characterization of the expected calibration accuracy.

3.5 Mission Timeline of Calibration Runs

A complete chronological listing of the official Spitzer focal plane survey calibration runs is depicted in Figure 3.2. IRAC runs are shown in blue, IRS runs in red, and MIPS runs in green. A solid box indicates calibration runs that were used to update the on-board frame table. Dashed boxes indicate runs that were officially delivered to the mission archive, but were used primarily for diagnostic and comparison purposes.

Run labels have the form XXXYYY where XXX denotes the run number, and YYY denotes the frame table number of the associated Prime frame (a number from 1 to 128). Pre-Coarse runs have run numbers containing the letter “P”; Coarse runs have run numbers less than 500; and Fine runs have run numbers greater than 500. It is seen that the surveys progressed from Pre-Coarse, to Coarse, to Fine, over the 3 month check-out period. An exception is a set of IRAC Pre-Coarse runs late in the checkout period which were used for comparison with other approaches, and the Post-IOC MIPS runs as discussed previously.

SPITZER SPACE TELESCOPE IOC/SV IPF TEAM ACTIVITIES

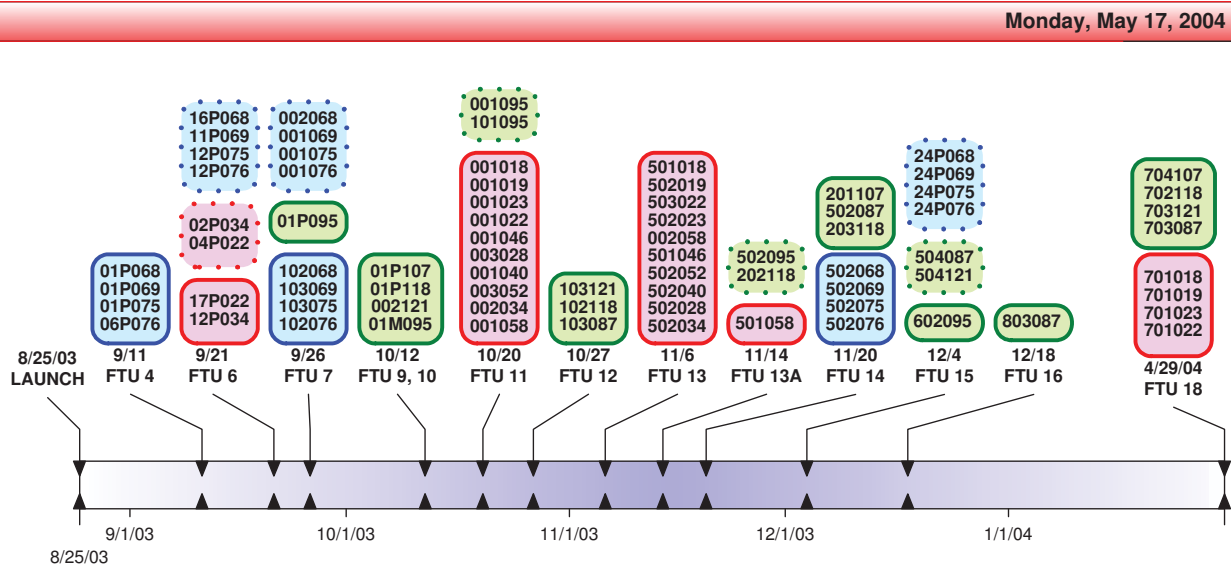


Figure 3.2: Mission Timeline of Calibration Runs

4 FRAMES AND COORDINATE SYSTEMS

4.1 Pointing-Relevant Frames

The main frames relevant to Spitzer pointing are shown in Figure 4.1. Here the focal plane is shown projected on the sky, as viewed by an observer who is located inside the celestial sphere. The key transformations between these frames are summarized in Table 4.1. For simplicity in presentation, the transformations A, R, T, C will denote 3×3 direction cosine matrices. (This is in contrast to the software implementation which uses quaternions for all numerical computations, but involves less recognizable expressions).

| Transformation | Description | From | To |
|----------------|--------------------|---------|--------------|
| A | Attitude | ICRS | Body |
| R | Alignment | Body | TPF |
| T | Instrument | TPF | IPF_0 |
| C | Scan Mirror Offset | IPF_0 | IPF_Γ |

Table 4.1: IPF Filter Transformations

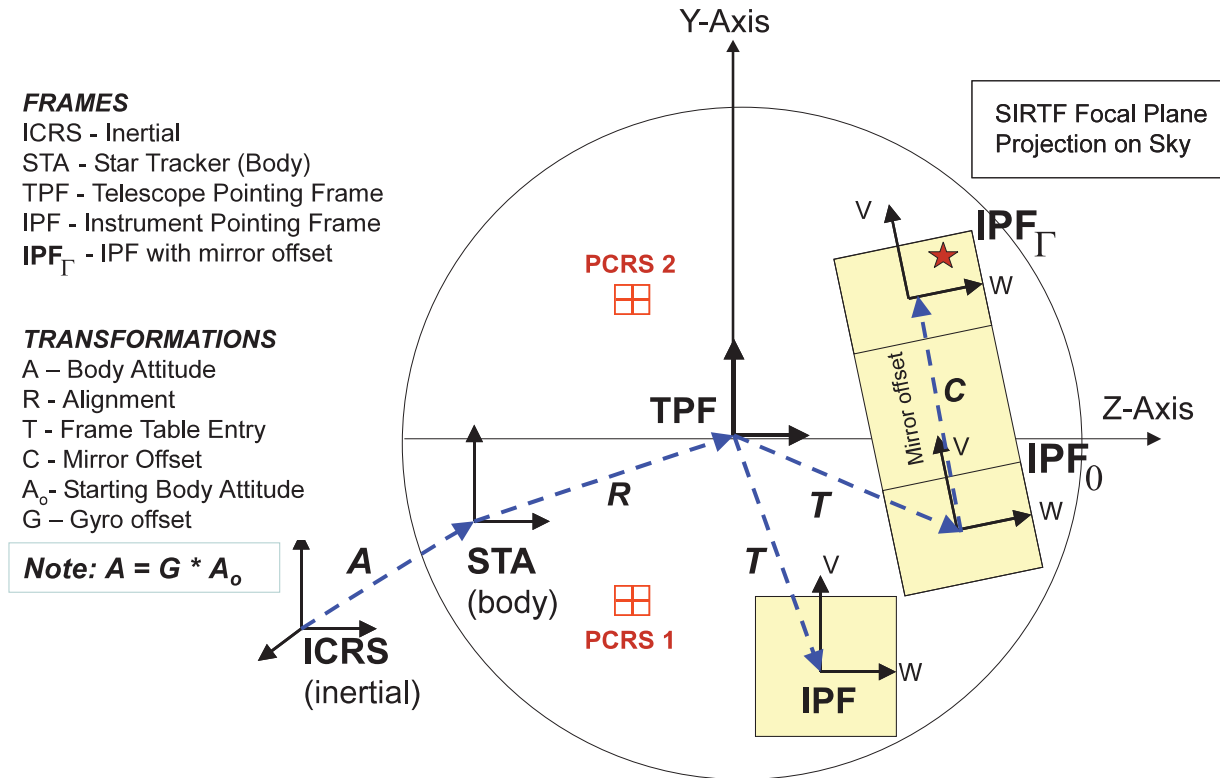


Figure 4.1: Spitzer Frames and Transformations

The International Celestial Reference System (ICRS) frame serves as the Spitzer's principle inertial reference frame. With a suitable relabelling, the star-tracker instrument frame serves as

the Spitzer’s Body frame (i.e., when spelled with its boresight as the x axis - see [3]). The mapping from ICRS to the Body Frame is denoted as the spacecraft attitude A . During each sandwich maneuver, only gyro propagated attitude solutions are used by the IPF filter to reconstruct attitude. The current attitude A is attained from a gyro propagated offset G relative to a starting attitude A_0 , i.e.,

$$A = GA_0 \tag{4.1}$$

where A_0 is available from the on-board attitude estimate. The Telescope Pointing Frame (TPF) has the telescope boresight as its x axis, and is defined rigorously in terms of the null points of the two PCRS sensors in [3]. Specifically, the TPF is defined by a fixed (3,2,1) Euler rotation from the line-of-centers frame (constructed by bisecting and crossing the two PCRS boresight vectors). The mapping from the Body Frame to the TPF is denoted as the alignment matrix R .

An Instrument Pointing Frame (IPF) is defined by a specific pixel location within a specific science array, such that its coordinate axes adopt the orientation of the corresponding pixel rows and columns of that array. The mapping from the TPF to any specified IPF is denoted generically as T . Best estimates of the IPF frames are stored in an on-board “Frame Table” as 128 values for T (stored as quaternions). The Frame Table is used extensively for commanding purposes. Certain important IPF frames are denoted as **Prime Frames** (typically defined at the center pixel location of each instrument array). Other frames are called **Inferred Frames** and are defined by a pixel offset relative to a nearby Prime frame. The nominal orientations of the science instruments and their associated Prime frames in the telescope focal plane have been shown earlier in Figure 2.1. Also shown are the mission-accepted conventions for the w and v directions, defined for each frame. Specifically, each IPF frame is defined by the u, v, w coordinate axes, where v, w are shown and $u = v \times w$ points outward to the sky. *The main goal of the IPF Kalman filter (as relevant to supporting on-board pointing capability) is to accurately estimate the IPF frame T for each of the 128 Prime and Inferred frames listed in the on-board Frame Table.*

The C matrix represents a scan mirror offset from a nominal starting position $\Gamma = 0$ to its current local offset position $\Gamma \neq 0$. For non-MIPS instruments, the C matrix is set to identity. For MIPS, the frame defined when the scan mirror is offset by angle Γ is denoted as IPF_Γ . Note that as the scan mirror moves there is an entire family of IPF_Γ frames generated as a continuous function of the variable Γ .

The attitude A is time-varying due to intentional telescope repositioning and unintentional control errors. The alignment matrix R is time-varying due to thermo-mechanically induced alignment drift. The mapping T from TPF to IPF is assumed constant due to the fact that the telescope focal plane is actively cooled. The mapping C is time-varying due to a constantly changing (but nominally known) scan-mirror offset angle Γ .

4.2 Standard Coordinates

Let $u \in \mathcal{R}^3$ be a unit vector associated with a star location in the ICRS frame, i.e.,

$$u = \begin{bmatrix} \cos(\text{DEC}) * \cos(\text{RA}) \\ \cos(\text{DEC}) * \sin(\text{RA}) \\ \sin(\text{DEC}) \end{bmatrix} \quad (4.2)$$

where RA, DEC denotes the Right Ascension and Declination of the source (in radians).

Let $\ell \in \mathcal{R}^3$ denote the unit vector after a velocity aberration correction has been applied (cf., [11]),

$$\ell = \frac{u + \frac{V_{SC}}{c}}{\|u + \frac{V_{SC}}{c}\|} \quad (4.3)$$

where c denotes the speed of light, and V_{SC} denotes the spacecraft velocity.

Define the vector s as the resolution of ℓ in the IPF_{Γ} frame to give,

$$s = CTRA\ell \quad (4.4)$$

When the current attitude is the result of a gyro-propagated offset G from an initial attitude A_0 one can decompose A as,

$$A = GA_0 \quad (4.5)$$

Substituting (4.5) into (4.4) gives,

$$s = CTRGA_0\ell \quad (4.6)$$

Equation (4.6) is useful because it shows the complete mapping of a star location vector ℓ in the ICRS frame to a unit vector s in the desired instrument pointing frame IPF_{Γ} . The next step will be to geometrically project s into the plane of the science array.

Let the components of s be given as,

$$s = \begin{bmatrix} s_x \\ s_y \\ s_z \end{bmatrix} \quad (4.7)$$

Since s is a unit vector in the IPF_{Γ} frame, it can be projected into focal plane coordinates to give,

$$z = \begin{bmatrix} z_w \\ z_v \end{bmatrix} = \begin{bmatrix} s_z/s_x \\ s_y/s_x \end{bmatrix} \quad (4.8)$$

The elements of $z \in \mathcal{R}^2$ will be said to be in **Standard Coordinates**.

Let the matrices C, T, R, G be parameterized in terms of the elements of the parameter vector p_{2f} (to be defined in detail in Section 5), and let A_0 be related to an available initial attitude estimate \hat{A}_0 as follows,

$$A_0 = (I - \psi^x)\hat{A}_0 \quad (4.9)$$

where $\psi \in \mathcal{R}^3$ denotes the initial attitude error. Then one can write (4.8) in the functional form,

$$z = h_z(p_{2f}, \psi) \quad (4.10)$$

This representation of the target source location in Standard Coordinates will be the starting point for the calibration process. A new initial attitude and attitude error is defined at the start of each sandwich maneuver. The initial attitude errors ψ are treated as zero-mean *correlated* measurement noise, since each one persists over the duration of a complete sandwich maneuver.

4.3 Oriented Angular Pixel (OAP) Coordinates

Typically, science centroids are obtained in units of pixels. However, calibration is more easily performed if pixel measurements are converted to units of angle (radians), and expressed with respect to an agreed upon origin and orientation. Oriented Angular Pixel (OAP) coordinates serve this purpose.

A pixel coordinate (CX, CY) (in the instrument (x, y) coordinate system) is converted to OAP coordinates using the following transformation,

$$y = \begin{bmatrix} y_w \\ y_v \end{bmatrix} = \begin{bmatrix} D11 & D12 \\ D21 & D22 \end{bmatrix} \begin{bmatrix} \text{PIX2RADX} & 0 \\ 0 & \text{PIX2RADY} \end{bmatrix} \begin{bmatrix} CX - CX0 \\ CY - CY0 \end{bmatrix} \quad (4.11)$$

Here, $\text{PIX2RADX}, \text{PIX2RADY}$ are nominal plate scales, and the pixel coordinate $(CX0, CY0)$ specifies the desired location where the Prime frame is to be embedded. The quantities $D11, D12, D21, D22$ are flip parameters (having values $0, -1, +1$), which specify how to map the instrument (x, y) coordinate directions into the focal plane (w, v) coordinate directions as defined in Figure 2.1.

4.4 Mapping OAP to Standard Coordinates

Let $y_{true} \in \mathcal{R}^2$ be a target source as observed in OAP coordinates assuming that there is no centroiding error,

$$y_{true} = \begin{bmatrix} y_{w_true} \\ y_{v_true} \end{bmatrix} \quad (4.12)$$

Generally, y_{true} will not coincide exactly with z in (4.10) due to imperfections in the optical system. To accommodate such imperfections, a model which maps y_{true} in OAP coordinates to z in Standard Coordinates is taken to be of the form,

$$z = \begin{bmatrix} z_w \\ z_v \end{bmatrix} = (I + M(p_1, \Gamma, y_{true})) \begin{bmatrix} y_{w_true} \\ y_{v_true} \end{bmatrix} \quad (4.13)$$

Here $M \in \mathcal{R}^{2 \times 2}$ is a perturbation matrix which captures imperfections such as optical distortions, plate scale errors, etc. The exact form of M will be discussed in Section 5.2 as a function of a set of distortion parameters (denoted as p_1), the scan mirror offset Γ , and the centroid location y_{true} .

The relation (4.13) assumes noiseless centroids. To generalize the model, a noisy centroid measurement y of the form (4.11) is introduced,

$$y = \begin{bmatrix} y_w \\ y_v \end{bmatrix} \quad (4.14)$$

The noisy centroid y is used to replace y_{true} in (4.13) according to the following relation,

$$z = \begin{bmatrix} z_w \\ z_v \end{bmatrix} = (I + M(p_1, \Gamma, y)) \begin{bmatrix} y_w \\ y_v \end{bmatrix} - \nu \quad (4.15)$$

where ν denotes the centroiding error in y . The motivation for choosing this model is that if M is small (which should always be the case), equation (4.15) is first-order equivalent to the more familiar additive noise model $y \simeq y_{true} + \nu$.

4.5 Calibration Equation

By equating (4.10) and (4.15) the following Calibration Equation is obtained,

$$\boxed{(I + M(p_1, \Gamma, y)) y = h_z(p_{2f}, \psi) + \nu} \quad (4.16)$$

This is the main equation to be used for all Spitzer's focal plane calibration. It is an end-to-end relation in the sense that it maps the source location on the sky (known from a star catalog with velocity correction applied) to the pixel location where the source is observed on the science instrument array. Accordingly, it contains both optical distortions parameterized by p_1 and systematic pointing errors parameterized by p_{2f} . The end-to-end pointing transformations associated with the Calibration Equation (4.16) are summarized in Figure 4.2.

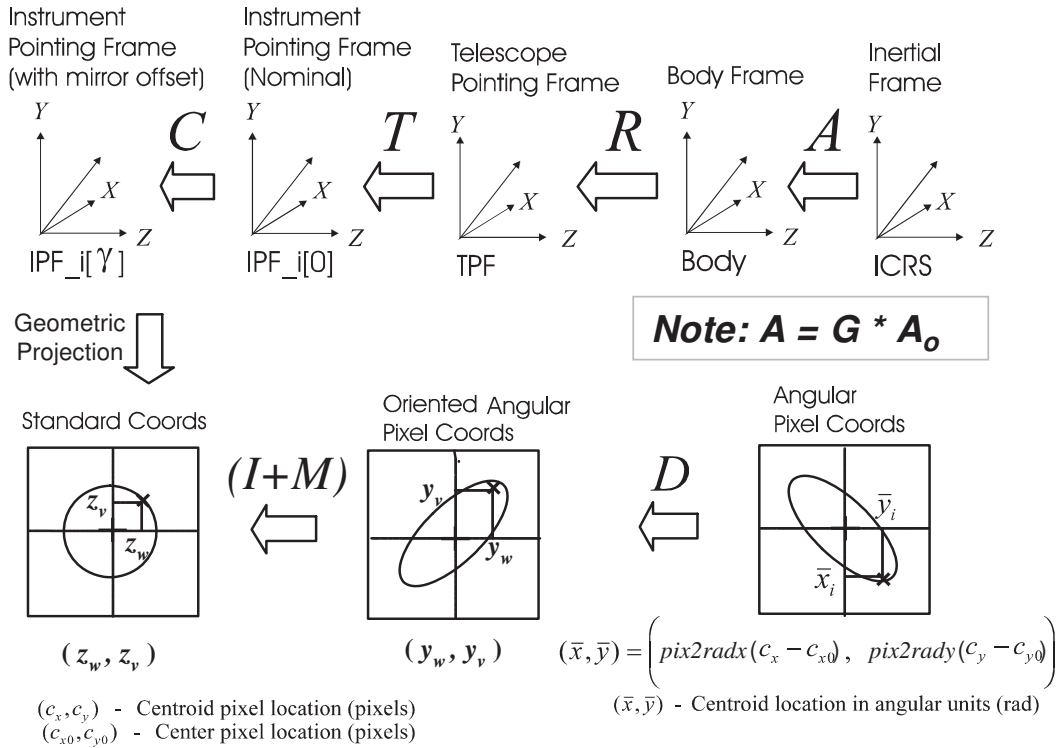


Figure 4.2: End-to-End Pointing Transformations

5 IPF FILTER PARAMETERS

5.1 Full State Description

The starting point for the Kalman filter design is the Calibration Equation (4.16). A full state vector x_f is defined as,

$$x_f = \begin{bmatrix} p_1 \\ p_{2f} \end{bmatrix} \tag{5.1}$$

where p_1 are the optical distortion parameters and p_{2f} are the systematic pointing errors in the Calibration Equation (4.16).

The parameters in p_1 and p_{2f} are defined such that they are constant with time. A summary of the states p_1 and p_{2f} is given in Table 5.1 and Table 5.2. The next few subsections will be devoted to giving a detailed description of each of these parameters.

| $p_1 \in \mathcal{R}^{17}$ | Description | $\delta p_1 \in \mathcal{R}^{17}$ |
|--|-----------------------------------|--|
| a_{00} b_{00} c_{00} | Constant Plate Scales | δa_{00} δb_{00} δc_{00} |
| a_{10} b_{10} c_{10} d_{10} | Γ Dependent Plate Scales | δa_{10} δb_{10} δc_{10} δd_{10} |
| a_{20} b_{20} c_{20} d_{20} | Γ^2 Dependent Plate Scales | δa_{20} δb_{20} δc_{20} δd_{20} |
| a_{01} b_{01} c_{01} d_{01} e_{01} f_{01} | Linear Plate Scales | δa_{01} δb_{01} δc_{01} δd_{01} δe_{01} δf_{01} |

Table 5.1: p_1 State Variables and Perturbations

| $p_2 \in \mathcal{R}^{24}$ | Description | $\delta p_2 \in \mathcal{R}^{20}$ |
|--|--------------------------|--|
| a_{m1} a_{m2} a_{m3} | mirror rotation axis | $\delta\alpha$ |
| β | scan mirror scale factor | $\delta\beta$ |
| q_{T1} q_{T2} q_{T3} q_{T4} | T quaternion | $\delta\theta_1$ $\delta\theta_2$ $\delta\theta_3$ |
| q_{R1} q_{R2} q_{R3} q_{R4} | R quaternion | δa_{rx} δa_{ry} δa_{rz} |
| b_{rx} b_{ry} b_{rz} | Linear Alignment | δb_{rx} δb_{ry} δb_{rz} |
| c_{rx} c_{ry} c_{rz} | Quadratic alignment | δc_{rx} δc_{ry} δc_{rz} |
| b_{gx} b_{gy} b_{gz} | Gyro Bias | δb_{gx} δb_{gy} δb_{gz} |
| c_{gx} c_{gy} c_{gz} | Gyro Bias Drift | δc_{gx} δc_{gy} δc_{gz} |

Table 5.2: p_2 State Variables and Perturbations

5.2 Optical Distortion Parameters

Optical distortion parameters capture imperfections and variations in the telescope and instrument which cause a star image to deviate from its idealized geometric projection. The optical distortions in the calibration equation (4.16) are parameterized in terms of the matrix $M \in \mathcal{R}^{2 \times 2}$ of the form,

$$M(p_1, \Gamma, y) = M_{00} + \Gamma M_{10} + \Gamma^2 M_{20} + M_{01}(y) \quad (5.2)$$

where,

$$M_{00} = \begin{bmatrix} a_{00} & c_{00} \\ c_{00} & b_{00} \end{bmatrix}; \quad M_{10} = \begin{bmatrix} a_{10} & c_{10} \\ d_{10} & b_{10} \end{bmatrix}; \quad M_{20} = \begin{bmatrix} a_{20} & c_{20} \\ d_{20} & b_{20} \end{bmatrix}; \quad (5.3)$$

$$M_{01}(y) = \begin{bmatrix} a_{01}y_w + c_{01}y_v & b_{01}y_v \\ d_{01}y_w & f_{01}y_w + e_{01}y_v \end{bmatrix}. \quad (5.4)$$

The parameter c_{00} is repeated symmetrically in M_{00} to disallow a redundant rotation with θ_1 of T (cf., [13]).

5.3 Scan Mirror Rotation Parameters

For science arrays having a scan mirror (i.e., MIPS arrays), the scan mirror rotation transformation can be defined by a direction cosine matrix C which maps the nominal IPF frame (denoted as IPF_0) to the IPF frame with a scan mirror offset (denoted as IPF_Γ). Mathematically, C is parametrized as an Euler axis rotation of the form,

$$C(p_{2f}, \Gamma) = \cos(\beta\Gamma) \cdot I + (1 - \cos(\beta\Gamma)) a_m a_m^T - \sin(\beta\Gamma) a_m^\times \quad (5.5)$$

Here $a_m = \begin{bmatrix} a_{m1} & a_{m2} & a_{m3} \end{bmatrix}^T$ is the scan mirror spin axis, Γ is the measured scan mirror angle (in radians), and β is the scale factor associated with measured mirror angle. The vector a_m is constrained to have unit norm, i.e.,

$$a_{m1}^2 + a_{m2}^2 + a_{m3}^2 = 1 \quad (5.6)$$

and the mirror transformation becomes the identity when the mirror is located in its nominal reference position ($\Gamma = 0$), i.e.,

$$C(p_{2f}, 0) = I. \quad (5.7)$$

For non-MIPS instruments (without a scan mirror), the condition $C = I$ is enforced.

5.4 Telescope Frame Parameters

The direction cosine matrix T transforms from TPF to IPF_0 and can be parameterized with a quaternion q_T as shown below.

$$T(q_T) = \begin{bmatrix} q_{T1}^2 - q_{T2}^2 - q_{T3}^2 + q_{T4}^2 & 2(q_{T1}q_{T2} + q_{T3}q_{T4}) & 2(q_{T1}q_{T3} - q_{T2}q_{T4}) \\ 2(q_{T1}q_{T2} - q_{T3}q_{T4}) & q_{T2}^2 - q_{T3}^2 + q_{T4}^2 - q_{T1}^2 & 2(q_{T2}q_{T3} + q_{T1}q_{T4}) \\ 2(q_{T1}q_{T3} + q_{T2}q_{T4}) & 2(q_{T2}q_{T3} - q_{T1}q_{T4}) & q_{T3}^2 + q_{T4}^2 - q_{T1}^2 - q_{T2}^2 \end{bmatrix} \quad (5.8)$$

5.5 Thermomechanical Drift Parameters

The direction cosine matrix R represents the time-varying mapping from the STA-defined Body frame to the TPF frame. The mapping is time-varying primarily due to thermomechanically induced boresight shifts over time. The IPF filter parametrizes R as a quadratic function of time, starting at an initial alignment R_0 , i.e.,

$$R \triangleq \left(I_{3 \times 3} - \left(b_r t + c_r \frac{t^2}{2} \right)^\times \right) R_0(q_R) \quad (5.9)$$

where,

$$b_r = \begin{bmatrix} b_{rx} \\ b_{ry} \\ b_{rz} \end{bmatrix}; \quad c_r = \begin{bmatrix} c_{rx} \\ c_{ry} \\ c_{rz} \end{bmatrix} \quad (5.10)$$

The time $t = 0$ in (5.9) corresponds to the time tag of the first centroid of the very first sandwich maneuver. Accordingly, the quantity R_0 is the static alignment at time $t = 0$. For notational simplicity, the quaternion equivalent of the initial alignment R_0 is denoted as q_R (rather than q_{R0}).

5.6 Attitude and Gyro Parameters

The gyro propagated offset G in (4.5) can be found by integrating the true rate $\omega \in \mathcal{R}^3$ as,

$$\dot{G} = -\omega^\times G \quad (5.11)$$

Since the true rate $\omega \in \mathcal{R}^3$ is not known exactly, an estimate must be generated. For computational convenience, this is done in two stages. First, the gyro pre-processor calculates a nominal rate vector estimate $\omega_m^\circ \in \mathcal{R}^3$, by subtracting (from the raw gyro measurement), a coarse estimate of gyro bias available from the on-board pointing system [3][1]. Second, an additive correction is applied to the nominal rate vector ω_m° to give the true rate in the form,

$$\omega = \omega_m^\circ + b_g + c_g t \quad (5.12)$$

The two-stage approach allows the gyro sensitivity equations to be computed once and stored, rather than requiring complete re-propagation every filter cycle. This assumes that the nominal rate used in the first step is sufficiently adequate to linearize the problem for all future iterations. (If this is not true, an option to re-propagate the sensitivities is provided).

5.7 IPF Parameter Mask

Not all parameters of the IPF filter are used for all runs. The IPF parameter mask vector is a list of ones and zeros, which specifies which parameters are to be estimated for a given calibration run. An example parameter mask is shown in Table 5.3 that has been used for the MIPS 24 μm array. In general, MIPS arrays use the most parameters since they have additional scan mirror parameters, while the IRS slits use the least parameters since the main interest is to characterize the size and shape of the entrance aperture.

| Con. Plate Scale | | | Γ Dependent | | | | Γ^2 Dependent | | | | Linear Plate Scale | | | | | | Mirror | |
|------------------|------------|------------|--------------------|----------|----------|----------|----------------------|----------|----------|----------|--------------------|-----------------|----------|----------|----------|----------|----------|---------|
| a_{00} | b_{00} | c_{00} | a_{10} | b_{10} | c_{10} | d_{10} | a_{20} | b_{20} | c_{20} | d_{20} | a_{01} | b_{01} | c_{01} | d_{01} | e_{01} | f_{01} | α | β |
| 1 | 2 | 3 | 4 | 5 | 6 | 7 | 8 | 9 | 10 | 11 | 12 | 13 | 14 | 15 | 16 | 17 | 18 | 19 |
| 1 | 1 | 1 | 1 | 1 | 1 | 1 | 0 | 0 | 0 | 0 | 1 | 1 | 1 | 1 | 1 | 1 | 1 | 1 |
| IPF (T) | | | Alignment R | | | | | | | | | Gyro Drift Bias | | | | | | |
| θ_1 | θ_2 | θ_3 | a_{rx} | a_{ry} | a_{rz} | b_{rx} | b_{ry} | b_{rz} | c_{rx} | c_{ry} | c_{rz} | b_{gx} | b_{gy} | b_{gz} | c_{gx} | c_{gy} | c_{gz} | |
| 20 | 21 | 22 | 23 | 24 | 25 | 26 | 27 | 28 | 29 | 30 | 31 | 32 | 33 | 34 | 35 | 36 | 37 | |
| 1 | 1 | 1 | 1 | 1 | 1 | 1 | 1 | 1 | 1 | 1 | 1 | 1 | 1 | 1 | 1 | 1 | 1 | |

Table 5.3: IPF filter execution mask vector assignment

6 TOP LEVEL SUMMARY

6.1 Focal Plane Survey Results

The calibration accuracy for each of the Prime frames is summarized in Table 6.1, in units of arcseconds, 1-sigma, radial. The last column, denoted as “REQ”, lists the requirements by Prime frame as provided in reference [14]. The second column from the right, denoted as “ACTL”, lists the actual calibration error in localizing the Prime Frame in the telescope focal plane. By comparing these last two columns, it is seen that all of the main focal plane survey requirements are met.

The column marked “PRED” gives the predicted accuracies based on the pre-flight analysis in [2]. Comparing this column with the “ACTL” column gives a comparison of how well the actual focal plane survey performed relative to the expected results. In general these two columns agree reasonably well. The IRAC arrays performed noticeably better than their predicts due to the improvement in the experiment design.

The IPF filter can estimate up to 37 parameters for calibration purposes, or any subset. The parameter execution mask used for each of the official calibration runs is indicated in Table 6.2.

| NF | RN | DESCRIPTION | BROWN ANGLE | | | ESTIM. ACCURACY | | |
|-----|-----|--------------------------------|-------------|---------|---------|--------------------------|--------|------|
| | | | [amin] | [amin] | [deg] | [asec] 1 σ radial | | |
| | | | theta_Y | theta_Z | angle | PRED | ACTL | REQ |
| 018 | 701 | IRS_Red_PeakUp_FOV_Center | -11.649 | 2.000 | 1.797 | 0.1279 | 0.0899 | 0.25 |
| 019 | 701 | IRS_Red_PeakUp_FOV_Sweet_Spot | -11.587 | 1.971 | 1.978 | 0.1009 | 0.0866 | 0.14 |
| 022 | 701 | IRS_Blue_PeakUp_FOV_Center | -13.520 | 1.897 | 1.704 | 0.1285 | 0.0966 | 0.25 |
| 023 | 701 | IRS_Blue_PeakUp_FOV_Sweet_Spot | -13.578 | 1.864 | 1.817 | 0.1014 | 0.0869 | 0.14 |
| 028 | 502 | IRS_ShortLo_1st_Ord_Center_Pos | -12.033 | -2.793 | -84.720 | 0.1056 | 0.1165 | 0.14 |
| 034 | 502 | IRS_ShortLo_2nd_Ord_Center_Pos | -11.913 | -4.093 | -84.720 | 0.1061 | 0.0909 | 0.14 |
| 040 | 502 | IRS_LongLo_1st_Ord_Center_Pos | -4.406 | -13.997 | -1.200 | 0.2571 | 0.1295 | 0.28 |
| 046 | 501 | IRS_LongLo_2nd_Ord_Center_Pos | -1.213 | -14.066 | -1.200 | 0.2587 | 0.2682 | 0.28 |
| 052 | 502 | IRS_ShortHi_Center_Position | -10.565 | 10.010 | -41.470 | 0.1037 | 0.0885 | 0.14 |
| 058 | 501 | IRS_LongHi_Center_Position | -10.418 | -10.232 | 43.340 | 0.1864 | 0.1027 | 0.28 |
| 068 | 502 | IRAC_Center_of_3.6umArray | -2.860 | 3.737 | -0.542 | 0.1358 | 0.0881 | 0.14 |
| 069 | 502 | IRAC_Center_of_5.8umArray | -2.843 | 3.607 | -0.301 | 0.1359 | 0.0889 | 0.14 |
| 075 | 502 | IRAC_Center_of_4.5umArray | -2.721 | -3.049 | -0.720 | 0.1103 | 0.0878 | 0.14 |
| 076 | 502 | IRAC_Center_of_8.0umArray | -2.752 | -3.068 | 0.017 | 0.1103 | 0.0895 | 0.14 |
| 087 | 703 | MIPS_160um_center_large_FOV | 6.711 | 11.987 | 0.814 | 0.2413 | 1.2056 | 3.70 |
| 095 | 602 | MIPS_24um_center | 6.716 | 4.246 | 0.638 | 0.1235 | 0.0884 | 0.14 |
| 107 | 704 | MIPS_70um_center | 6.550 | -8.069 | -2.862 | 0.2957 | 0.2847 | 2.60 |
| 118 | 702 | MIPS_70um_fine_center | 7.126 | -6.809 | -8.474 | 0.2117 | 0.3038 | 1.10 |
| 121 | 703 | MIPS_SED_center | 6.056 | -9.431 | 0.062 | 0.6392 | 0.9998 | 1.10 |

Table 6.1: Top Level Performance Summary (Predicted, Actual and Required)

| Parameter Description | | Const. Plate Scale | | | | Γ Dependent | | | | Γ^2 Dependent | | | | Linear Plate Scale | | | | | | | | | |
|-------------------------|-----|--------------------|----------|----------|------------|--------------------|------------|-------------|----------|----------------------|----------|-----------------|----------|--------------------|----------|----------|----------|----------|----------|----------|----------|----------|---|
| p_1 Parameters | | a_{00} | b_{00} | c_{00} | a_{10} | b_{10} | c_{10} | d_{10} | a_{20} | b_{20} | c_{20} | d_{20} | a_{01} | b_{01} | c_{01} | d_{01} | e_{01} | f_{01} | | | | | |
| Instrument Name | RN | 1 | 2 | 3 | 4 | 5 | 6 | 7 | 8 | 9 | 10 | 11 | 12 | 13 | 14 | 15 | 16 | 17 | | | | | |
| IRS_Red_PkUp_Cntr | 18 | 701 | 1 | 1 | 0 | 0 | 0 | 0 | 0 | 0 | 0 | 0 | 1 | 1 | 1 | 1 | 1 | 1 | | | | | |
| IRS_Red_PkUp_SwtsSpot | 19 | 701 | 1 | 1 | 0 | 0 | 0 | 0 | 0 | 0 | 0 | 0 | 0 | 0 | 0 | 0 | 0 | 0 | | | | | |
| IRS_Blue_PkUp_Cntr | 22 | 701 | 1 | 1 | 0 | 0 | 0 | 0 | 0 | 0 | 0 | 0 | 1 | 1 | 1 | 1 | 1 | 1 | | | | | |
| IRS_Blue_PkUp_SwtsSpot | 23 | 701 | 1 | 1 | 0 | 0 | 0 | 0 | 0 | 0 | 0 | 0 | 0 | 0 | 0 | 0 | 0 | 0 | | | | | |
| IRS_ShortLo_1stOrd_Cntr | 28 | 502 | 1 | 0 | 0 | 0 | 0 | 0 | 0 | 0 | 0 | 0 | 0 | 0 | 0 | 0 | 0 | 0 | | | | | |
| IRS_ShortLo_2ndOrd_Cntr | 34 | 502 | 1 | 0 | 0 | 0 | 0 | 0 | 0 | 0 | 0 | 0 | 0 | 0 | 0 | 0 | 0 | 0 | | | | | |
| IRS_LongLo_1stOrd_Cntr | 40 | 502 | 1 | 0 | 0 | 0 | 0 | 0 | 0 | 0 | 0 | 0 | 0 | 0 | 0 | 0 | 0 | 0 | | | | | |
| IRS_LongLo_2ndOrd_Cntr | 46 | 501 | 1 | 0 | 0 | 0 | 0 | 0 | 0 | 0 | 0 | 0 | 0 | 0 | 0 | 0 | 0 | 0 | | | | | |
| IRS_ShortHi_Cntr | 52 | 502 | 1 | 0 | 0 | 0 | 0 | 0 | 0 | 0 | 0 | 0 | 0 | 0 | 0 | 0 | 0 | 0 | | | | | |
| IRS_LongHi_Cntr | 58 | 501 | 1 | 0 | 0 | 0 | 0 | 0 | 0 | 0 | 0 | 0 | 0 | 0 | 0 | 0 | 0 | 0 | | | | | |
| IRAC_Cntr_3.6umArray | 68 | 502 | 1 | 1 | 0 | 0 | 0 | 0 | 0 | 0 | 0 | 0 | 1 | 1 | 1 | 1 | 1 | 1 | | | | | |
| IRAC_Cntr_5.8umArray | 69 | 502 | 1 | 1 | 0 | 0 | 0 | 0 | 0 | 0 | 0 | 0 | 1 | 1 | 1 | 1 | 1 | 1 | | | | | |
| IRAC_Cntr_4.5umArray | 75 | 502 | 1 | 1 | 0 | 0 | 0 | 0 | 0 | 0 | 0 | 0 | 1 | 1 | 1 | 1 | 1 | 1 | | | | | |
| IRAC_Cntr_8.0umArray | 76 | 502 | 1 | 1 | 0 | 0 | 0 | 0 | 0 | 0 | 0 | 0 | 1 | 1 | 1 | 1 | 1 | 1 | | | | | |
| MIPS_160um_CntrLgFOV | 87 | 703 | 0 | 0 | 0 | 0 | 0 | 0 | 0 | 0 | 0 | 0 | 0 | 0 | 0 | 0 | 0 | 0 | | | | | |
| MIPS_24um_Cntr | 95 | 602 | 1 | 1 | 1 | 0 | 0 | 0 | 0 | 0 | 0 | 0 | 1 | 1 | 1 | 1 | 1 | 1 | | | | | |
| MIPS_70um_Cntr | 107 | 704 | 1 | 1 | 0 | 0 | 0 | 0 | 0 | 0 | 0 | 0 | 0 | 0 | 0 | 0 | 0 | 0 | | | | | |
| MIPS_70um_fine_Cntr | 118 | 702 | 1 | 1 | 0 | 0 | 0 | 0 | 0 | 0 | 0 | 0 | 0 | 0 | 0 | 0 | 0 | 0 | | | | | |
| MIPS_SED_Cntr | 121 | 703 | 0 | 0 | 0 | 0 | 0 | 0 | 0 | 0 | 0 | 0 | 0 | 0 | 0 | 0 | 0 | 0 | | | | | |
| Parameter Description | | Mirror | | | IPF (T) | | | Alignment R | | | | Gyro Drift Bias | | | | | | | | | | | |
| Instrument Name | NF | RN | α | β | θ_1 | θ_2 | θ_3 | a_{rx} | a_{ry} | a_{rz} | b_{rx} | b_{ry} | b_{rz} | c_{rx} | c_{ry} | c_{rz} | b_{gx} | b_{gy} | b_{gz} | c_{gx} | c_{gy} | c_{gz} | |
| IRS_Red_PkUp_Cntr | 18 | 701 | 0 | 0 | 1 | 1 | 1 | 1 | 1 | 1 | 1 | 1 | 1 | 1 | 1 | 1 | 1 | 1 | 1 | 1 | 1 | 1 | 1 |
| IRS_Red_PkUp_SwtsSpot | 19 | 701 | 0 | 0 | 1 | 1 | 1 | 1 | 1 | 1 | 1 | 1 | 1 | 1 | 1 | 1 | 1 | 1 | 1 | 1 | 1 | 1 | 1 |
| IRS_Blue_PkUp_Cntr | 22 | 701 | 0 | 0 | 1 | 1 | 1 | 1 | 1 | 1 | 1 | 1 | 1 | 1 | 1 | 1 | 1 | 1 | 1 | 1 | 1 | 1 | 1 |
| IRS_Blue_PkUp_SwtsSpot | 23 | 701 | 0 | 0 | 1 | 1 | 1 | 1 | 1 | 1 | 1 | 1 | 1 | 1 | 1 | 1 | 1 | 1 | 1 | 1 | 1 | 1 | 1 |
| IRS_ShortLo_1stOrd_Cntr | 28 | 502 | 0 | 0 | 1 | 1 | 1 | 1 | 1 | 1 | 1 | 1 | 1 | 1 | 1 | 1 | 1 | 1 | 1 | 1 | 1 | 1 | 1 |
| IRS_ShortLo_2ndOrd_Cntr | 34 | 502 | 0 | 0 | 1 | 1 | 1 | 1 | 1 | 1 | 1 | 1 | 1 | 1 | 1 | 1 | 1 | 1 | 1 | 1 | 1 | 1 | 1 |
| IRS_LongLo_1stOrd_Cntr | 40 | 502 | 0 | 0 | 1 | 1 | 1 | 1 | 1 | 1 | 1 | 1 | 1 | 1 | 1 | 1 | 1 | 1 | 1 | 1 | 1 | 1 | 1 |
| IRS_LongLo_2ndOrd_Cntr | 46 | 501 | 0 | 0 | 1 | 1 | 1 | 1 | 1 | 1 | 1 | 1 | 1 | 1 | 1 | 1 | 1 | 1 | 1 | 1 | 1 | 1 | 1 |
| IRS_ShortHi_Cntr | 52 | 502 | 0 | 0 | 1 | 1 | 1 | 1 | 1 | 1 | 1 | 1 | 1 | 1 | 1 | 1 | 1 | 1 | 1 | 1 | 1 | 1 | 1 |
| IRS_LongHi_Cntr | 58 | 501 | 0 | 0 | 1 | 1 | 1 | 1 | 1 | 1 | 1 | 1 | 1 | 1 | 1 | 1 | 1 | 1 | 1 | 1 | 1 | 1 | 1 |
| IRAC_Cntr_3.6umArray | 68 | 502 | 0 | 0 | 1 | 1 | 1 | 1 | 1 | 0 | 0 | 0 | 0 | 0 | 0 | 0 | 1 | 1 | 1 | 1 | 1 | 1 | 1 |
| IRAC_Cntr_5.8umArray | 69 | 502 | 0 | 0 | 1 | 1 | 1 | 1 | 1 | 0 | 0 | 0 | 0 | 0 | 0 | 0 | 1 | 1 | 1 | 1 | 1 | 1 | 1 |
| IRAC_Cntr_4.5umArray | 75 | 502 | 0 | 0 | 1 | 1 | 1 | 1 | 1 | 0 | 0 | 0 | 0 | 0 | 0 | 0 | 1 | 1 | 1 | 1 | 1 | 1 | 1 |
| IRAC_Cntr_8.0umArray | 76 | 502 | 0 | 0 | 1 | 1 | 1 | 1 | 1 | 0 | 0 | 0 | 0 | 0 | 0 | 0 | 1 | 1 | 1 | 1 | 1 | 1 | 1 |
| MIPS_160um_CntrLgFOV | 87 | 703 | 1 | 0 | 1 | 1 | 1 | 1 | 1 | 0 | 0 | 0 | 0 | 0 | 0 | 0 | 0 | 0 | 0 | 0 | 0 | 0 | 0 |
| MIPS_24um_Cntr | 95 | 602 | 1 | 1 | 1 | 1 | 1 | 1 | 1 | 1 | 1 | 1 | 1 | 1 | 1 | 1 | 1 | 1 | 1 | 1 | 1 | 1 | 1 |
| MIPS_70um_Cntr | 107 | 704 | 1 | 1 | 1 | 1 | 1 | 1 | 1 | 1 | 1 | 1 | 1 | 1 | 1 | 1 | 1 | 1 | 1 | 1 | 1 | 1 | 1 |
| MIPS_70um_fine_Cntr | 118 | 702 | 1 | 1 | 1 | 1 | 1 | 1 | 1 | 1 | 1 | 1 | 1 | 1 | 1 | 1 | 1 | 1 | 1 | 1 | 1 | 1 | 1 |
| MIPS_SED_Cntr | 121 | 703 | 1 | 1 | 1 | 1 | 1 | 1 | 1 | 1 | 1 | 1 | 1 | 1 | 1 | 1 | 1 | 1 | 1 | 1 | 1 | 1 | 1 |

Table 6.2: Final Mask Vector Assignment for p_1 (mask1) and p_2 (mask2) State Variables

A large improvement was seen in the achieved performance for the IRAC 3.6 and 5.8 μm array centers (frames 068, 069), where a 36 percent margin was achieved compared to a predicted 3 percent margin. This improvement can be attributed to a change in the experiment design by the IRAC team from a five-of-diamonds pattern to a “simultaneous star cluster” calibration set. The latter design contains a significantly larger number of centroids which helped improve estimates of the optical distortion parameters.

In contrast, the MIPS 160 μm (frame 087) had much less margin than predicted from pre-flight analysis. The main reason is the use of a Seyfert galaxy as the calibration source, which had significant positional uncertainty (approx 1 arcsec) compared to other sources typically used for calibration (approx 0.1 arcsec). This 1” error mapped directly into the final frame calibration error.

When interpreting the present results, it is worth reminding the reader that the IRS Peakup arrays use units of centi-pixels, while all other arrays use units of pixels. Also, the entrance apertures associated with the IRS spectroscopy slits do not have physical pixels associated with them, so they are assigned a 1 arcsecond “artificial” pixel for calibration purposes.

| NF | FTU 0 | | | FTU18 | | | DIFF: FTU18 - FTU0 | | |
|-----|-------------|----------|----------|-------------|----------|----------|--------------------|---------|----------|
| | BROWN ANGLE | | | BROWN ANGLE | | | BROWN ANGLE | | |
| | Theta X | Theta Y | Theta Z | Theta X | Theta Y | Theta Z | Theta X | Theta Y | Theta Z |
| | [amin] | [amin] | [deg] | [amin] | [amin] | [deg] | [amin] | [amin] | [deg] |
| 18 | -11.7080 | 2.1380 | 2.9600 | -11.6492 | 2.0004 | 1.7966 | 0.0588 | -0.1376 | -1.1634 |
| 19 | -11.6496 | 2.1709 | 2.9600 | -11.5870 | 1.9713 | 1.9779 | 0.0626 | -0.1996 | -0.9821 |
| 22 | -13.7500 | 2.0370 | 2.9600 | -13.5203 | 1.8967 | 1.7044 | 0.2297 | -0.1403 | -1.2556 |
| 23 | -13.8114 | 2.0640 | 2.9600 | -13.5784 | 1.8644 | 1.8172 | 0.2330 | -0.1996 | -1.1428 |
| 28 | -12.1660 | -2.6690 | 275.2800 | -12.0326 | -2.7926 | 275.2800 | 0.1334 | -0.1236 | 0.0000 |
| 34 | -12.0450 | -3.9910 | 275.2800 | -11.9131 | -4.0932 | 275.2800 | 0.1319 | -0.1022 | 0.0000 |
| 40 | -4.6060 | -13.8890 | 358.8000 | -4.4057 | -13.9970 | 358.8000 | 0.2003 | -0.1080 | 0.0000 |
| 46 | -1.1980 | -13.9600 | 358.8000 | -1.2134 | -14.0662 | 358.8000 | -0.0154 | -0.1062 | 0.0000 |
| 52 | -10.7640 | 10.1330 | 318.5300 | -10.5647 | 10.0097 | 318.5300 | 0.1993 | -0.1233 | 0.0000 |
| 58 | -10.5440 | -10.1580 | 43.3400 | -10.4177 | -10.2319 | 43.3400 | 0.1263 | -0.0739 | 0.0000 |
| 68 | -3.1240 | 3.6340 | 0.0000 | -2.8605 | 3.7375 | 359.4577 | 0.2635 | 0.1035 | 359.4577 |
| 69 | -3.1170 | 3.5160 | 0.0000 | -2.8433 | 3.6067 | 359.6989 | 0.2737 | 0.0907 | 359.6989 |
| 75 | -2.9600 | -2.9500 | 0.0000 | -2.7206 | -3.0487 | 359.2799 | 0.2394 | -0.0987 | 359.2799 |
| 76 | -2.9800 | -2.9910 | 0.0000 | -2.7518 | -3.0679 | 0.0171 | 0.2282 | -0.0769 | 0.0171 |
| 87 | 6.6690 | 11.5170 | 0.0000 | 6.7110 | 11.9874 | 0.8143 | 0.0420 | 0.4704 | 0.8143 |
| 95 | 6.6410 | 3.9310 | 0.0000 | 6.7221 | 4.2538 | 0.6319 | 0.0811 | 0.3228 | 0.6319 |
| 107 | 6.4450 | -8.5920 | 0.0000 | 6.5504 | -8.0689 | 357.1381 | 0.1054 | 0.5231 | 357.1381 |
| 118 | 6.8590 | -8.8470 | 0.0000 | 7.1226 | -6.8087 | 351.5257 | 0.2636 | 2.0383 | 351.5257 |
| 121 | 6.0730 | -11.0980 | 0.0000 | 6.0563 | -9.4312 | 0.0620 | -0.0167 | 1.6668 | 0.0620 |

Table 6.3: FTU 0 to FTU 18 Brown Angles

7 FOCAL PLANE SURVEYS

In total, the IPF Kalman filter was used to process 76 separate calibration data sets over the period of IOC/SV and Post-IOC. This consisted of 19 Pre-Coarse Survey runs, 29 Coarse Survey runs, and 28 Fine survey runs. Based on these runs, approximately 1500 calibration parameters were estimated associated with frame alignments, pointing systematic errors, plate scales and optical distortions. Pre-Coarse, Coarse and Fine survey runs are summarized in Section 7.1, Section 7.2, and Section 7.3, respectively. With only a few exceptions, the requirements for the Pre-Coarse and Coarse surveys are 5.0 and 1.0 arcseconds, respectively. The Fine survey requirements are more specialized and differ from array to array.

7.1 Pre-Coarse Surveys

Results of the Pre-Coarse focal plane surveys are summarized in Table 7.1. The column marked TOTAL gives the total calibration error in arcseconds, 1-sigma, radial. It should be compared to the the column marked REQ, which shows the calibration requirement in the same units.

| NF | RN | DESCRIPTION | ANALYSIS | TOTAL | REQ |
|-----|-----|--------------------------------|----------------------|--------|------|
| 022 | 04P | IRS_Blue_PeakUp_FOV_Center | IOC Precoarse Survey | 0.2579 | 5.00 |
| 022 | 17P | IRS_Blue_PeakUp_FOV_Center | IOC Precoarse Survey | 0.1185 | 5.00 |
| 034 | 02P | IRS_ShortLo_2nd_Ord_Center_Pos | IOC Precoarse Survey | 0.4180 | 5.00 |
| 034 | 12P | IRS_ShortLo_2nd_Ord_Center_Pos | IOC Precoarse Survey | 0.9994 | 5.00 |
| 068 | 01P | IRAC_Center_of_3.6umArray | IOC Precoarse Survey | 4.5301 | 5.00 |
| 068 | 16P | IRAC_Center_of_3.6umArray | IOC Precoarse Survey | 0.2239 | 5.00 |
| 069 | 01P | IRAC_Center_of_5.8umArray | IOC Precoarse Survey | 3.2011 | 5.00 |
| 069 | 11P | IRAC_Center_of_5.8umArray | IOC Precoarse Survey | 0.2113 | 5.00 |
| 075 | 01P | IRAC_Center_of_4.5umArray | IOC Precoarse Survey | 1.2774 | 5.00 |
| 075 | 12P | IRAC_Center_of_4.5umArray | IOC Precoarse Survey | 0.2473 | 5.00 |
| 076 | 06P | IRAC_Center_of_8.0umArray | IOC Precoarse Survey | 1.5944 | 5.00 |
| 076 | 12P | IRAC_Center_of_8.0umArray | IOC Precoarse Survey | 0.2366 | 5.00 |
| 095 | 01P | MIPS_24um_center | IOC Precoarse Survey | 4.2958 | 5.00 |
| 107 | 01P | MIPS_70um_center | IOC Precoarse Survey | 1.6417 | 5.00 |
| 118 | 01P | MIPS_70um_fine_center | IOC Precoarse Survey | 2.0543 | 5.00 |
| 068 | 24P | IRAC_Center_of_3.6umArray | Plate Scale Test | N/A | 5.00 |
| 069 | 24P | IRAC_Center_of_5.8umArray | Plate Scale Test | N/A | 5.00 |
| 075 | 24P | IRAC_Center_of_4.5umArray | Plate Scale Test | N/A | 5.00 |
| 076 | 24P | IRAC_Center_of_8.0umArray | Plate Scale Test | N/A | 5.00 |

Table 7.1: Top Level Calibration Summary (Pre-Coarse) ([arcsec], 1-sigma, radial)

7.2 Coarse Surveys

Results of the Coarse focal plane surveys are summarized in Table 7.2.

| NF | RN | DESCRIPTION | ANALYSIS | TOTAL | REQ |
|-----|-----|--------------------------------|-------------------|---------|------|
| 018 | 001 | IRS_Red_PeakUp_FOV_Center | IOC Coarse Survey | 0.1109 | 1.00 |
| 019 | 001 | IRS_Red_PeakUp_FOV_Sweet_Spot | IOC Coarse Survey | 0.0957 | 1.00 |
| 022 | 001 | IRS_Blue_PeakUp_FOV_Center | IOC Coarse Survey | 0.1350 | 1.00 |
| 023 | 001 | IRS_Blue_PeakUp_FOV_Sweet_Spot | IOC Coarse Survey | 0.0998 | 1.00 |
| 028 | 003 | IRS_ShortLo_1st_Ord_Center_Pos | IOC Coarse Survey | 0.7680 | 1.00 |
| 034 | 002 | IRS_ShortLo_2nd_Ord_Center_Pos | IOC Coarse Survey | 2.5814 | 1.00 |
| 040 | 001 | IRS_LongLo_1st_Ord_Center_Pos | IOC Coarse Survey | 0.8900 | 1.00 |
| 046 | 001 | IRS_LongLo_2nd_Ord_Center_Pos | IOC Coarse Survey | 0.9278 | 1.00 |
| 052 | 003 | IRS_ShortHi_Center_Position | IOC Coarse Survey | 1.1260 | 1.00 |
| 058 | 001 | IRS_LongHi_Center_Position | IOC Coarse Survey | 2.1282 | 1.00 |
| 058 | 002 | IRS_LongHi_Center_Position | IOC Coarse Survey | 1.3895 | 1.00 |
| 068 | 002 | IRAC_Center_of_3.6umArray | IOC Coarse Survey | 0.3658 | 1.00 |
| 068 | 102 | IRAC_Center_of_3.6umArray | IOC Coarse Survey | 0.1128 | 1.00 |
| 069 | 001 | IRAC_Center_of_5.8umArray | IOC Coarse Survey | 0.3833 | 1.00 |
| 069 | 103 | IRAC_Center_of_5.8umArray | IOC Coarse Survey | 0.1130 | 1.00 |
| 075 | 001 | IRAC_Center_of_4.5umArray | IOC Coarse Survey | 0.3287 | 1.00 |
| 075 | 103 | IRAC_Center_of_4.5umArray | IOC Coarse Survey | 0.1033 | 1.00 |
| 076 | 001 | IRAC_Center_of_8.0umArray | IOC Coarse Survey | 0.4474 | 1.00 |
| 076 | 102 | IRAC_Center_of_8.0umArray | IOC Coarse Survey | 0.1045 | 1.00 |
| 087 | 103 | MIPS_160um_center_large_FOV | IOC Coarse Survey | 3.7858 | 3.75 |
| 095 | 001 | MIPS_24um_center | IOC Coarse Survey | 0.1307 | 1.00 |
| 095 | 101 | MIPS_24um_center | IOC Coarse Survey | 0.1151 | 1.00 |
| 095 | 01M | MIPS_24um_center | IOC Multi-Run | 0.1054 | 1.00 |
| 107 | 201 | MIPS_70um_center | IOC Coarse Survey | 0.4898 | 2.65 |
| 118 | 102 | MIPS_70um_fine_center | IOC Coarse Survey | 0.3473 | 1.12 |
| 118 | 202 | MIPS_70um_fine_center | IOC Coarse Survey | 0.3013 | 1.12 |
| 118 | 203 | MIPS_70um_fine_center | IOC Coarse Survey | 0.3013 | 1.12 |
| 121 | 002 | MIPS_SED_center | IOC Coarse Survey | 26.4392 | 1.15 |
| 121 | 103 | MIPS_SED_center | IOC Coarse Survey | 1.6069 | 1.15 |

Table 7.2: Top Level Calibration Summary (Coarse) ([arcsec], 1-sigma, radial)

7.3 Fine Surveys

Results of the Fine focal plane surveys are summarized in Table 7.3. Run numbers (NF) which have been incorporated into the recent Frame Table 18 are denoted with an asterisk *.

An exception to this convention is for the MIPS 24 um array (frame 095). Because of scan mirror non-repeatability, Prime frame 095 and its inferred frames were ultimately derived by the MIPS team using a weighted average of the frame locations in two separate IPF calibration runs 502095 and 602095. These derived frames should be accurate and repeatable to approximately 0.5 arcseconds, based on the experience of the MIPS team in dealing with this non-ideal behavior.

| NF | RN | DESCRIPTION | ANALYSIS | TOTAL | REQ |
|-----|------|--------------------------------|-----------------|--------|------|
| 018 | 501 | IRS_Red_PeakUp_FOV_Center | IOC Fine Survey | 0.0899 | 0.25 |
| 018 | 701* | IRS_Red_PeakUp_FOV_Center | IOC Fine Survey | 0.0899 | 0.25 |
| 019 | 502 | IRS_Red_PeakUp_FOV_Sweet_Spot | IOC Fine Survey | 0.0866 | 0.14 |
| 019 | 701* | IRS_Red_PeakUp_FOV_Sweet_Spot | IOC Fine Survey | 0.0866 | 0.14 |
| 022 | 503 | IRS_Blue_PeakUp_FOV_Center | IOC Fine Survey | 0.0968 | 0.25 |
| 022 | 701* | IRS_Blue_PeakUp_FOV_Center | IOC Fine Survey | 0.0966 | 0.25 |
| 023 | 502 | IRS_Blue_PeakUp_FOV_Sweet_Spot | IOC Fine Survey | 0.0868 | 0.14 |
| 023 | 701* | IRS_Blue_PeakUp_FOV_Sweet_Spot | IOC Fine Survey | 0.0869 | 0.14 |
| 028 | 502* | IRS_ShortLo_1st_Ord_Center_Pos | IOC Fine Survey | 0.1165 | 0.14 |
| 034 | 502* | IRS_ShortLo_2nd_Ord_Center_Pos | IOC Fine Survey | 0.0909 | 0.14 |
| 040 | 502* | IRS_LongLo_1st_Ord_Center_Pos | IOC Fine Survey | 0.1295 | 0.28 |
| 046 | 501* | IRS_LongLo_2nd_Ord_Center_Pos | IOC Fine Survey | 0.2682 | 0.28 |
| 052 | 502* | IRS_ShortHi_Center_Position | IOC Fine Survey | 0.0885 | 0.14 |
| 058 | 501* | IRS_LongHi_Center_Position | IOC Fine Survey | 0.1027 | 0.28 |
| 068 | 502* | IRAC_Center_of_3.6umArray | IOC Fine Survey | 0.0881 | 0.14 |
| 069 | 502* | IRAC_Center_of_5.8umArray | IOC Fine Survey | 0.0889 | 0.14 |
| 075 | 502* | IRAC_Center_of_4.5umArray | IOC Fine Survey | 0.0878 | 0.14 |
| 076 | 502* | IRAC_Center_of_8.0umArray | IOC Fine Survey | 0.0895 | 0.14 |
| 087 | 502 | MIPS_160um_center_large_FOV | IOC Fine Survey | 0.6254 | 3.70 |
| 087 | 504 | MIPS_160um_center_large_FOV | IOC Fine Survey | 0.3694 | 3.70 |
| 087 | 803 | MIPS_160um_center_large_FOV | IOC Fine Survey | 1.8519 | 3.70 |
| 087 | 703* | MIPS_160um_center_large_FOV | IOC Fine Survey | 1.2056 | 3.70 |
| 095 | 502 | MIPS_24um_center | IOC Fine Survey | 0.0906 | 0.14 |
| 095 | 602* | MIPS_24um_center | IOC Fine Survey | 0.0884 | 0.14 |
| 107 | 704* | MIPS_70um_center | IOC Fine Survey | 0.2847 | 2.60 |
| 118 | 702* | MIPS_70um_fine_center | IOC Fine Survey | 0.3038 | 1.10 |
| 121 | 504 | MIPS_SED_center | IOC Fine Survey | 0.3988 | 1.10 |
| 121 | 703* | MIPS_SED_center | IOC Fine Survey | 0.9998 | 1.10 |

Table 7.3: Top Level Calibration Summary (Fine) ([arcsec], 1-sigma, radial)

8 DETAILED EXAMPLES

In this section, four examples are highlighted in detail. These examples represent official Fine Survey runs which have been delivered to the project and have been incorporated into the latest on-board frame table.

- Example 1: IRS Red Peak-Up Array (frame 018)
- Example 2: IRS Short-Lo Slit (frame 028)
- Example 3: IRAC 3.6 um Array (frame 068)
- Example 4: MIPS 24 um Array (frame 095)

It is emphasized that estimated corrections from Fine Survey runs are generally very small because large errors were already removed in earlier Pre-Coarse and Coarse calibration runs.

8.1 Example 1: IRS Red Peak-Up Array (frame 018)

The experiment design for the IRS Peak-Up array is shown in Figure 8.1. The design involves putting a star on PCRS1 (leg 1), moving it to PCRS2 (leg 2), moving it to the Peak-Up array where it is placed at each point on a 3x3 grid (legs 4-11) and then back to PCRS2 (leg 12).

REMARK 8.1 Aside from scaling and shift the grid of points, this same experiment design is used for calibrating all of the Peakup array frames (i.e., frames 018, 019, 022, 023). Specifically, the experiment design is repeated 7 times for the Acquisition frames (frames 018 and 022) which have a 0.28 arcsec calibration requirement, and is repeated 21 times for the Sweet Spot frames (frames 019 and 023) which have a tighter 0.14 arcsec calibration requirement.

In this run (and for all IRS Peakup arrays), the tables list “pixels” but values are actually reported in “centi-pixels”. The physical pixel of the IRS Peakup array has a true angular size of approximately 1.8 arcseconds.

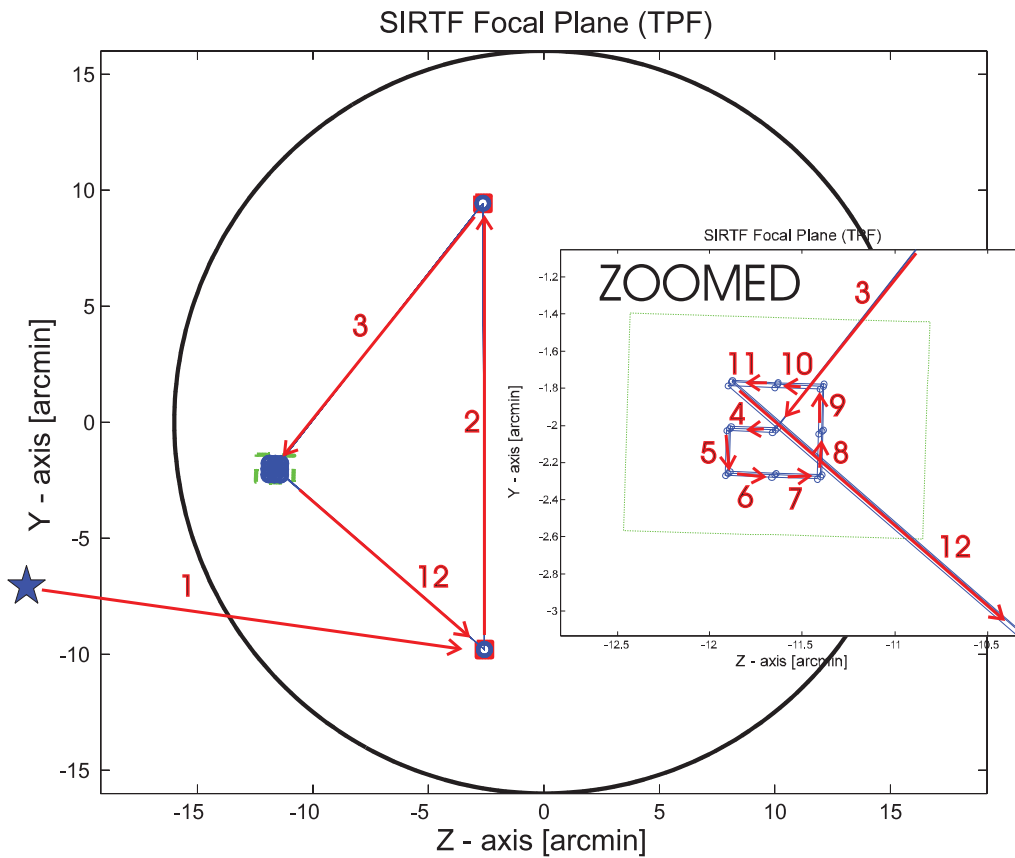


Figure 8.1: Experiment Design for IRS Red Peak-Up Array [ID701018]

FOCAL PLANE SURVEY ANALYSIS: IOC Fine Survey.
INSTRUMENT NAME: IRS_Red_PeakUp_FOV_Center NF: 18
PIX2RADW: 8.72660000E-008[rad/pixel] = 1.8000E-002[arcsec/pixel]
PIX2RADV: 8.72660000E-008[rad/pixel] = 1.8000E-002[arcsec/pixel]

| FRAME | DESCRIPTION | IPF ¹ | SF ² | TOTAL | REQ |
|--------|---------------------------|------------------|-----------------|--------|------|
| 018(P) | IRS_Red_PeakUp_FOV_Center | 0.0279 | 0.0855 | 0.0899 | 0.25 |

Table 8.1: IPF calibration error summary ([arcsec], 1-sigma, radial)

| RMS METRIC | A PRIORI ³ | A POSTERIORI ³ | ATT. CORRECTED ⁴ | UNITS |
|------------|-----------------------|---------------------------|-----------------------------|--------|
| Radial | 1.3635 | 0.1075 | 0.0509 | arcsec |
| W-Axis | 1.3367 | 0.0645 | 0.0390 | arcsec |
| V-Axis | 0.2690 | 0.0859 | 0.0327 | arcsec |
| Radial | 75.7489 | 5.9702 | 2.8271 | pixels |
| W-Axis | 74.2600 | 3.5845 | 2.1658 | pixels |
| V-Axis | 14.9450 | 4.7743 | 1.8171 | pixels |

Table 8.2: Science measurement prediction error summary (1-sigma)

| Con. Plate Scale | | | Γ Dependent | | | | Γ^2 Dependent | | | | Linear Plate Scale | | | | | | Mirror | |
|------------------|------------|------------|--------------------|----------|----------|----------|----------------------|----------|----------|----------|--------------------|-----------------|----------|----------|----------|----------|----------|---------|
| a_{00} | b_{00} | c_{00} | a_{10} | b_{10} | c_{10} | d_{10} | a_{20} | b_{20} | c_{20} | d_{20} | a_{01} | b_{01} | c_{01} | d_{01} | e_{01} | f_{01} | α | β |
| 1 | 2 | 3 | 4 | 5 | 6 | 7 | 8 | 9 | 10 | 11 | 12 | 13 | 14 | 15 | 16 | 17 | 18 | 19 |
| 1 | 1 | 1 | 0 | 0 | 0 | 0 | 0 | 0 | 0 | 0 | 1 | 1 | 1 | 1 | 1 | 1 | 0 | 0 |
| IPF (T) | | | Alignment R | | | | | | | | | Gyro Drift Bias | | | | | | |
| θ_1 | θ_2 | θ_3 | a_{rx} | a_{ry} | a_{rz} | b_{rx} | b_{ry} | b_{rz} | c_{rx} | c_{ry} | c_{rz} | b_{gx} | b_{gy} | b_{gz} | c_{gx} | c_{gy} | c_{gz} | |
| 20 | 21 | 22 | 23 | 24 | 25 | 26 | 27 | 28 | 29 | 30 | 31 | 32 | 33 | 34 | 35 | 36 | 37 | |
| 1 | 1 | 1 | 1 | 1 | 1 | 1 | 1 | 1 | 1 | 1 | 1 | 1 | 1 | 1 | 1 | 1 | 1 | |

Table 8.3: IPF filter execution mask vector assignment

¹IPF filter removes systematic pointing errors due to: thermomechanical alignment drift (Body to TPF), gyro bias and bias drift, centroiding error, attitude error, and optical distortion. IPF SIGMA presented here is “Scaled” by the Least Squares Scale factor. The Least Squares Scale Factor was: 0.541872. It is assumed that the gyro Angle Random Walk contribution is captured with the Least Squares scaling. The gyro ARW contribution can be approximately calculated as 0.0788 arcseconds, given that $ARW = 100 \mu deg/\sqrt{hr}$, with 6.043555e+002 second Maneuver time (max), and 7 independent Maneuvers.

²Gyro Scale Factor(GSF) assumes 95 ppm error over 0.250 degree maneuver.

³This can be interpreted as estimate of ”pixel to sky” pointing reconstruction error if no science data is used.

⁴This can be interpreted as estimate of achieved S/I centroiding error

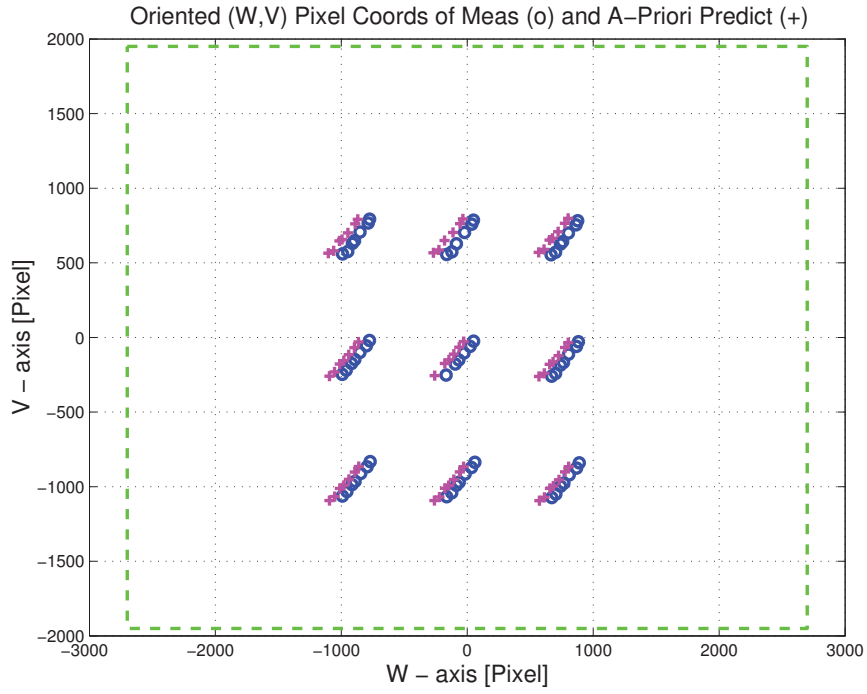


Figure 8.2: Oriented Pixel Coords of measurements and a-priori predicts [RUN701018]

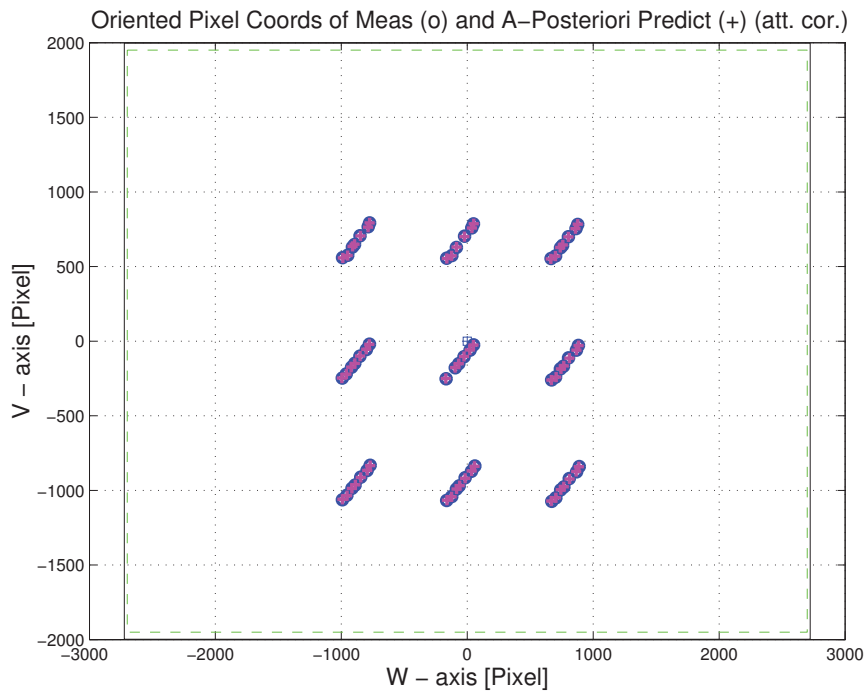


Figure 8.3: Oriented Pixel Coords of meas. and a-posteriori predicts (attitude corrected) [RUN701018]

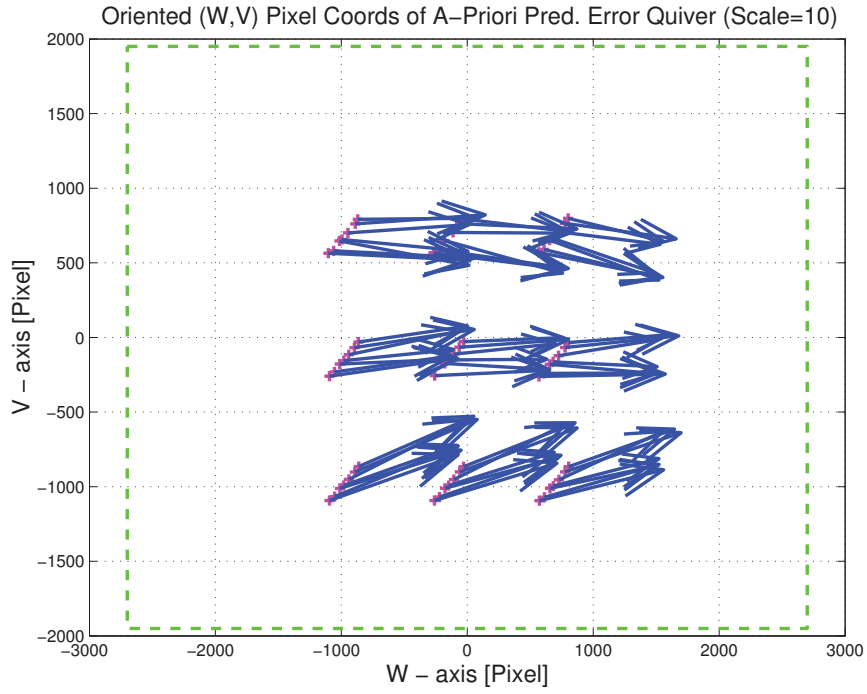


Figure 8.4: Oriented (W,V) Pixel Coords of A-Priori Prediction Error Quiver Plot [RUN701018]

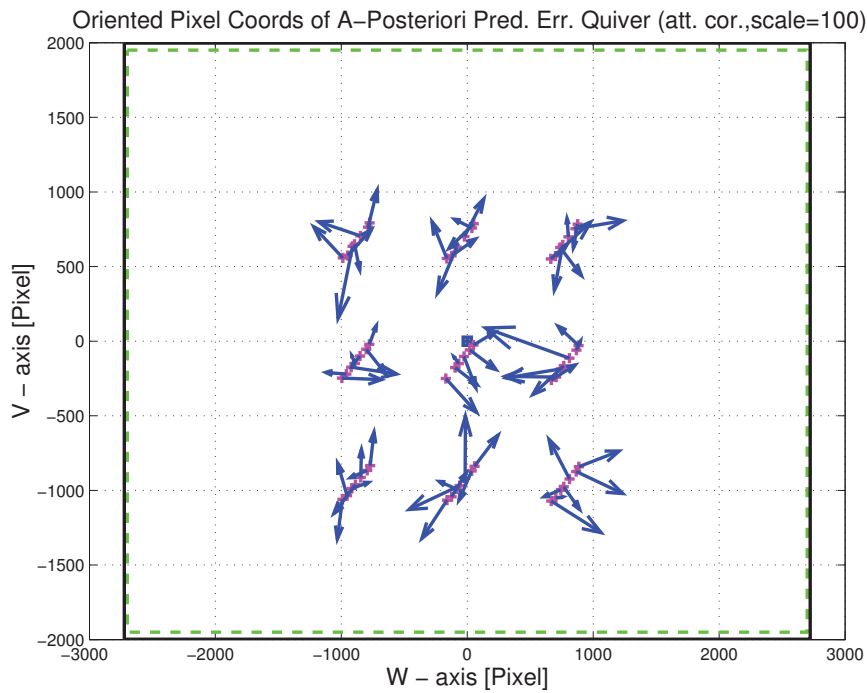


Figure 8.5: A-Posteriori Science Centroid Prediction Error Quiver (Att. Cor.) [RUN701018]

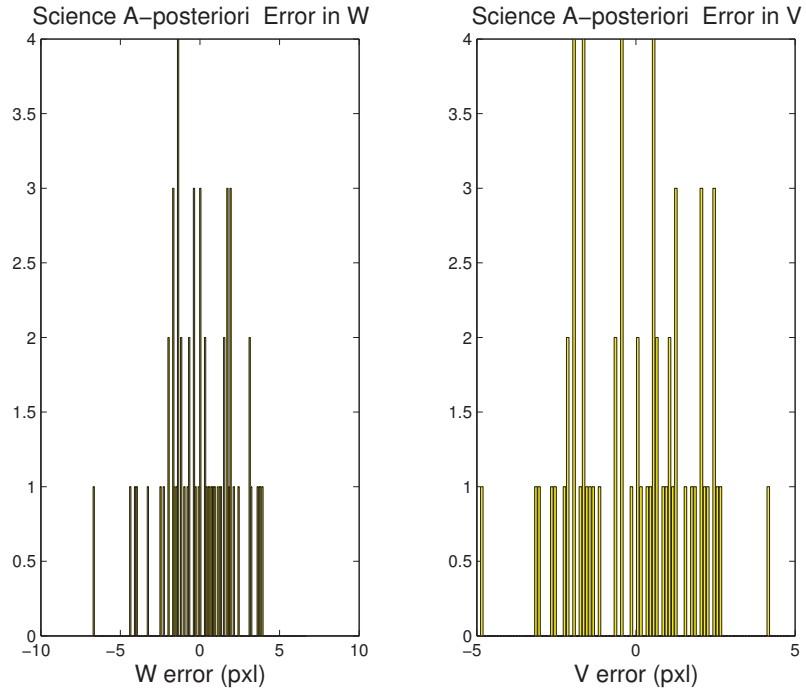


Figure 8.6: Histograms of science a-posteriori residuals (or innovations) [RUN701018]

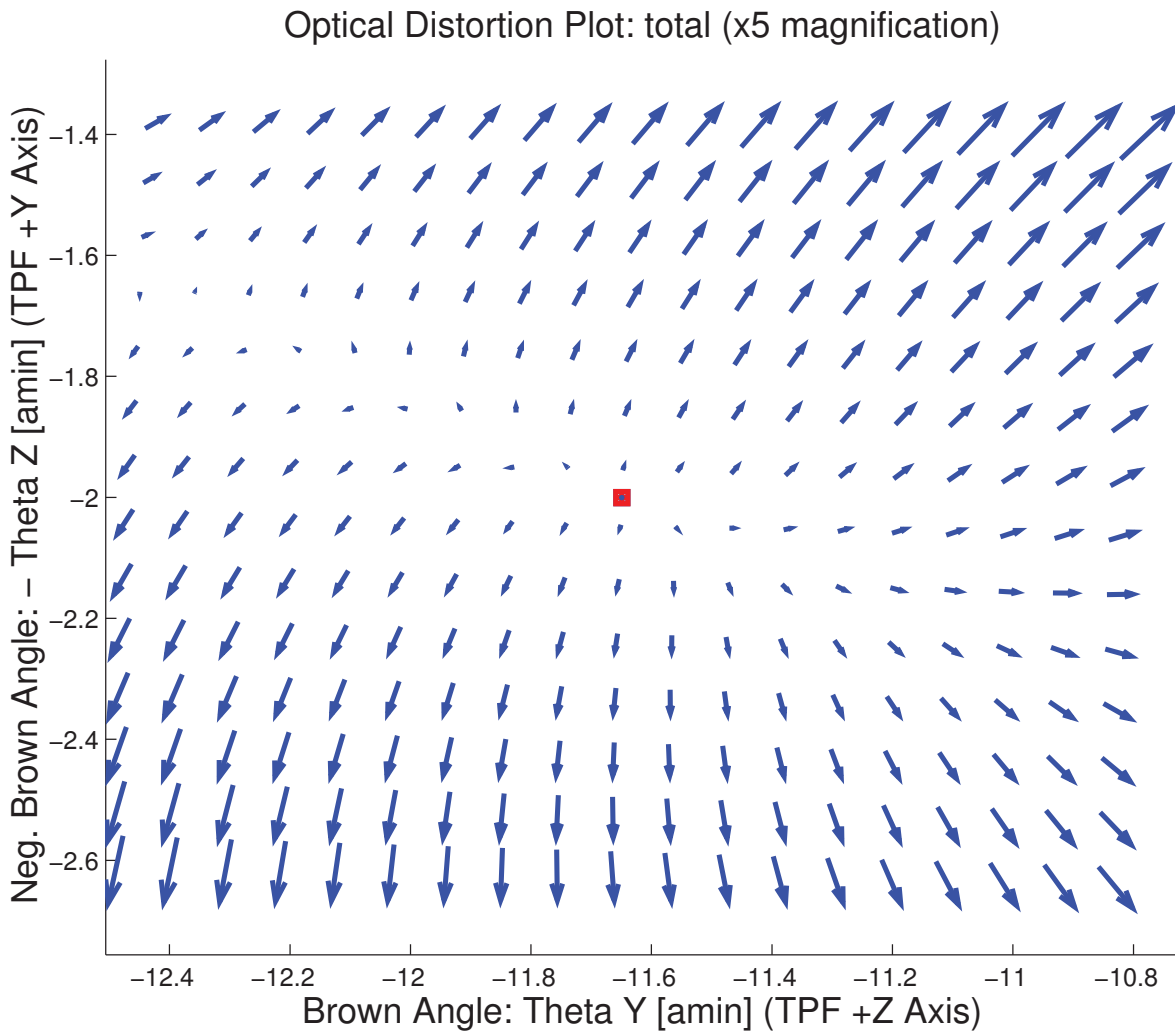


Figure 8.7: Optical Distortion Plot: total (x5 magnification) [RUN701018]

OUTPUT FILE NAME: IFmini701018.dat DATE: 26-Apr-2004 TIME: 10:29
 INSTRUMENT NAME: IRS_Red_PeakUp_FOV_Center NF: 18
 IPF FILTER VERSION: IPF.V4.0.0 SW RELEASE DATE: January 30, 2004
 FRAME TABLE USED: BodyFrames_FTU_17a

----- IPF BROWN ANGLE SUMMARY -----

| Frame Number | WAS | | | IS | | |
|--------------|------------------|------------------|-------------|------------------|------------------|-------------|
| | theta_Y (arcmin) | theta_Z (arcmin) | angle (deg) | theta_Y (arcmin) | theta_Z (arcmin) | angle (deg) |
| 018 | -11.634104 | +2.000761 | +1.797497 | -11.649227 | +2.000391 | +1.796568 |

OFFSET NF Delta_CW Delta_CV
 0 18 +0.000 +0.000 pixels

OFFSET FRAME NAME: IRS_Red_PeakUp_FOV_Center
 Brown Angle theta_Y(arcmin) theta_Z(arcmin) angle(deg)
 WAS(FTB) -11.634104 +2.000761 +1.797497
 IS (EST) -11.649227 +2.000391 +1.796568
 dT_EST -0.015122 -0.000370 -0.000929
 T_sSIGMA +0.000343 +0.000314 +0.027035
 dT_EST/T_sSIGMA -44.145328 -1.179646 -0.034381

| VARNAME | MEAN | SIGMA | SCALED_SIGMA |
|------------|--------------------------|--------------------------|--------------------------|
| a00 | +8.3450700080643682E-003 | +1.1273567124418847E-003 | +6.1088293297998969E-004 |
| b00 | +2.4451506019239577E-002 | +1.4793499350343783E-003 | +8.0161817217560096E-004 |
| c00 | +6.9999743657076785E-003 | +8.7540744264380868E-004 | +4.7435870138780892E-004 |
| a01 | +1.1248577582585527E+001 | +2.5755386292958942E+001 | +1.3956120316697406E+001 |
| b01 | +5.7551828493173169E+001 | +2.6436266228613896E+001 | +1.4325070026678015E+001 |
| c01 | -8.8694976875352811E+000 | +1.8462630582075413E+001 | +1.0004380863688421E+001 |
| d01 | -8.2959472672241539E+000 | +2.5976959878197114E+001 | +1.4076184818134580E+001 |
| e01 | -1.9967256641951010E+001 | +2.7887173104844319E+001 | +1.5111275704304798E+001 |
| f01 | +8.2634102587626721E+000 | +1.9039395020480583E+001 | +1.0316913310502295E+001 |
| del_theta1 | +3.8673030706634637E-013 | +8.7076274322244471E-004 | +4.7184186924939243E-004 |
| del_theta2 | +2.3100620027209200E-016 | +1.8389176895891647E-007 | +9.9645783745925455E-008 |
| del_theta3 | -7.2814657915123895E-018 | +1.6852041764747993E-007 | +9.1316480279361660E-008 |
| del_arx | -1.1794819525771548E-013 | +4.4691893314850053E-005 | +2.4217281511074331E-005 |
| del_ary | -1.2444422772602969E-017 | +4.1320408664020520E-006 | +2.2390368689901116E-006 |
| del_arz | +1.0424518391060012E-015 | +4.1328896599874182E-006 | +2.2394968063898723E-006 |
| brx | -7.4250778782522904E-009 | +4.2628402179686213E-008 | +2.3099133632133062E-008 |
| bry | -5.5139723484908851E-010 | +4.9752052316802564E-009 | +2.6959239525199515E-009 |
| brz | +1.3323473199365649E-010 | +4.9765515288145841E-009 | +2.6966534731171182E-009 |
| crx | +1.8010742375275293E-012 | +1.9044106701084413E-011 | +1.0319466437861868E-011 |
| cry | +2.6361801087110402E-013 | +2.4468321782871572E-012 | +1.3258696214654676E-012 |
| crz | -7.4853164468114418E-014 | +2.4475046095252647E-012 | +1.3262339930635865E-012 |
| bgx | -1.1525072612839652E-006 | +6.5550525259180096E-007 | +3.5519988204949896E-007 |
| bgy | +8.4040468426487263E-009 | +5.0146161860984653E-009 | +2.7172796415940759E-009 |
| bgz | +2.4630372118899584E-009 | +5.8819295556110879E-009 | +3.1872523921292719E-009 |
| cgx | +7.7404924268011984E-012 | +2.1272758775495873E-010 | +1.1527110390111448E-010 |
| cgy | +4.1964546732329322E-013 | +2.4576115666657468E-012 | +1.3317106692152788E-012 |
| cgz | +1.1250680144746528E-012 | +2.6554335245667130E-012 | +1.4389048310246589E-012 |

LSQF RESIDUAL SIGMA SCALE = +5.4187190818849251E-001

Summary of Results (IRS Red Peak-Up Array)

There were 7 sandwiches maneuvers with 61 science centroids and 49 PCRS measurements. The IPF filter estimated 27 parameters consisting of: 3 constant and 6 linear plate scales, 3 IPF alignment angles, 3 STA-to-PCRS alignment angles, 6 STA-to-PCRS thermomechanical drift parameters, and 3 gyro bias and 3 gyro bias-drift parameters.

Results indicate constant plate scale errors on the order of 24 parts per thousand. The linear plate scales were needed in this run to estimate centroids accurately. The optical distortion quiver plot in Figure 8.7 indicates the presence of these high order distortions. However, the data set contained no centroids near the edge of the array so the extrapolation of the linear plate scales to these edge locations may not be accurate.

The recommended Brown angle offset of 0.9" is due primarily to a redefinition of the Prime frame by 1/2 pixel (with 1.8 arcsecond pixels) made by the IRS team just prior to this run. The histograms indicate that the IRS Peak-Up array is achieving a centroiding accuracy on the order of 5 centi-pixels, or 1/20 of a 1.8" pixel with the chosen calibration source.

The frame calibration is accurate to 0.09 arcsecond which satisfies its Fine Survey requirement of 0.25 arcsecond by a good margin.

8.2 Example 2: IRS Short-Lo Slit (frame 028)

The experiment design for the IRS Short-Lo slit is shown in Figure 8.8. The design involves putting a star on PCRS1 (leg 1), moving it to PCRS2 (leg 2), moving it to the IRS Short-Lo slit (leg 3), and then crossing the slit four times back and forth in the dispersion direction (legs 4-11), then crossing in the cross-dispersion direction (legs 13, 14), and then back to PCRS2 (leg 15). Since centroids are not available for a slit (in contrast to a CCD array), a different approach is taken. Specifically, for each slit crossing a centroid is reported at the slit center at the time instant when the light intensity (total dn) is at its maximum.

REMARK 8.2 Except for changes in numbers, separations, and speeds of slit crossings, a similar experiment design is used for all of the IRS slits (i.e., frames 028, 034, 040, 046, 052, 058). Interestingly, a similar experiment design was also used for the MIPS SED (i.e., frame 121, which is a long-wavelength spectroscopy slit), and for the MIPS 160 μm array (frame 087) which resembles a slit because it consists of two rows of pixels separated by a missing row of pixels. However, one difference in the MIPS calibrations is that the source was switched to an IR target when the maneuver approached the MIPS 160 μm and SED arrays, since the PCRS source would be too faint at these longer wavelengths. Another difference is that the MIPS sources were stepped across the SED slit and 160 μm array using a “step-and-stare” motion instead of a continuous scan, in order to allow longer integration times.

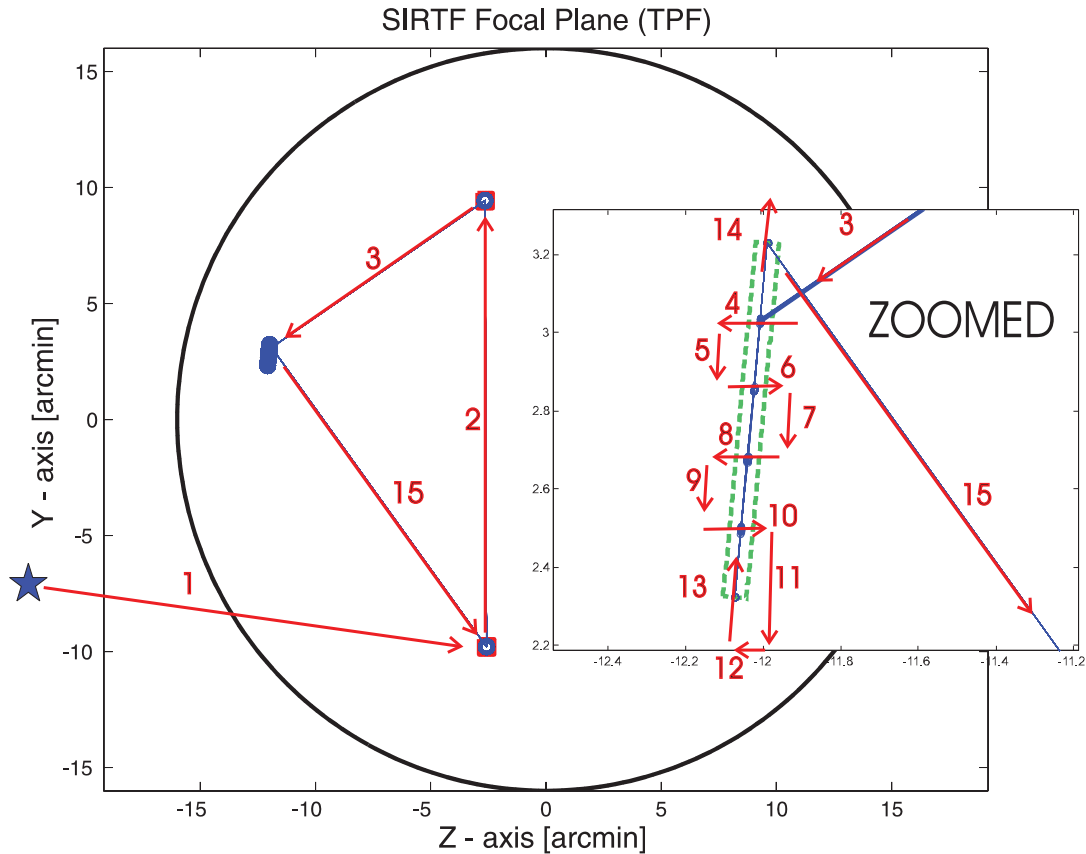


Figure 8.8: Experiment Design for IRS Short-Lo Slit [ID502028]

FOCAL PLANE SURVEY ANALYSIS: IOC Fine Survey.
INSTRUMENT NAME: IRS_ShortLo_1st_Ord_Center_Pos NF: 28
PIX2RADW: 4.84813681E-006[rad/pixel] = 1.0000E+000[arcsec/pixel]
PIX2RADV: 4.84813681E-006[rad/pixel] = 1.0000E+000[arcsec/pixel]

| FRAME | DESCRIPTION | IPF ¹ | SF ² | TOTAL | REQ |
|--------|--------------------------------|------------------|-----------------|--------|------|
| 028(P) | IRS_ShortLo_1st_Ord_Center_Pos | 0.0791 | 0.0855 | 0.1165 | 0.14 |
| 026(I) | IRS_ShortLo_1st_Ord_1st_Pos | 0.0821 | 0.0855 | 0.1186 | N/A |
| 027(I) | IRS_ShortLo_1st_Ord_2nd_Pos | 0.0772 | 0.0855 | 0.1152 | N/A |
| 029(I) | IRS_ShortLo_Module_Center | 0.0809 | 0.0855 | 0.1177 | N/A |

Table 8.4: IPF calibration error summary ([arcsec], 1-sigma, radial)

| RMS METRIC | A PRIORI ³ | A POSTERIORI ³ | ATT. CORRECTED ⁴ | UNITS |
|------------|-----------------------|---------------------------|-----------------------------|--------|
| Radial | 1.5786 | 0.6289 | 0.5543 | arcsec |
| W-Axis | 1.3875 | 0.5477 | 0.5429 | arcsec |
| V-Axis | 0.7528 | 0.3092 | 0.1115 | arcsec |
| Radial | 1.5786 | 0.6289 | 0.5543 | pixels |
| W-Axis | 1.3875 | 0.5477 | 0.5429 | pixels |
| V-Axis | 0.7528 | 0.3092 | 0.1115 | pixels |

Table 8.5: Science measurement prediction error summary (1-sigma)

| Con. Plate Scale | | | Γ Dependent | | | | Γ^2 Dependent | | | | Linear Plate Scale | | | | | | Mirror | |
|------------------|------------|------------|--------------------|----------|----------|----------|----------------------|----------|----------|----------|--------------------|-----------------|----------|----------|----------|----------|----------|---------|
| a_{00} | b_{00} | c_{00} | a_{10} | b_{10} | c_{10} | d_{10} | a_{20} | b_{20} | c_{20} | d_{20} | a_{01} | b_{01} | c_{01} | d_{01} | e_{01} | f_{01} | α | β |
| 1 | 2 | 3 | 4 | 5 | 6 | 7 | 8 | 9 | 10 | 11 | 12 | 13 | 14 | 15 | 16 | 17 | 18 | 19 |
| 1 | 0 | 0 | 0 | 0 | 0 | 0 | 0 | 0 | 0 | 0 | 0 | 0 | 0 | 0 | 0 | 0 | 0 | 0 |
| IPF (T) | | | Alignment R | | | | | | | | | Gyro Drift Bias | | | | | | |
| θ_1 | θ_2 | θ_3 | a_{rx} | a_{ry} | a_{rz} | b_{rx} | b_{ry} | b_{rz} | c_{rx} | c_{ry} | c_{rz} | b_{gx} | b_{gy} | b_{gz} | c_{gx} | c_{gy} | c_{gz} | |
| 20 | 21 | 22 | 23 | 24 | 25 | 26 | 27 | 28 | 29 | 30 | 31 | 32 | 33 | 34 | 35 | 36 | 37 | |
| 0 | 1 | 1 | 1 | 1 | 1 | 1 | 1 | 1 | 1 | 1 | 1 | 1 | 1 | 1 | 1 | 1 | 1 | 1 |

Table 8.6: IPF filter execution mask vector assignment

¹IPF filter removes systematic pointing errors due to: thermomechanical alignment drift (Body to TPF), gyro bias and bias drift, centroiding error, attitude error, and optical distortion. IPF SIGMA presented here is “Scaled” by the Least Squares Scale factor. The Least Squares Scale Factor was: 3.485288. It is assumed that the gyro Angle Random Walk contribution is captured with the Least Squares scaling. The gyro ARW contribution can be approximately calculated as 0.0387 arcseconds, given that $ARW = 100 \mu deg/\sqrt{hr}$, with $6.872852e+002$ second Maneuver time (max), and 33 independent Maneuvers.

²Gyro Scale Factor(GSF) assumes 95 ppm error over 0.250 degree maneuver.

³This can be interpreted as estimate of ”pixel to sky” pointing reconstruction error if no science data is used.

⁴This can be interpreted as estimate of achieved S/I centroiding error

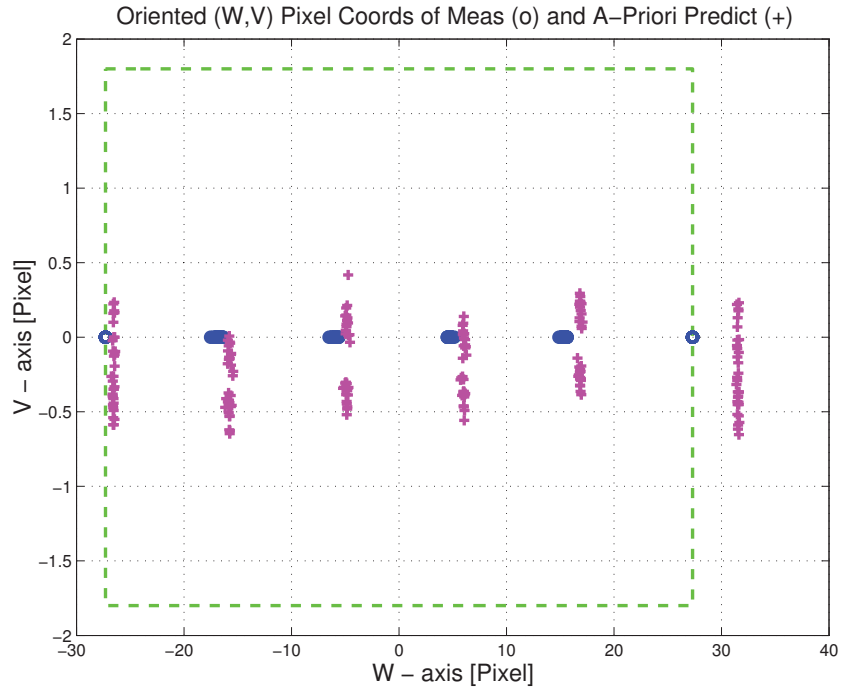


Figure 8.9: Oriented Pixel Coords of measurements and a-priori predicts [RUN502028]

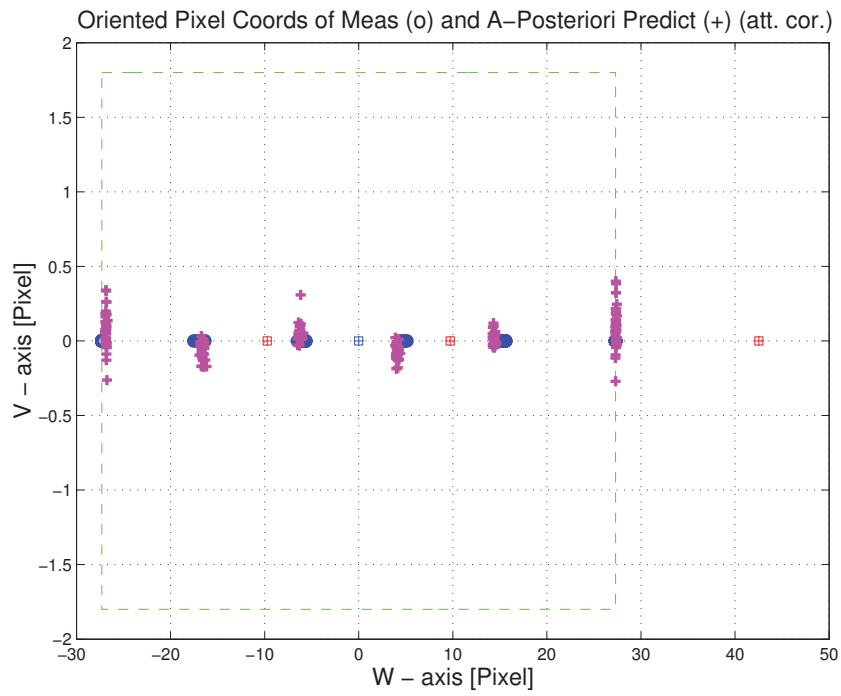


Figure 8.10: Oriented Pixel Coords of meas. and a-posteriori predicts (attitude corrected) [RUN502028]

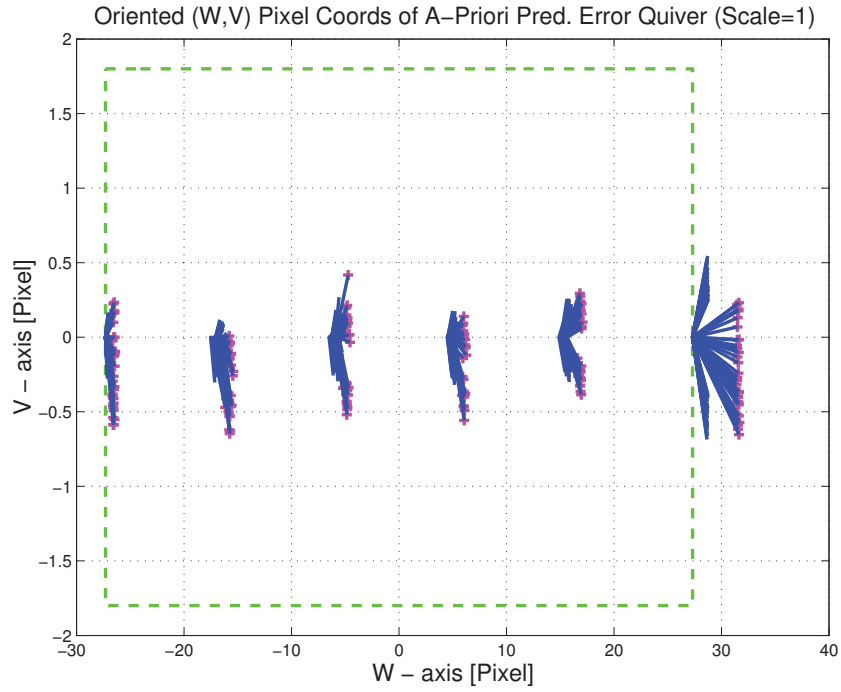


Figure 8.11: Oriented (W,V) Pixel Coords of A-Priori Prediction Error Quiver Plot [RUN502028]

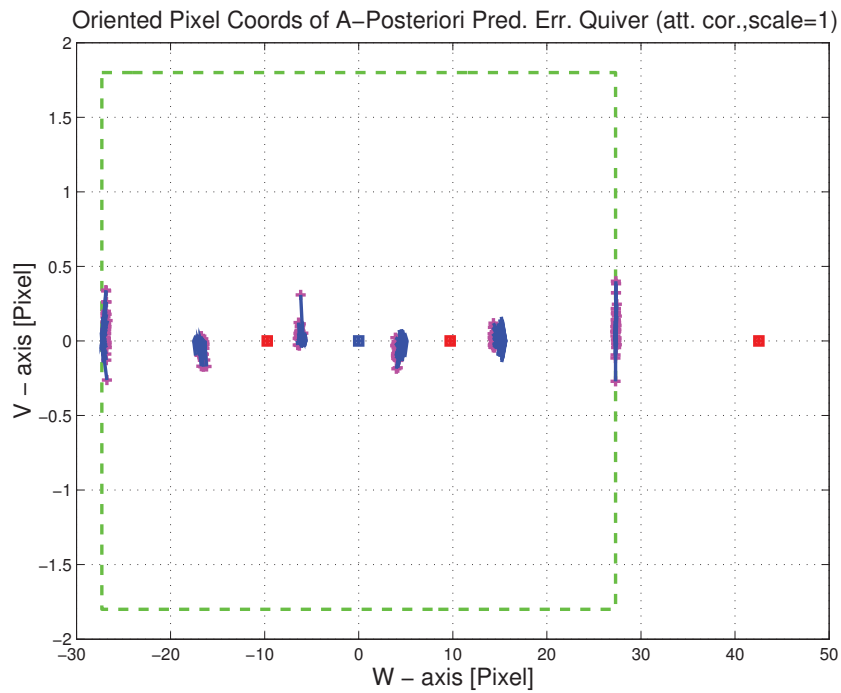


Figure 8.12: A-Posteriori Science Centroid Prediction Error Quiver (Att. Cor.) [RUN502028]

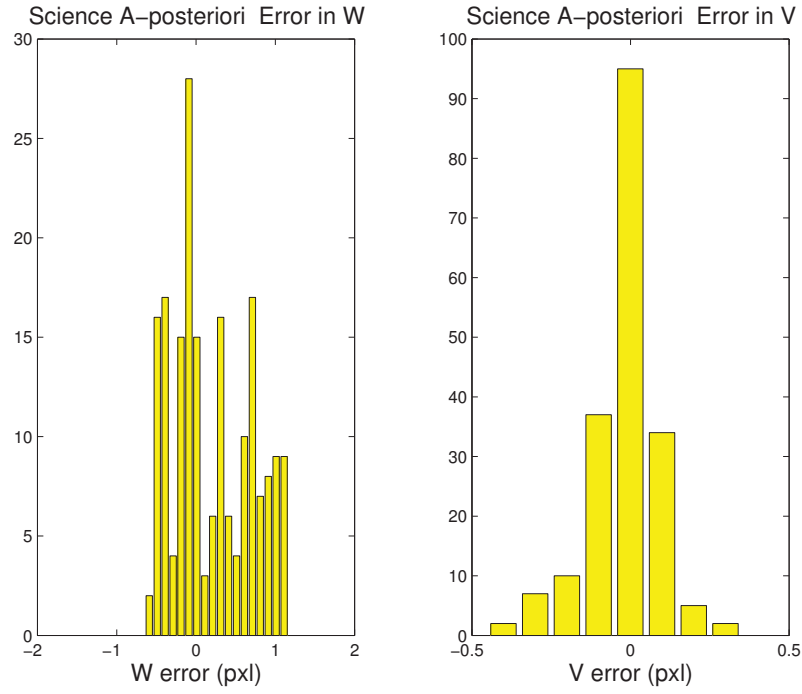


Figure 8.13: Histograms of science a-posteriori residuals (or innovations) [RUN502028]

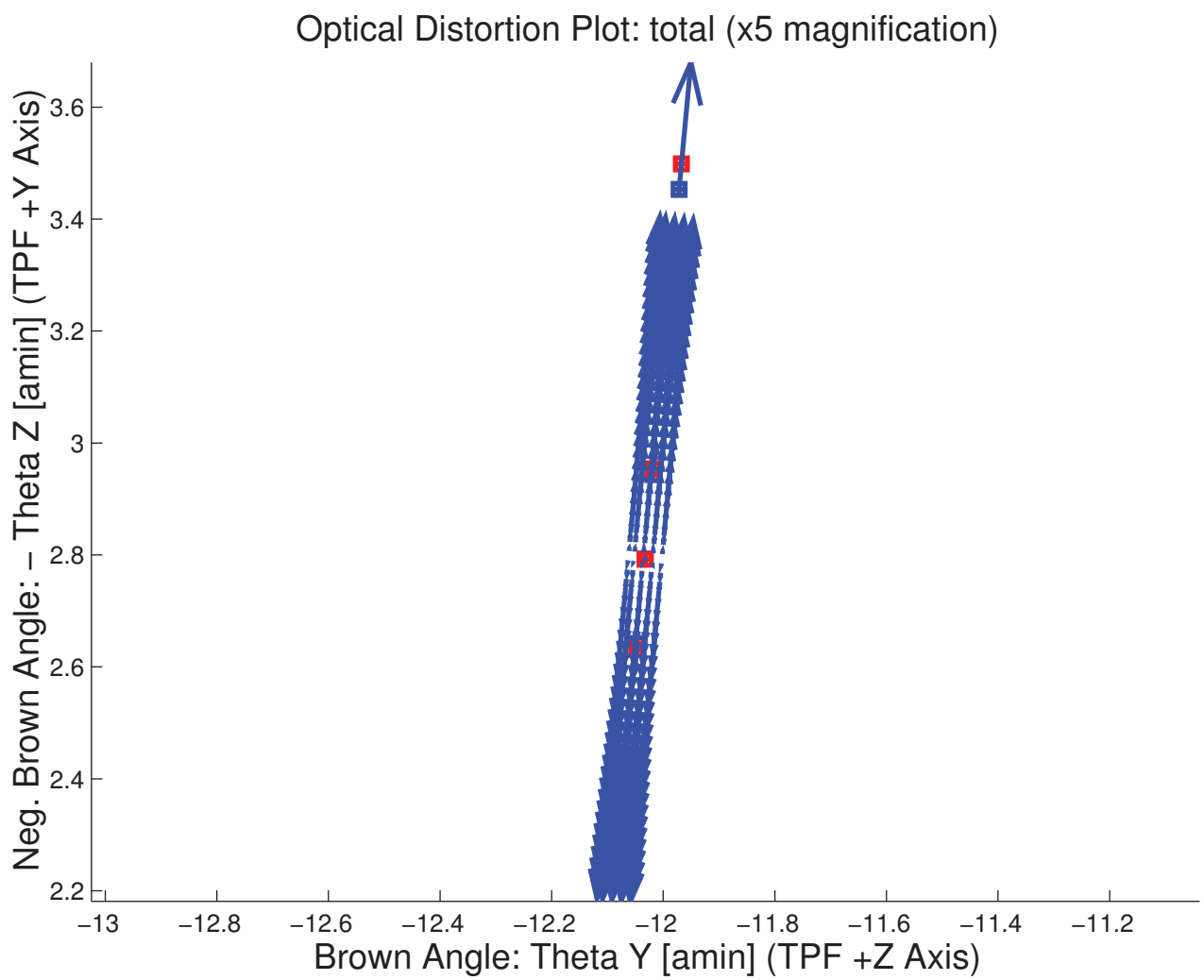


Figure 8.14: Optical Distortion Plot: total (x5 magnification) [RUN502028]

OUTPUT FILE NAME: IFmini502028.dat DATE: 06-Nov-2003 TIME: 14:58
 INSTRUMENT NAME: IRS_ShortLo_1st_Ord_Center_Pos NF: 28
 IPF FILTER VERSION: IPF.V3.0.0B SW RELEASE DATE: November 3, 2003
 FRAME TABLE USED: BodyFrames_FTU_12b

----- IPF BROWN ANGLE SUMMARY -----

OFFSET NF Delta_CW Delta_CV
 0 28 +0.000 +0.000 pixels

OFFSET FRAME NAME: IRS_ShortLo_1st_Ord_Center_Pos
 Brown Angle theta_Y(arcmin) theta_Z(arcmin) angle(deg)
 WAS(FTB) -12.031014 -2.776537 -84.719994
 IS (EST) -12.032552 -2.792599 -84.719993
 dT_EST -0.001538 -0.016062 +0.000001
 T_sSIGMA +0.000985 +0.000875 +999.999999
 dT_EST/T_sSIGMA -1.561550 -18.349747 +999.999999

OFFSET NF Delta_CW Delta_CV
 1 26 -9.100 +0.000 pixels

OFFSET FRAME NAME: IRS_ShortLo_1st_Ord_1st_Pos
 Brown Angle theta_Y(arcmin) theta_Z(arcmin) angle(deg)
 WAS(FTB) -12.044971 -2.625513 -84.719994
 IS (EST) -12.047468 -2.631200 -84.719993
 dT_EST -0.002497 -0.005688 +0.000001
 T_sSIGMA +0.001052 +0.000875 +999.999999
 dT_EST/T_sSIGMA -2.372454 -6.497895 +999.999999

OFFSET NF Delta_CW Delta_CV
 2 27 +9.100 +0.000 pixels

OFFSET FRAME NAME: IRS_ShortLo_1st_Ord_2nd_Pos
 Brown Angle theta_Y(arcmin) theta_Z(arcmin) angle(deg)
 WAS(FTB) -12.017057 -2.927561 -84.719994
 IS (EST) -12.017636 -2.953997 -84.719993
 dT_EST -0.000579 -0.026436 +0.000001
 T_sSIGMA +0.000944 +0.000875 +999.999999
 dT_EST/T_sSIGMA -0.613791 -30.201598 +999.999999

OFFSET NF Delta_CW Delta_CV
 3 29 +39.800 +0.000 pixels

OFFSET FRAME NAME: IRS_ShortLo_Module_Center
 Brown Angle theta_Y(arcmin) theta_Z(arcmin) angle(deg)
 WAS(FTB) -11.969972 -3.437059 -84.719994
 IS (EST) -11.967317 -3.498495 -84.719993
 dT_EST +0.002655 -0.061435 +0.000001
 T_sSIGMA +0.001026 +0.000875 +999.999999
 dT_EST/T_sSIGMA +2.588876 -70.185304 +999.999999

| VARNAME | MEAN | SIGMA | SCALED_SIGMA |
|------------|--------------------------|--------------------------|--------------------------|
| a00 | +6.8693071855212465E-002 | +3.2245121394587015E-004 | +1.1238351992073983E-003 |
| del_theta2 | -4.7805196201717925E-017 | +8.2205919979670894E-008 | +2.8651126887024126E-007 |
| del_theta3 | -3.6541304423526956E-016 | +7.3056749687733810E-008 | +2.5462377962249540E-007 |

LSQF RESIDUAL SIGMA SCALE = +3.4852875430515713E+000

Summary of Results (IRS Short-Lo Slit)

Because of the large effective centroiding errors along the v-axis caused by the slit-scanning process, the plate scale along the v-axis direction and orientation of the slit are not estimated.

There were 32 sandwiches maneuvers with 192 science centroids and 224 PCRS measurements. The IPF filter estimated 18 parameters consisting of: 1 constant plate scale (along W-axis), 2 IPF alignment angles, 3 STA-to-PCRS alignment angles, 6 STA-to-PCRS thermomechanical drift parameters, and 3 gyro bias and 3 gyro bias-drift parameters. Recommendations were made for updating frames 28, 26, 27 and 29, with adjustments of about 0.1 and 0.96 arcseconds in Y and Z. The frame calibration is accurate to 0.1165 arcsecond which satisfies its Fine Survey requirement of 0.14 arcsecond.

8.3 Example 3: IRAC 3.6 um Array (frame 068)

The experiment design for the IRAC 3.6 um array is shown in Figure 8.15. The design involves putting a star on PCRS1 (leg 1), and simultaneously imaging a cluster of stars on the IRAC 3.6 um array, and then dithering the cluster to several different positions to get additional centroids on the array (leg 2), and then moving the star to PCRS 2 (leg 3), and then back to PCRS1 (leg 4), where the entire maneuver is repeated.

REMARK 8.3 The approach of dithering a cluster of stars was originally suggested by Peter Eisenhardt as an alternative to the original baselined approach of using a “five-of-diamonds” pattern obtained with only a single star. Although the five-of-diamonds experiment design was validated in [2] and shown to meet calibration requirements, the cluster approach has the advantage of providing many centroids for calibration purposes. This gives better coverage of the entire array, and allows the plate scales and optical distortions to be learned better. The same cluster approach was used for calibrating all other IRAC frames (i.e., 069, 075, and 076).

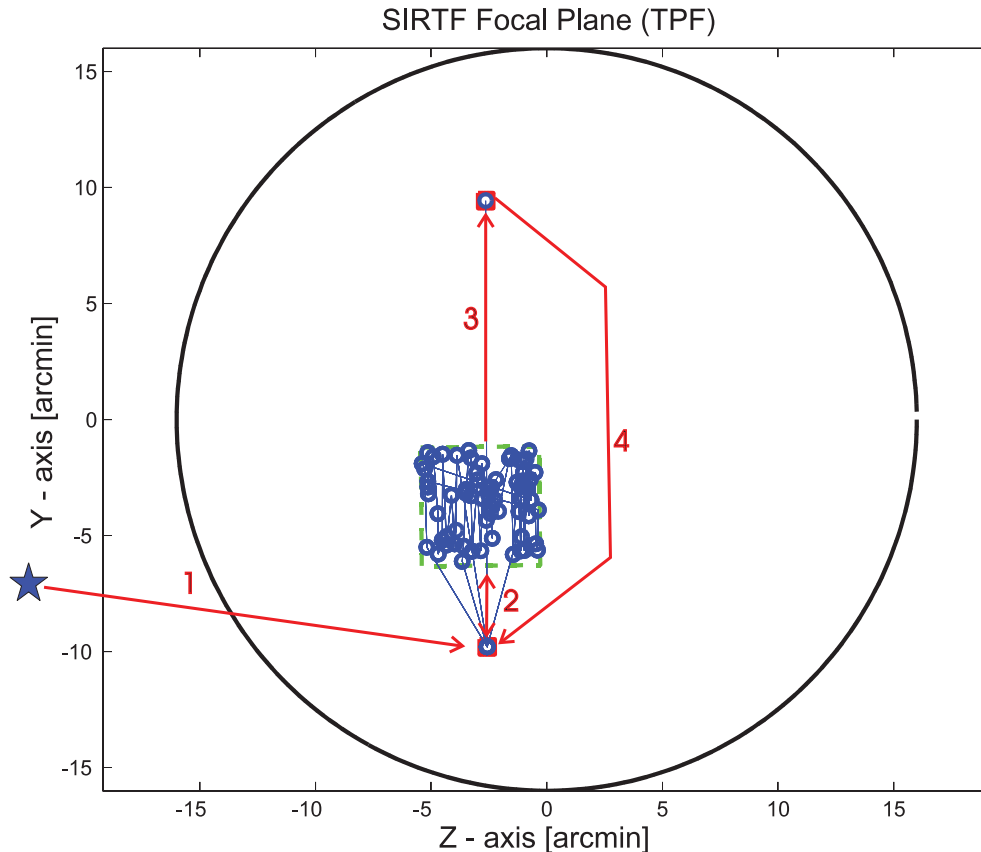


Figure 8.15: Experiment Design for IRAC 3.6 um Array [ID502068]

FOCAL PLANE SURVEY ANALYSIS: IOC Fine Survey.
INSTRUMENT NAME: IRAC_Center_of_3.6umArray NF: 68
PIX2RADW: 5.86625000E-006[rad/pixel] = 1.2100E+000[arcsec/pixel]
PIX2RADV: 5.86625000E-006[rad/pixel] = 1.2100E+000[arcsec/pixel]

| FRAME | DESCRIPTION | IPF ¹ | SF ² | TOTAL | REQ |
|--------|-------------------------------|------------------|-----------------|--------|------|
| 068(P) | IRAC_Center_of_3.6umArray | 0.0212 | 0.0855 | 0.0881 | 0.14 |
| 070(I) | IRAC_Center_of_3.6umSub-array | 0.0325 | 0.0855 | 0.0915 | N/A |

Table 8.7: IPF calibration error summary ([arcsec], 1-sigma, radial)

| RMS METRIC | A PRIORI ³ | A POSTERIORI ³ | ATT. CORRECTED ⁴ | UNITS |
|------------|-----------------------|---------------------------|-----------------------------|--------|
| Radial | 1.2942 | 0.3671 | 0.3099 | arcsec |
| W-Axis | 1.0238 | 0.2994 | 0.2408 | arcsec |
| V-Axis | 0.7917 | 0.2124 | 0.1951 | arcsec |
| Radial | 1.0696 | 0.3034 | 0.2561 | pixels |
| W-Axis | 0.8461 | 0.2474 | 0.1990 | pixels |
| V-Axis | 0.6543 | 0.1756 | 0.1613 | pixels |

Table 8.8: Science measurement prediction error summary (1-sigma)

| Con. Plate Scale | | | Γ Dependent | | | | Γ^2 Dependent | | | | Linear Plate Scale | | | | | | Mirror | |
|------------------|------------|------------|--------------------|----------|----------|----------|----------------------|----------|----------|----------|--------------------|-----------------|----------|----------|----------|----------|----------|---------|
| a_{00} | b_{00} | c_{00} | a_{10} | b_{10} | c_{10} | d_{10} | a_{20} | b_{20} | c_{20} | d_{20} | a_{01} | b_{01} | c_{01} | d_{01} | e_{01} | f_{01} | α | β |
| 1 | 2 | 3 | 4 | 5 | 6 | 7 | 8 | 9 | 10 | 11 | 12 | 13 | 14 | 15 | 16 | 17 | 18 | 19 |
| 1 | 1 | 1 | 0 | 0 | 0 | 0 | 0 | 0 | 0 | 0 | 1 | 1 | 1 | 1 | 1 | 1 | 0 | 0 |
| IPF (T) | | | Alignment R | | | | | | | | | Gyro Drift Bias | | | | | | |
| θ_1 | θ_2 | θ_3 | a_{rx} | a_{ry} | a_{rz} | b_{rx} | b_{ry} | b_{rz} | c_{rx} | c_{ry} | c_{rz} | b_{gx} | b_{gy} | b_{gz} | c_{gx} | c_{gy} | c_{gz} | |
| 20 | 21 | 22 | 23 | 24 | 25 | 26 | 27 | 28 | 29 | 30 | 31 | 32 | 33 | 34 | 35 | 36 | 37 | |
| 1 | 1 | 1 | 1 | 1 | 1 | 0 | 0 | 0 | 0 | 0 | 0 | 1 | 1 | 1 | 1 | 1 | 1 | |

Table 8.9: IPF filter execution mask vector assignment

¹IPF filter removes systematic pointing errors due to: thermomechanical alignment drift (Body to TPF), gyro bias and bias drift, centroiding error, attitude error, and optical distortion. IPF SIGMA presented here is “Scaled” by the Least Squares Scale factor. The Least Squares Scale Factor was: 0.777790. It is assumed that the gyro Angle Random Walk contribution is captured with the Least Squares scaling. The gyro ARW contribution can be approximately calculated as 0.1390 arcseconds, given that $ARW = 100 \mu deg/\sqrt{hr}$, with 1.073400e+003 second Maneuver time (max), and 4 independent Maneuvers.

²Gyro Scale Factor(GSF) assumes 95 ppm error over 0.250 degree maneuver.

³This can be interpreted as estimate of ”pixel to sky” pointing reconstruction error if no science data is used.

⁴This can be interpreted as estimate of achieved S/I centroiding error

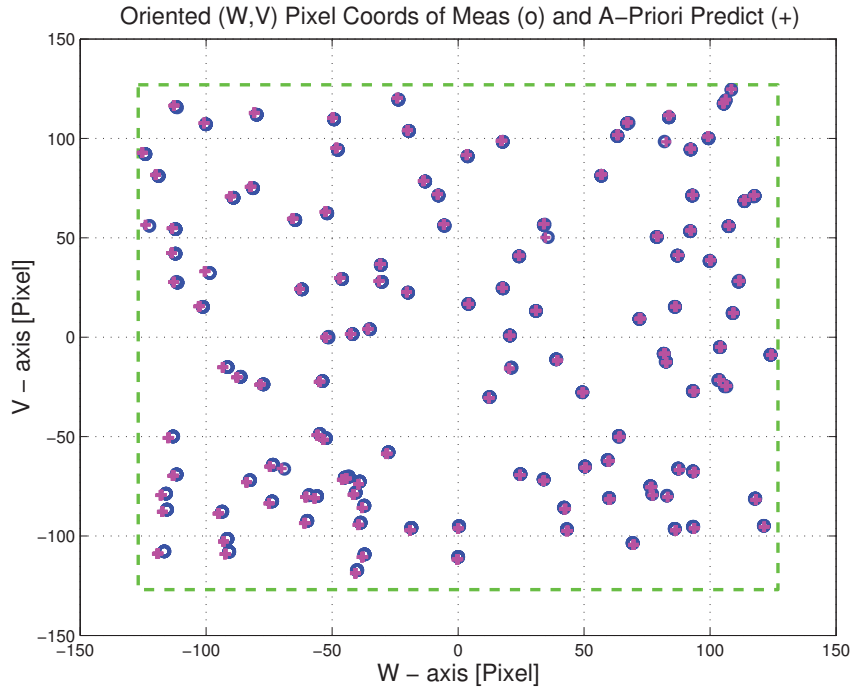


Figure 8.16: Oriented Pixel Coords of measurements and a-priori predicts [RUN502068]

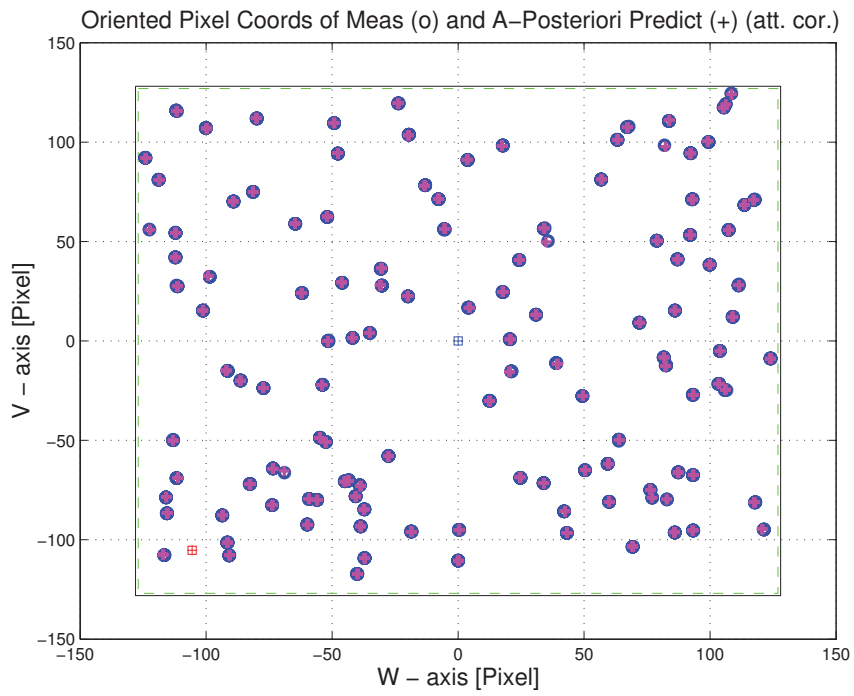


Figure 8.17: Oriented Pixel Coords of meas. and a-posteriori predicts (attitude corrected) [RUN502068]

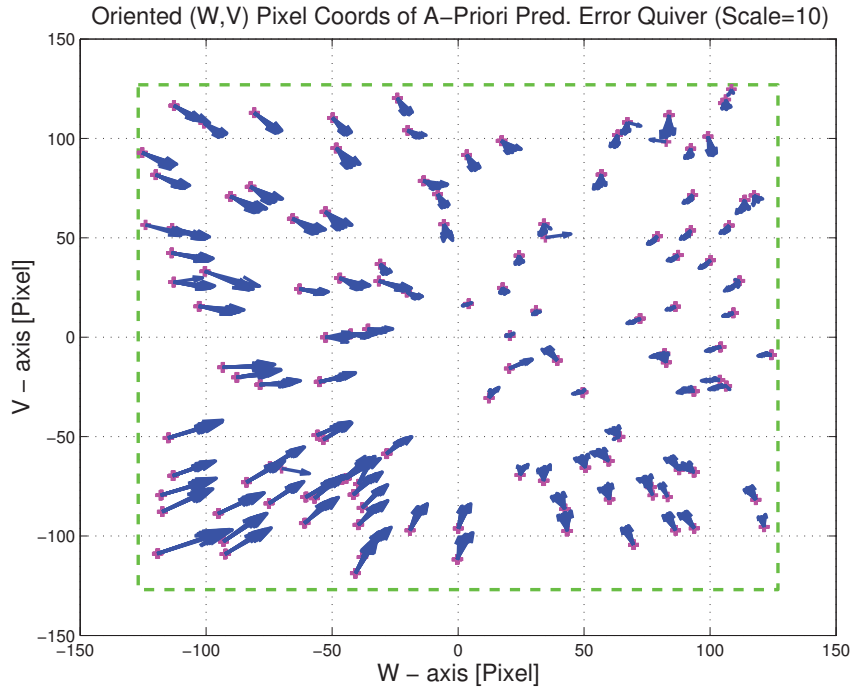


Figure 8.18: Oriented (W,V) Pixel Coords of A-Priori Prediction Error Quiver Plot [RUN502068]

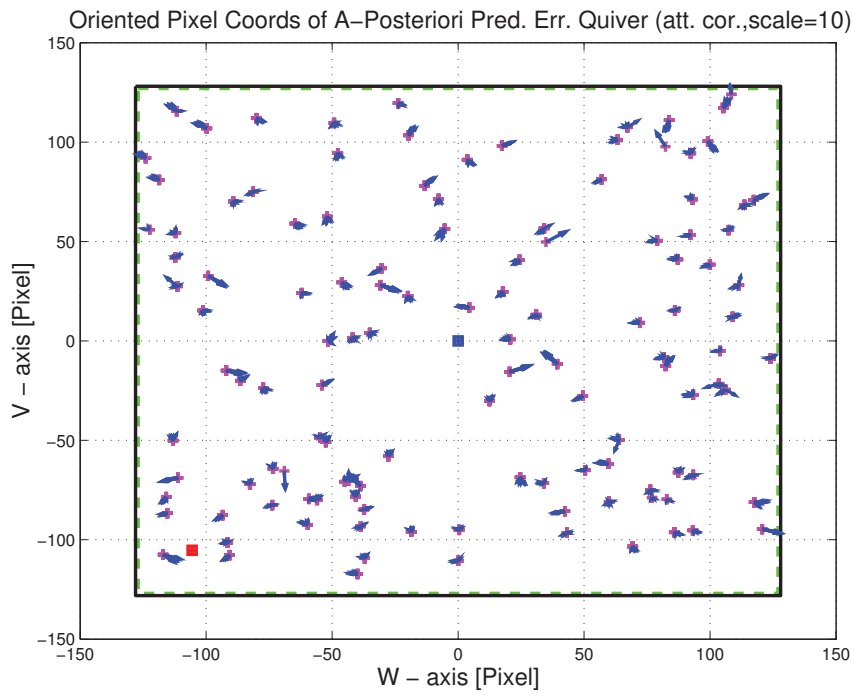


Figure 8.19: A-Posteriori Science Centroid Prediction Error Quiver (Att. Cor.) [RUN502068]

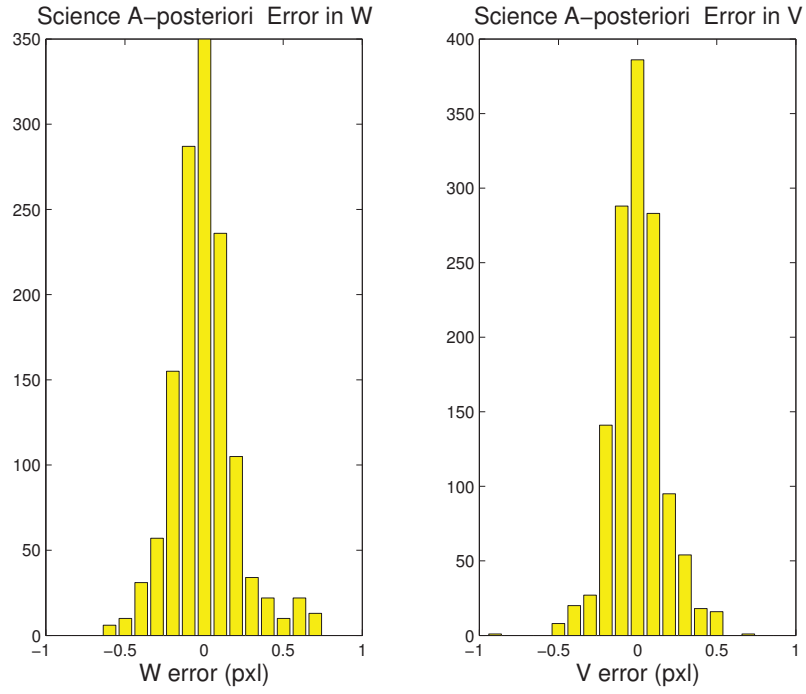


Figure 8.20: Histograms of science a-posteriori residuals (or innovations) [RUN502068]

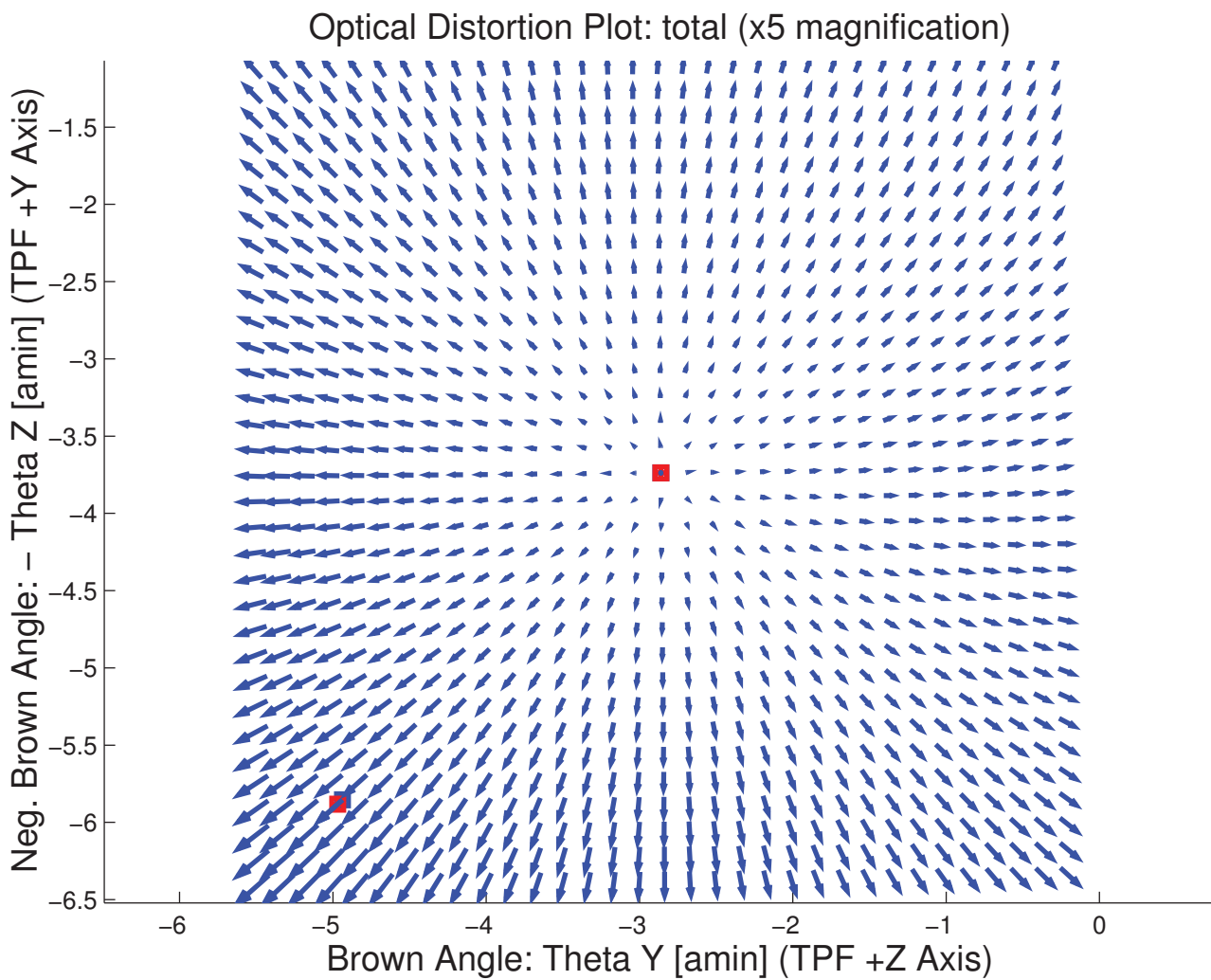


Figure 8.21: Optical Distortion Plot: total (x5 magnification) [RUN502068]

OUTPUT FILE NAME: IFmini502068.dat DATE: 19-Nov-2003 TIME: 12:12
 INSTRUMENT NAME: IRAC_Center_of_3.6umArray NF: 68
 IPF FILTER VERSION: IPF.V3.0.0B SW RELEASE DATE: November 3, 2003
 FRAME TABLE USED: BodyFrames_FTU_13Aa

----- IPF BROWN ANGLE SUMMARY -----

OFFSET NF Delta_CW Delta_CV
 0 68 +0.000 +0.000 pixels

OFFSET FRAME NAME: IRAC_Center_of_3.6umArray
 Brown Angle theta_Y(arcmin) theta_Z(arcmin) angle(deg)
 WAS(FTB) -2.865619 +3.739370 -0.539874
 IS (EST) -2.860490 +3.737451 -0.542312
 dT_EST +0.005129 -0.001919 -0.002438
 T_sSIGMA +0.000272 +0.000226 +0.003164
 dT_EST/T_sSIGMA +18.881001 -8.505326 -0.770604

OFFSET NF Delta_CW Delta_CV
 1 70 -104.000 -104.000 pixels

OFFSET FRAME NAME: IRAC_Center_of_3.6umSub-array
 Brown Angle theta_Y(arcmin) theta_Z(arcmin) angle(deg)
 WAS(FTB) -4.971810 +5.885570 -0.539874
 IS (EST) -4.968435 +5.881740 -0.542312
 dT_EST +0.003375 -0.003829 -0.002438
 T_sSIGMA +0.000404 +0.000360 +0.003164
 dT_EST/T_sSIGMA +8.350197 -10.631991 -0.770605

| VARNAME | MEAN | SIGMA | SCALED_SIGMA |
|------------|--------------------------|--------------------------|--------------------------|
| a00 | +8.6567481549441796E-003 | +9.1801811889912827E-005 | +7.1402506449035275E-005 |
| b00 | +8.8227569599375229E-003 | +9.7566630034760874E-005 | +7.5886322795259880E-005 |
| c00 | +3.4518023057434564E-004 | +6.7425663149458238E-005 | +5.2442988310873119E-005 |
| a01 | -4.4714770404084110E+000 | +2.5565147357977580E-001 | +1.9884309051411081E-001 |
| b01 | +2.0941117430397604E-001 | +2.8527265601429963E-001 | +2.2188214199106251E-001 |
| c01 | -5.0638595726863738E+000 | +2.1870419148259213E-001 | +1.7010587396132554E-001 |
| d01 | +1.1448074467261384E+000 | +2.5544051045268179E-001 | +1.9867900556052731E-001 |
| e01 | -4.0456797551742580E+000 | +2.8446090281247699E-001 | +2.2125076868769383E-001 |
| f01 | -3.0985497128440800E+000 | +2.1845806171393192E-001 | +1.6991443675510642E-001 |
| del_theta1 | -7.8793240920575769E-015 | +7.1004571365643790E-005 | +5.5226626364696468E-005 |
| del_theta2 | -1.2759122809468156E-017 | +1.0160004659029562E-007 | +7.9023472767458421E-008 |
| del_theta3 | -7.3152995465173397E-018 | +8.4388224512850358E-008 | +6.5636294327470879E-008 |

LSQF RESIDUAL SIGMA SCALE = +7.7778972962603332E-001

Summary of Results (IRAC 3.6 μm Array)

The delivered data set contained 1473 IRAC science centroids and 148 PCRS centroids, of which 135 science centroids were removed based on a 3.75 sigma criteria (approximately 3/4 pixel). A total of 21 parameters were estimated, including the constant and linear plate scales. Recommendations were made for updating frame 068 with adjustments of about 0.3 and 0.06 arcseconds in Y and Z. The frame calibration is accurate to 0.09 arcsecond which satisfies its Fine Survey requirement of 0.14 arcsecond.

8.4 Example 4: MIPS 24 um Array (frame 095)

The experiment design for the MIPS 24 um array is shown in Figure 8.15. The experiment design calls for a 7 by 3 grid of observations, where each row of 3 uses a separate sandwich maneuver. At each point in a row the spacecraft attitude is fixed, and there are six scan mirror offsets which move the source 3 positions up and 3 positions down in approximately 25 arcsecond increments (some of which fall off the array and are not recorded).

REMARK 8.4 Except for changes in grid size and scan mirror offsets, a similar experiment design is used for the MIPS 70 um wide and narrow arrays (frames 107, 118). However, an important difference is that two separate sources must be used: a visible source for the PCRS centroids and a separate IR source for the science centroids.

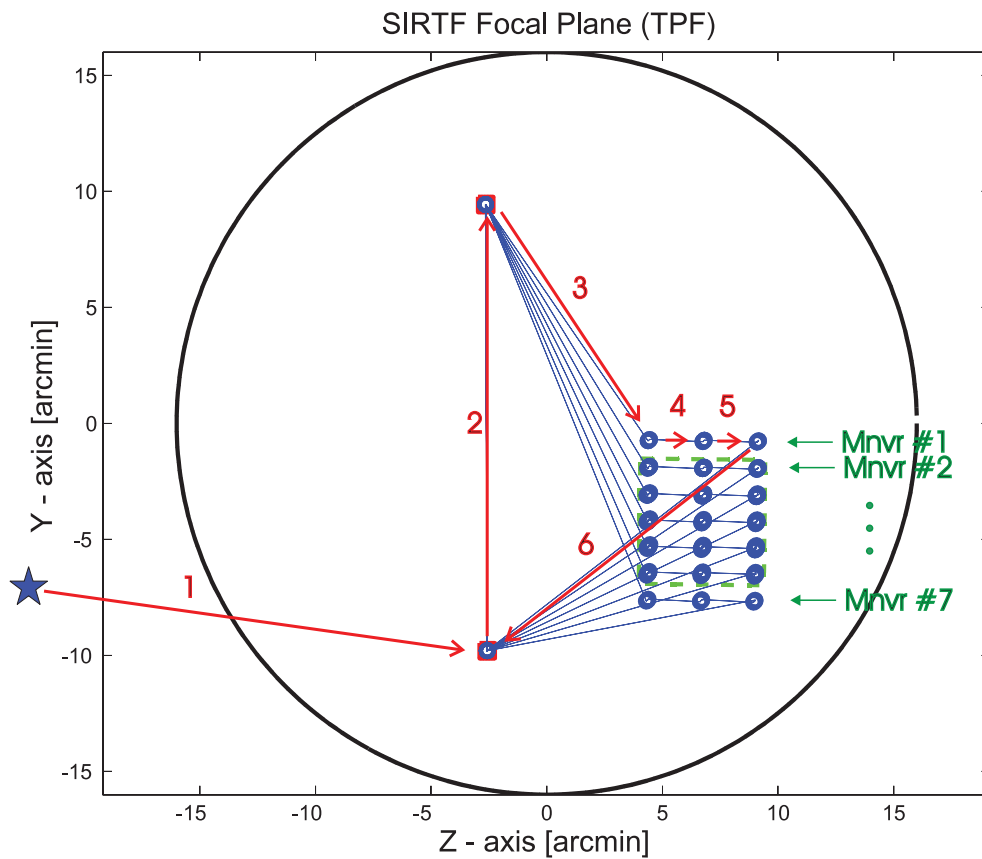


Figure 8.22: Experiment Design for MIPS 24 um Array [ID602095]

FOCAL PLANE SURVEY ANALYSIS: IOC Fine Survey.

INSTRUMENT NAME: MIPS_24um_center NF: 95

PIX2RADW: 1.20874169E-005 [rad/pixel] = 2.4932E+000 [arcsec/pixel]

PIX2RADV: 1.25959084E-005 [rad/pixel] = 2.5981E+000 [arcsec/pixel]

| FRAME | DESCRIPTION | IPF ¹ | SF ² | TOTAL | REQ |
|--------|----------------------|------------------|-----------------|--------|------|
| 095(P) | MIPS_24um_center | 0.0224 | 0.0855 | 0.0884 | 0.14 |
| 096(I) | MIPS_24um_plusY_edge | 0.0328 | 0.0855 | 0.0916 | N/A |
| 099(I) | MIPS_24um_small_FOV1 | 0.0214 | 0.0855 | 0.0881 | N/A |
| 100(I) | MIPS_24um_small_FOV2 | 0.0214 | 0.0855 | 0.0881 | N/A |
| 103(I) | MIPS_24um_large_FOV1 | 0.0224 | 0.0855 | 0.0884 | N/A |
| 104(I) | MIPS_24um_large_FOV2 | 0.0224 | 0.0855 | 0.0884 | N/A |

Table 8.10: IPF calibration error summary ([arcsec], 1-sigma, radial)

| RMS METRIC | A PRIORI ³ | A POSTERIORI ³ | ATT. CORRECTED ⁴ | UNITS |
|------------|-----------------------|---------------------------|-----------------------------|--------|
| Radial | 2.4059 | 0.1785 | 0.1634 | arcsec |
| W-Axis | 1.4388 | 0.1059 | 0.0892 | arcsec |
| V-Axis | 1.9283 | 0.1437 | 0.1369 | arcsec |
| Radial | 0.9401 | 0.0697 | 0.0637 | pixels |
| W-Axis | 0.5771 | 0.0425 | 0.0358 | pixels |
| V-Axis | 0.7422 | 0.0553 | 0.0527 | pixels |

Table 8.11: Science measurement prediction error summary (1-sigma)

| Con. Plate Scale | | | Γ Dependent | | | | Γ ² Dependent | | | | Linear Plate Scale | | | | | | Mirror | |
|------------------|-----------------|-----------------|-----------------|-----------------|-----------------|-----------------|--------------------------|-----------------|-----------------|-----------------|--------------------|-----------------|-----------------|-----------------|-----------------|-----------------|-----------------|----|
| a ₀₀ | b ₀₀ | c ₀₀ | a ₁₀ | b ₁₀ | c ₁₀ | d ₁₀ | a ₂₀ | b ₂₀ | c ₂₀ | d ₂₀ | a ₀₁ | b ₀₁ | c ₀₁ | d ₀₁ | e ₀₁ | f ₀₁ | α | β |
| 1 | 2 | 3 | 4 | 5 | 6 | 7 | 8 | 9 | 10 | 11 | 12 | 13 | 14 | 15 | 16 | 17 | 18 | 19 |
| 1 | 1 | 1 | 1 | 1 | 1 | 1 | 0 | 0 | 0 | 0 | 1 | 1 | 1 | 1 | 1 | 1 | 1 | 1 |
| IPF (T) | | | Alignment R | | | | | | | | | Gyro Drift Bias | | | | | | |
| θ ₁ | θ ₂ | θ ₃ | a _{rx} | a _{ry} | a _{rz} | b _{rx} | b _{ry} | b _{rz} | c _{rx} | c _{ry} | c _{rz} | b _{gx} | b _{gy} | b _{gz} | c _{gx} | c _{gy} | c _{gz} | |
| 20 | 21 | 22 | 23 | 24 | 25 | 26 | 27 | 28 | 29 | 30 | 31 | 32 | 33 | 34 | 35 | 36 | 37 | |
| 1 | 1 | 1 | 1 | 1 | 1 | 1 | 1 | 1 | 1 | 1 | 1 | 1 | 1 | 1 | 1 | 1 | 1 | 1 |

Table 8.12: IPF filter execution mask vector assignment

¹IPF filter removes systematic pointing errors due to: thermomechanical alignment drift (Body to TPF), gyro bias and bias drift, centroiding error, attitude error, and optical distortion. IPF SIGMA presented here is “Scaled” by the Least Squares Scale factor. The Least Squares Scale Factor was: 0.945293. It is assumed that the gyro Angle Random Walk contribution is captured with the Least Squares scaling. The gyro ARW contribution can be approximately calculated as 0.0517 arcseconds, given that $ARW = 100 \mu deg / \sqrt{hr}$, with 5.567000e+002 second Maneuver time (max), and 15 independent Maneuvers.

²Gyro Scale Factor(GSF) assumes 95 ppm error over 0.250 degree maneuver.

³This can be interpreted as estimate of ”pixel to sky” pointing reconstruction error if no science data is used.

⁴This can be interpreted as estimate of achieved S/I centroiding error

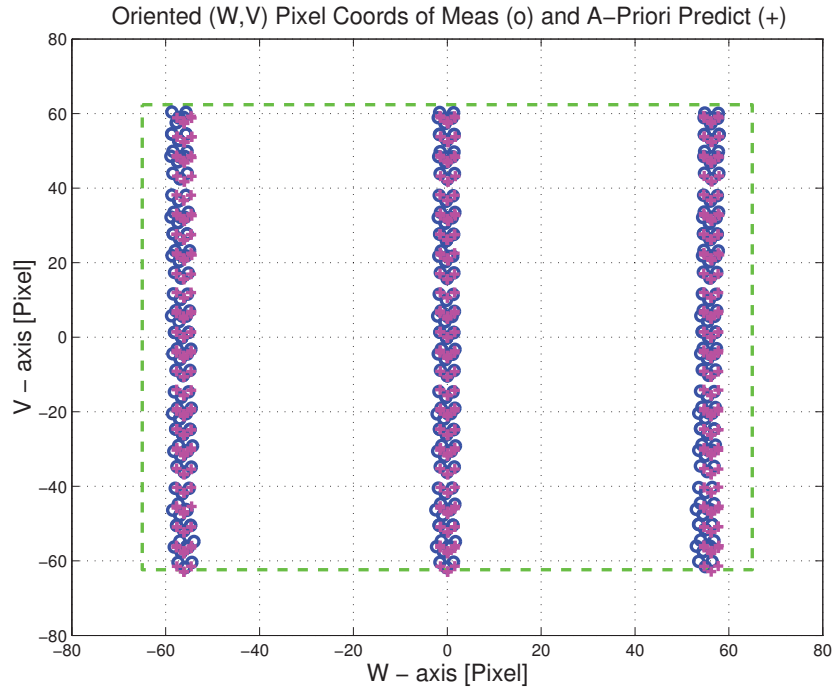


Figure 8.23: Oriented Pixel Coords of measurements and a-priori predicts [RUN602095]

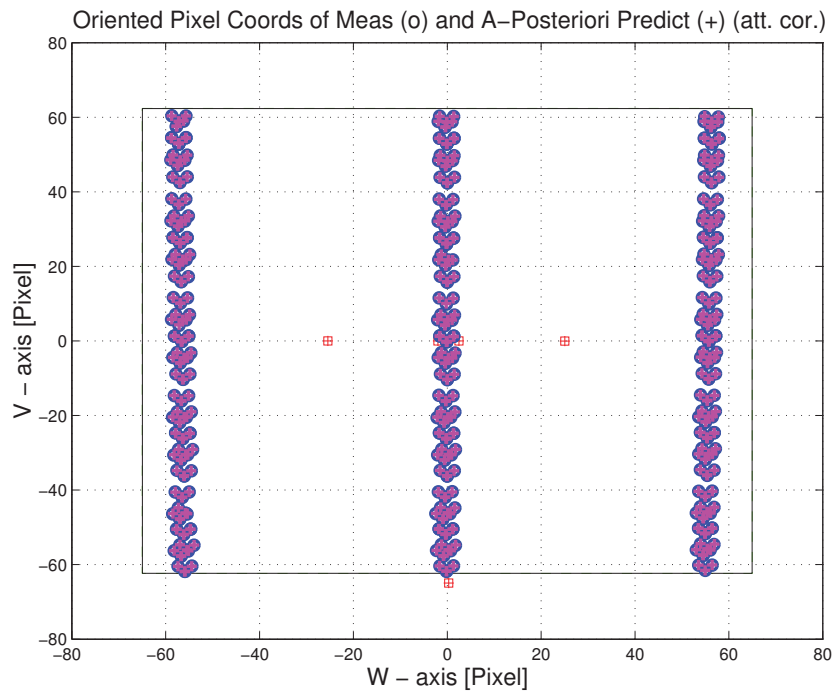


Figure 8.24: Oriented Pixel Coords of meas. and a-posteriori predicts (attitude corrected) [RUN602095]

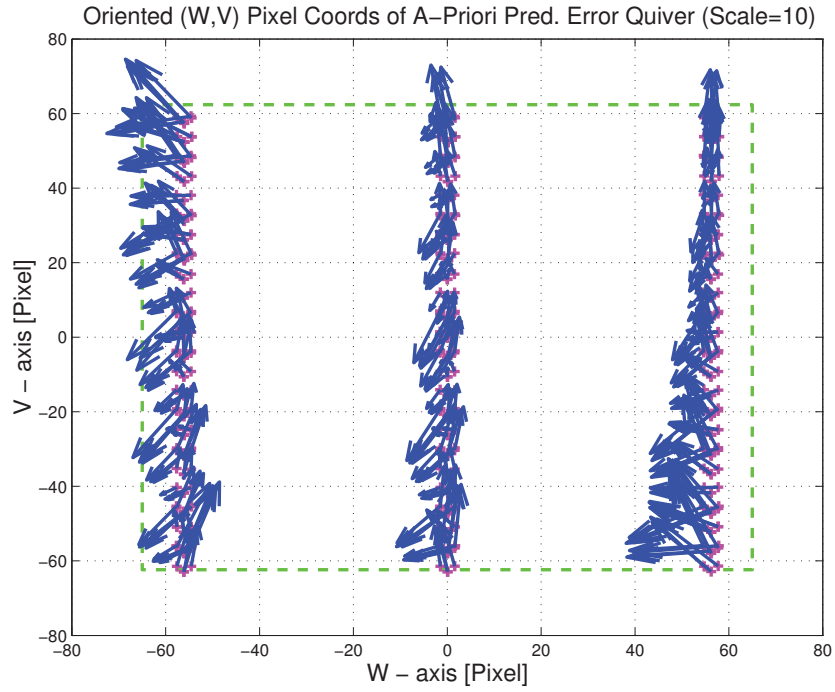


Figure 8.25: Oriented (W,V) Pixel Coords of A-Priori Prediction Error Quiver Plot [RUN602095]

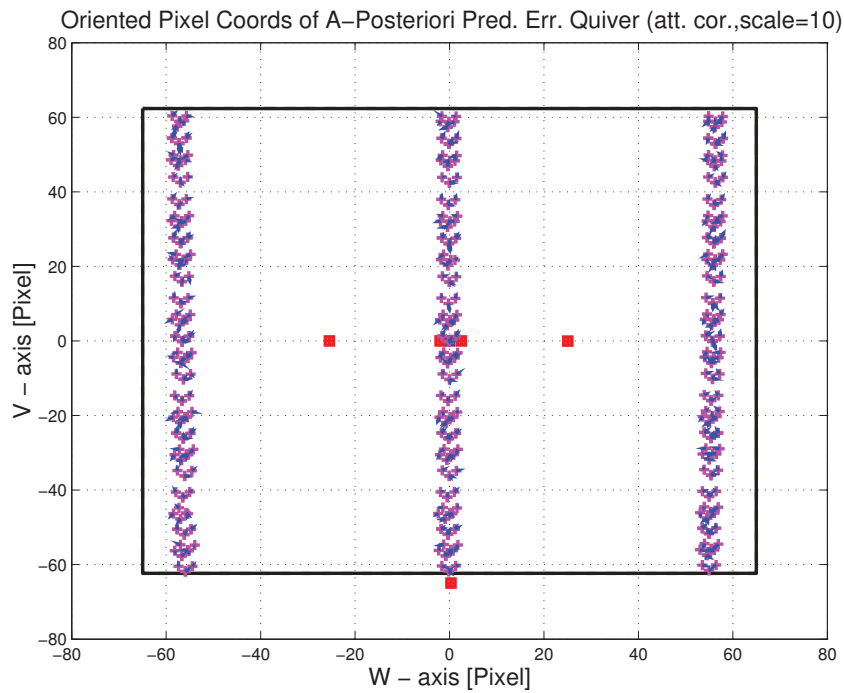


Figure 8.26: A-Posteriori Science Centroid Prediction Error Quiver (Att. Cor.) [RUN602095]

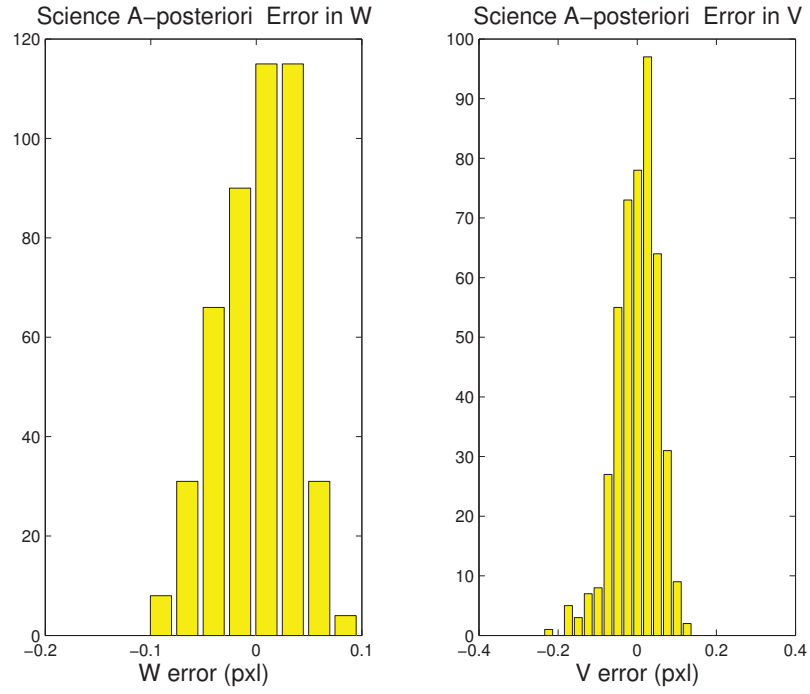


Figure 8.27: Histograms of science a-posteriori residuals (or innovations) [RUN602095]

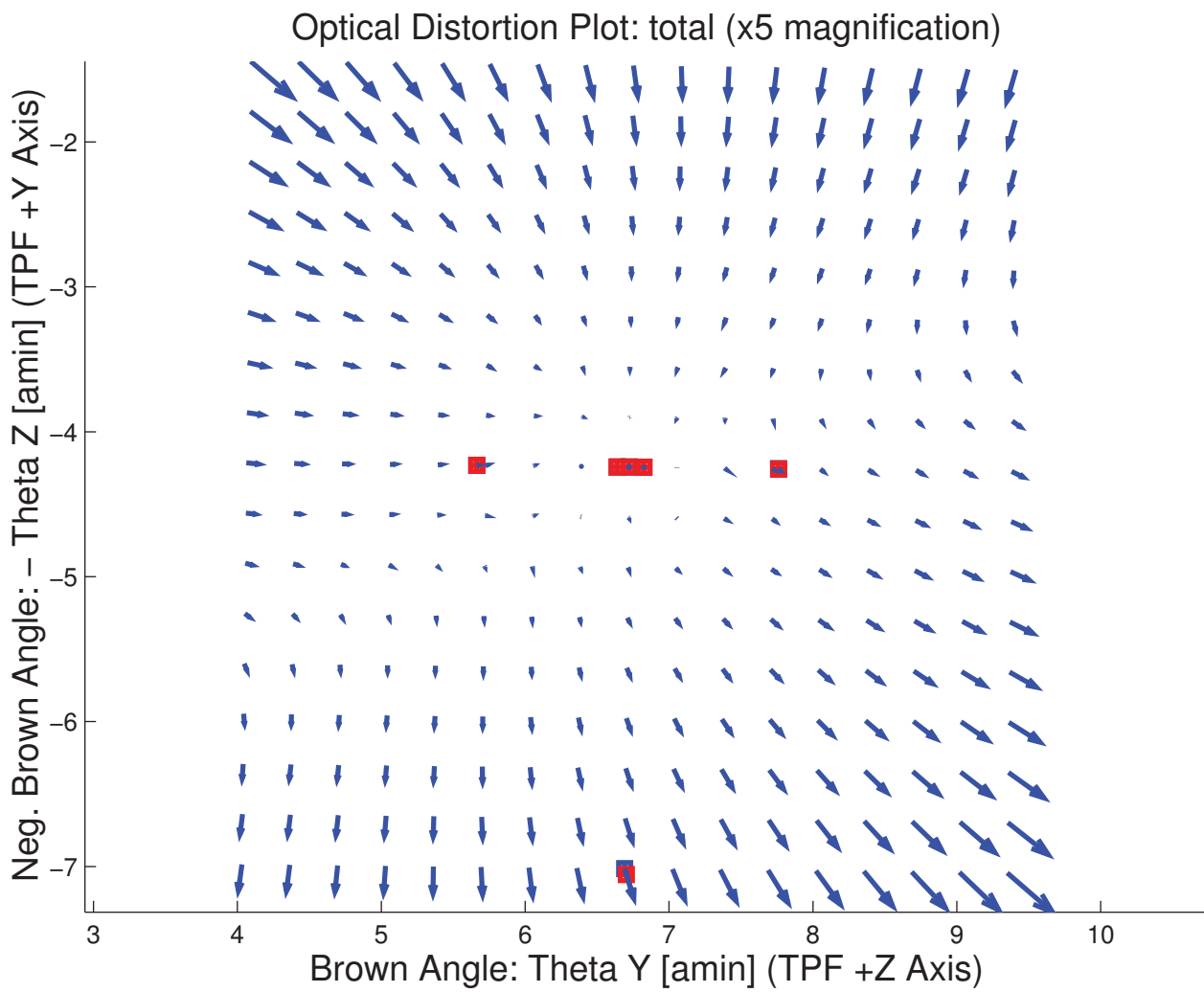


Figure 8.28: Optical Distortion Plot: total (x5 magnification) [RUN602095]

24 μm : Distorted-Undistorted pixels($u-p',v-q'$)
Mirror Angle= 0.0000

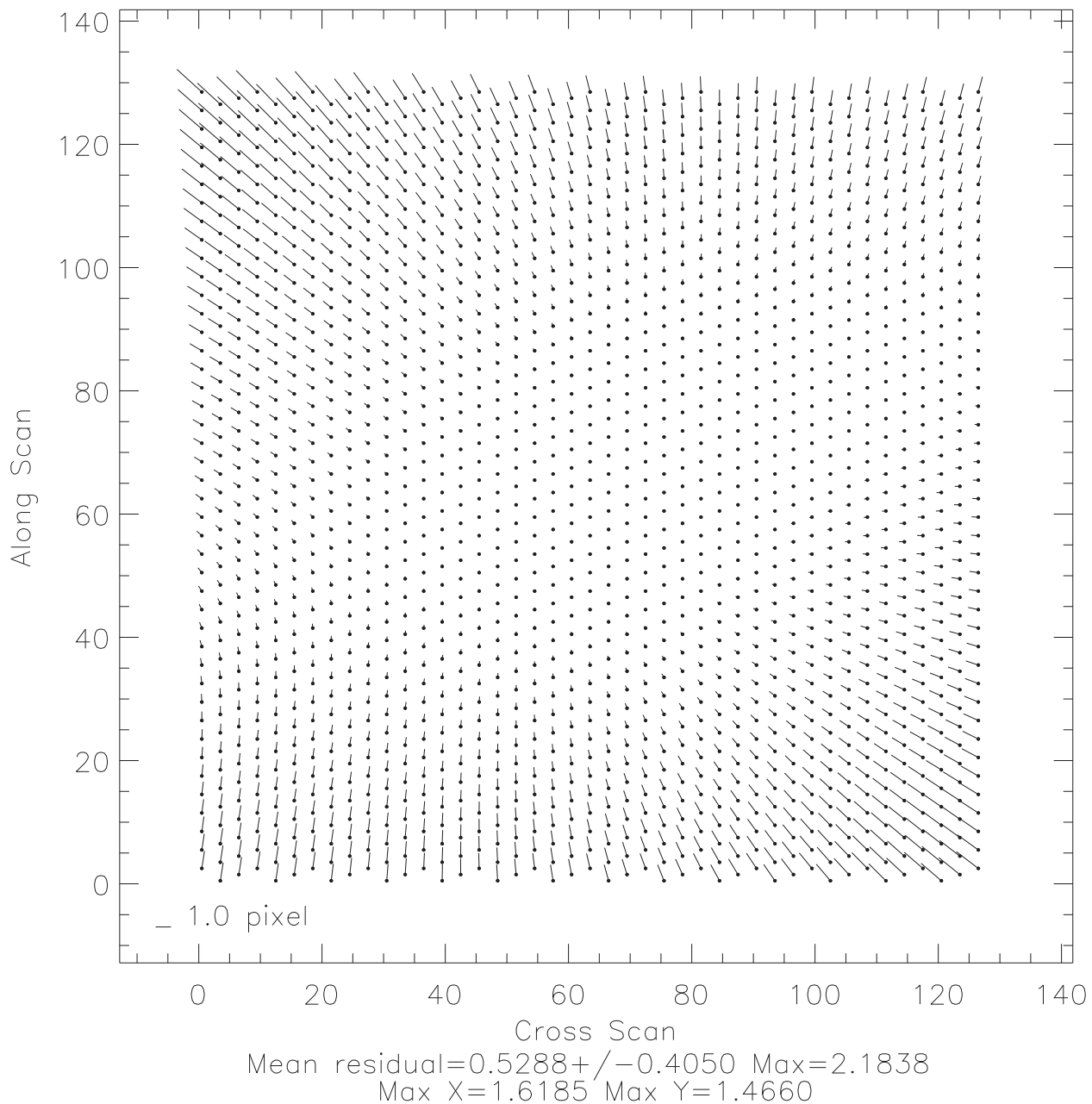


Figure 8.29: Optical Distortion Plot Based on Code V (courtesy of Jane Morrison, Univ. of Arizona)

OUTPUT FILE NAME: IFmini602095.dat DATE: 02-Dec-2003 TIME: 19:18
 INSTRUMENT NAME: MIPS_24um_center NF: 95
 IPF FILTER VERSION: IPF.V3.0.0B SW RELEASE DATE: November 3, 2003
 FRAME TABLE USED: BodyFrames_FTU_14a

----- IPF BROWN ANGLE SUMMARY -----

OFFSET NF Delta_CW Delta_CV
 0 95 +0.000 +0.000 pixels

OFFSET FRAME NAME: MIPS_24um_center

| Brown Angle | theta_Y(arcmin) | theta_Z(arcmin) | angle(deg) |
|-----------------|-----------------|-----------------|------------|
| WAS(FTB) | +6.716105 | +4.246060 | +0.637930 |
| IS (EST) | +6.721826 | +4.243820 | +0.628212 |
| dT_EST | +0.005721 | -0.002240 | -0.009717 |
| T_sSIGMA | +0.000268 | +0.000261 | +0.002879 |
| dT_EST/T_sSIGMA | +21.373226 | -8.591985 | -3.375556 |

OFFSET NF Delta_CW Delta_CV
 1 96 +0.000 -64.000 pixels

OFFSET FRAME NAME: MIPS_24um_plusY_edge

| Brown Angle | theta_Y(arcmin) | theta_Z(arcmin) | angle(deg) |
|-----------------|-----------------|-----------------|------------|
| WAS(FTB) | +6.695190 | +7.060913 | +0.637930 |
| IS (EST) | +6.703859 | +7.055562 | +0.628212 |
| dT_EST | +0.008670 | -0.005350 | -0.009717 |
| T_sSIGMA | +0.000390 | +0.000383 | +0.002879 |
| dT_EST/T_sSIGMA | +22.245672 | -13.953343 | -3.375558 |

OFFSET NF Delta_CW Delta_CV
 2 99 +25.000 +0.000 pixels

OFFSET FRAME NAME: MIPS_24um_small_FOV1

| Brown Angle | theta_Y(arcmin) | theta_Z(arcmin) | angle(deg) |
|-----------------|-----------------|-----------------|------------|
| WAS(FTB) | +7.756798 | +4.259313 | +0.637930 |
| IS (EST) | +7.762937 | +4.257169 | +0.628212 |
| dT_EST | +0.006139 | -0.002144 | -0.009717 |
| T_sSIGMA | +0.000255 | +0.000251 | +0.002879 |
| dT_EST/T_sSIGMA | +24.118740 | -8.550594 | -3.375557 |

OFFSET NF Delta_CW Delta_CV
 3 100 -25.500 +0.000 pixels

OFFSET FRAME NAME: MIPS_24um_small_FOV2

| Brown Angle | theta_Y(arcmin) | theta_Z(arcmin) | angle(deg) |
|-----------------|-----------------|-----------------|------------|
| WAS(FTB) | +5.659609 | +4.234140 | +0.637930 |
| IS (EST) | +5.665074 | +4.231696 | +0.628212 |
| dT_EST | +0.005465 | -0.002444 | -0.009717 |
| T_sSIGMA | +0.000258 | +0.000246 | +0.002879 |
| dT_EST/T_sSIGMA | +21.179236 | -9.944902 | -3.375556 |

OFFSET NF Delta_CW Delta_CV
 4 103 +2.500 +0.000 pixels

OFFSET FRAME NAME: MIPS_24um_large_FOV1

| Brown Angle | theta_Y(arcmin) | theta_Z(arcmin) | angle(deg) |
|-----------------|-----------------|-----------------|------------|
| WAS(FTB) | +6.819955 | +4.247316 | +0.637930 |
| IS (EST) | +6.825711 | +4.245090 | +0.628212 |
| dT_EST | +0.005755 | -0.002225 | -0.009717 |
| T_sSIGMA | +0.000267 | +0.000261 | +0.002879 |
| dT_EST/T_sSIGMA | +21.528771 | -8.536610 | -3.375556 |

OFFSET NF Delta_CW Delta_CV
 5 104 -2.000 +0.000 pixels

OFFSET FRAME NAME: MIPS_24um_large_FOV2

| Brown Angle | theta_Y(arcmin) | theta_Z(arcmin) | angle(deg) |
|-----------------|-----------------|-----------------|------------|
| WAS(FTB) | +6.633060 | +4.245067 | +0.637930 |
| IS (EST) | +6.638755 | +4.242815 | +0.628212 |
| dT_EST | +0.005695 | -0.002252 | -0.009717 |
| T_sSIGMA | +0.000268 | +0.000260 | +0.002879 |
| dT_EST/T_sSIGMA | +21.269327 | -8.646350 | -3.375556 |

```

-----
VARNAME          MEAN          SIGMA          SCALED_SIGMA
a00              -1.5877962194911865E-004 +5.6074167712169990E-005 +5.3006527472556519E-005
b00              -2.1263046444906114E-004 +7.8358920515259108E-005 +7.4072151981499629E-005
c00              -1.1905880467921641E-003 +4.9209568729192622E-005 +4.6517468973337786E-005
a10              +4.5903737071241908E+000 +2.0395174313832184E-001 +1.9279418878277785E-001
b10              +4.4617004892088712E+000 +2.8099692687996636E-001 +2.6562447437154285E-001
c10              +1.1012184796910059E+001 +2.8359172768657320E-001 +2.6807732183861932E-001
d10              -1.1496388061253342E+000 +2.1147192429963435E-001 +1.9990296463428639E-001
a01              +8.0348888827276834E+000 +1.3175140408091843E-001 +1.2454370175961439E-001
b01              +4.2815218751340707E+000 +1.7711292169398987E-001 +1.6742363431423132E-001
c01              -1.6160111270247537E+001 +1.1506208563998141E-001 +1.0876740310853740E-001
d01              -2.2181116354195640E+000 +1.3724961133427385E-001 +1.2974111949608025E-001
e01              -1.8377235746694279E+001 +1.7688354552245991E-001 +1.6720680658706538E-001
f01              +2.5538655928081306E+000 +1.1794872495709381E-001 +1.1149612352488469E-001
del_alpha       +7.1143720255240073E-015 +1.2847549721851603E-004 +1.2144700939333995E-004
beta            +9.6245187272690003E-001 +1.7581747981171902E-004 +1.6619906195723872E-004
del_theta1     +9.6141966458331007E-016 +5.3151343703491090E-005 +5.0243601914593024E-005
del_theta2     -1.5603988014759517E-017 +8.2370910167444326E-008 +7.7864658377845363E-008
del_theta3     +3.5243250916405872E-017 +8.0211236041361491E-008 +7.5823133187786526E-008
-----
LSQF RESIDUAL SIGMA SCALE =          +9.4529316502101757E-001
-----

```

```

-----
          a_mirror(1)          a_mirror(2)          a_mirror(3)
a_mirror_ipf  +0.0000000000000000E+000 +1.2565262419800743E-002 +9.9992105397392328E-001
a_mirror_tpf -1.9533180461764328E-003 +1.6036329010015136E-003 +9.999680644996536E-001
beta          beta_0          beta          beta_total
          +2.8047410000000001E-006 +9.6245187272690003E-001 +2.6994282279639184E-006
-----

```

Summary of Results (MIPS 24 um Array)

There were 15 sandwich maneuvers with 460 science centroids (7 centroids were removed from the original 467 centroids, at the 3-sigma level) and 126 PCRS measurements. The IPF filter estimated 33 parameters consisting of: 3 constant and 6 linear plate scales, 4 Gamma Dependent parameters, 2 mirror parameters, 3 IPF alignment angles, 3 STA-to-PCRS alignment angles, 6 STA-to-PCRS thermomechanical drift parameters, and 3 gyro bias and 3 gyro bias-drift parameters.

Results indicate constant plate scale errors on the order of 1 part in a thousand, and significant high order optical distortions. The scan mirror has approximately a 4 percent scale factor error and a .7 degree misalignment with respect to the orientation of the 24 um array.

The optical distortions estimated by the IPF Kalman filter (at zero scan mirror offset) are plotted in the quiver plot Figure 8.28. As a comparison, the optical distortions obtained using a purely physical modeling approach (i.e., a Code V program) are shown in Figure 8.29, courtesy of Jane Morrison at the University of Arizona. It can be seen that the quiver directions and sizes are in excellent agreement. This provides an independent validation of the optical modeling approach which is based on purely on physical principles, and the IPF calibration approach which is based purely on empirical measurements.

The accuracy of this focal plane calibration is 0.09 arcseconds meeting the requirement of 0.14 arcseconds. However, when the Brown angles recommendations in this run were compared to an earlier Fine Survey run (ID502095) they were found to disagree by 1" in the V direction. This indicates a non-repeatability in the scan mirror Gamma angle on the order of 1". Subsequent experience by the MIPS team working with this non-repeatability has indicated that it tends to be a long-term effect in the sense that variations are predominantly seen from campaign to campaign rather than within any single campaign.

To moderate the effect of non-repeatability, the MIPS team recently redefined the MIPS 24 um Prime and Inferred frames to be an average of results from two separate IPF calibration (this run 602095 and the previous run 502095). This derived frame should be accurate to approximately 0.5 arcseconds, based on these two calibration data sets, and subsequent experience obtained by the MIPS team in dealing with the scan mirror non-repeatability.

9 INDIVIDUAL RUN SUMMARIES

Execution summaries are provided in this section for all individual Prime frames. Each execution summary contains two tables. The first table is a calibration error summary. The second table is a prediction error summary. This latter table is not available for MIPS multi-runs. These two tables are discussed below.

IPF Calibration Error Table

The calibration error summary table shows the specific Prime frame and all of its Inferred frames. The table shows the total error from the earlier Table 6.1 in the column denoted as “TOTAL” and how it is broken down into the root-sum-square (RSS) combination of two separate errors: IPF and SF. Here, the IPF error corresponds to errors which are directly modeled by the IPF filter covariances (systematic pointing errors, alignments, and optical distortions); and SF is due to the gyro scale factor error. The SF error is not directly modeled by the IPF filter and must be added in an RSS fashion. While the gyro has an additional error due to Angle Random Walk (ARW), the ARW error is observable in the least-squares residual, and is already captured in the IPF error column.

IPF Science Measurement Prediction Error Table

This table shows a summary of prediction errors incurred by the IPF Kalman filter. The errors are shown a-priori (the prediction errors **before** calibration) and a-posteriori (the prediction errors **after** calibration) to demonstrate the improvement due to calibration. The a-posteriori error can be roughly interpreted as the pixel-to-sky pointing reconstruction accuracy that was achieved by the IPF filter after calibration. This includes star tracker errors and tracker-to-telescope alignment errors, so it is expected to be between 1 and 5 arcseconds based on current understanding of the pointing system. The Attitude Corrected error is useful because it can be interpreted as an estimate of the achieved centroiding accuracy associated with science centroids taken on the specified array. Centroiding errors are typically between .05 and .2 pixels, depending on the signal-to-noise of the observation. IRS slits have “artificial” pixels scaled to 1 arcsecond, and do not hold to this convention. Pickup arrays use units of centi-pixels, so one would expect centroiding errors between 5 and 20 centi-pixel units.

9.1 IPF EXECUTION SUMMARY OF ID701018

FOCAL PLANE SURVEY ANALYSIS: IOC Fine Survey.

INSTRUMENT NAME: IRS_Red_PeakUp_FOV_Center NF: 18

PIX2RADW: 8.72660000E-008[rad/pixel] = 1.8000E-002[arcsec/pixel]

PIX2RADV: 8.72660000E-008[rad/pixel] = 1.8000E-002[arcsec/pixel]

| FRAME | DESCRIPTION | IPF ¹ | SF ² | TOTAL | REQ |
|--------|---------------------------|------------------|-----------------|--------|------|
| 018(P) | IRS_Red_PeakUp_FOV_Center | 0.0279 | 0.0855 | 0.0899 | 0.25 |

Table 9.1: IPF calibration error summary ([arcsec], 1-sigma, radial)

| RMS METRIC | A PRIORI ³ | A POSTERIORI ³ | ATT. CORRECTED ⁴ | UNITS |
|------------|-----------------------|---------------------------|-----------------------------|--------|
| Radial | 1.3635 | 0.1075 | 0.0509 | arcsec |
| W-Axis | 1.3367 | 0.0645 | 0.0390 | arcsec |
| V-Axis | 0.2690 | 0.0859 | 0.0327 | arcsec |
| Radial | 75.7489 | 5.9702 | 2.8271 | pixels |
| W-Axis | 74.2600 | 3.5845 | 2.1658 | pixels |
| V-Axis | 14.9450 | 4.7743 | 1.8171 | pixels |

Table 9.2: Science measurement prediction error summary (1-sigma)

¹IPF filter removes systematic pointing errors due to: thermomechanical alignment drift (Body to TPF), gyro bias and bias drift, centroiding error, attitude error, and optical distortion. IPF SIGMA presented here is "Scaled" by the Least Squares Scale factor. The Least Squares Scale Factor was: 0.541872. It is assumed that the gyro Angle Random Walk contribution is captured with the Least Squares scaling. The gyro ARW contribution can be approximately calculated as 0.0788 arcseconds, given that $ARW = 100 \mu deg/\sqrt{hr}$, with $6.043555e+002$ second Maneuver time (max), and 7 independent Maneuvers.

²Gyro Scale Factor(GSF) assumes 95 ppm error over 0.250 degree maneuver.

³This can be interpreted as estimate of "pixel to sky" pointing reconstruction error if no science data is used.

⁴This can be interpreted as estimate of achieved S/I centroiding error

9.2 IPF EXECUTION SUMMARY OF ID701019

FOCAL PLANE SURVEY ANALYSIS: IOC Fine Survey.

INSTRUMENT NAME: IRS_Red_PeakUp_FOV_Sweet_Spot NF: 19

PIX2RADW: 8.72660000E-08[rad/pixel] = 1.8000E-02[arcsec/pixel]

PIX2RADV: 8.72660000E-08[rad/pixel] = 1.8000E-02[arcsec/pixel]

| FRAME | DESCRIPTION | IPF ¹ | SF ² | TOTAL | REQ |
|--------|-------------------------------|------------------|-----------------|--------|------|
| 019(P) | IRS_Red_PeakUp_FOV_Sweet_Spot | 0.0138 | 0.0855 | 0.0866 | 0.14 |

Table 9.3: IPF calibration error summary ([arcsec], 1-sigma, radial)

| RMS METRIC | A PRIORI ³ | A POSTERIORI ³ | ATT. CORRECTED ⁴ | UNITS |
|------------|-----------------------|---------------------------|-----------------------------|--------|
| Radial | 1.2220 | 0.1035 | 0.0662 | arcsec |
| W-Axis | 1.2153 | 0.0773 | 0.0538 | arcsec |
| V-Axis | 0.1276 | 0.0689 | 0.0385 | arcsec |
| Radial | 67.8890 | 5.7517 | 3.6757 | pixels |
| W-Axis | 67.5178 | 4.2937 | 2.9886 | pixels |
| V-Axis | 7.0904 | 3.8271 | 2.1397 | pixels |

Table 9.4: Science measurement prediction error summary (1-sigma)

¹IPF filter removes systematic pointing errors due to: thermomechanical alignment drift (Body to TPF), gyro bias and bias drift, centroiding error, attitude error, and optical distortion. IPF SIGMA presented here is “Scaled” by the Least Squares Scale factor. The Least Squares Scale Factor was: 0.727871. It is assumed that the gyro Angle Random Walk contribution is captured with the Least Squares scaling. The gyro ARW contribution can be approximately calculated as 0.0453 arcseconds, given that $ARW = 100 \mu deg/\sqrt{hr}$, with 5.980000e+02 second Maneuver time (max), and 21 independent Maneuvers.

²Gyro Scale Factor(GSF) assumes 95 ppm error over 0.250 degree maneuver.

³This can be interpreted as estimate of ”pixel to sky” pointing reconstruction error if no science data is used.

⁴This can be interpreted as estimate of achieved S/I centroiding error

9.3 IPF EXECUTION SUMMARY OF ID701022

FOCAL PLANE SURVEY ANALYSIS: IOC Fine Survey.

INSTRUMENT NAME: IRS_Blue_PeakUp_FOV_Center NF: 22

PIX2RADW: 8.72660000E-008[rad/pixel] = 1.8000E-002[arcsec/pixel]

PIX2RADV: 8.72660000E-008[rad/pixel] = 1.8000E-002[arcsec/pixel]

| FRAME | DESCRIPTION | IPF ¹ | SF ² | TOTAL | REQ |
|--------|----------------------------|------------------|-----------------|--------|------|
| 022(P) | IRS_Blue_PeakUp_FOV_Center | 0.0449 | 0.0855 | 0.0966 | 0.25 |

Table 9.5: IPF calibration error summary ([arcsec], 1-sigma, radial)

| RMS METRIC | A PRIORI ³ | A POSTERIORI ³ | ATT. CORRECTED ⁴ | UNITS |
|------------|-----------------------|---------------------------|-----------------------------|--------|
| Radial | 1.5993 | 0.0972 | 0.0682 | arcsec |
| W-Axis | 0.7167 | 0.0754 | 0.0455 | arcsec |
| V-Axis | 1.4297 | 0.0613 | 0.0509 | arcsec |
| Radial | 88.8505 | 5.3991 | 3.7911 | pixels |
| W-Axis | 39.8168 | 4.1907 | 2.5279 | pixels |
| V-Axis | 79.4294 | 3.4041 | 2.8253 | pixels |

Table 9.6: Science measurement prediction error summary (1-sigma)

¹IPF filter removes systematic pointing errors due to: thermomechanical alignment drift (Body to TPF), gyro bias and bias drift, centroiding error, attitude error, and optical distortion. IPF SIGMA presented here is “Scaled” by the Least Squares Scale factor. The Least Squares Scale Factor was: 0.870666. It is assumed that the gyro Angle Random Walk contribution is captured with the Least Squares scaling. The gyro ARW contribution can be approximately calculated as 0.0853 arcseconds, given that $ARW = 100 \mu deg/\sqrt{hr}$, with 6.060556e+002 second Maneuver time (max), and 6 independent Maneuvers.

²Gyro Scale Factor(GSF) assumes 95 ppm error over 0.250 degree maneuver.

³This can be interpreted as estimate of ”pixel to sky” pointing reconstruction error if no science data is used.

⁴This can be interpreted as estimate of achieved S/I centroiding error

9.4 IPF EXECUTION SUMMARY OF ID701023

FOCAL PLANE SURVEY ANALYSIS: IOC Fine Survey.

INSTRUMENT NAME: IRS_Blue_PeakUp_FOV_Sweet_Spot NF: 23

PIX2RADW: 8.72660000E-008[rad/pixel] = 1.8000E-002[arcsec/pixel]

PIX2RADV: 8.72660000E-008[rad/pixel] = 1.8000E-002[arcsec/pixel]

| FRAME | DESCRIPTION | IPF ¹ | SF ² | TOTAL | REQ |
|--------|--------------------------------|------------------|-----------------|--------|------|
| 023(P) | IRS_Blue_PeakUp_FOV_Sweet_Spot | 0.0157 | 0.0855 | 0.0869 | 0.14 |

Table 9.7: IPF calibration error summary ([arcsec], 1-sigma, radial)

| RMS METRIC | A PRIORI ³ | A POSTERIORI ³ | ATT. CORRECTED ⁴ | UNITS |
|------------|-----------------------|---------------------------|-----------------------------|--------|
| Radial | 1.2491 | 0.1536 | 0.0669 | arcsec |
| W-Axis | 0.4280 | 0.1276 | 0.0576 | arcsec |
| V-Axis | 1.1735 | 0.0855 | 0.0339 | arcsec |
| Radial | 69.3972 | 8.5322 | 3.7155 | pixels |
| W-Axis | 23.7752 | 7.0870 | 3.2014 | pixels |
| V-Axis | 65.1975 | 4.7511 | 1.8857 | pixels |

Table 9.8: Science measurement prediction error summary (1-sigma)

¹IPF filter removes systematic pointing errors due to: thermomechanical alignment drift (Body to TPF), gyro bias and bias drift, centroiding error, attitude error, and optical distortion. IPF SIGMA presented here is “Scaled” by the Least Squares Scale factor. The Least Squares Scale Factor was: 0.831187. It is assumed that the gyro Angle Random Walk contribution is captured with the Least Squares scaling. The gyro ARW contribution can be approximately calculated as 0.0454 arcseconds, given that $ARW = 100 \mu deg/\sqrt{hr}$, with 6.004369e+002 second Maneuver time (max), and 21 independent Maneuvers.

²Gyro Scale Factor(GSF) assumes 95 ppm error over 0.250 degree maneuver.

³This can be interpreted as estimate of ”pixel to sky” pointing reconstruction error if no science data is used.

⁴This can be interpreted as estimate of achieved S/I centroiding error

9.5 IPF EXECUTION SUMMARY OF ID502028

FOCAL PLANE SURVEY ANALYSIS: IOC Fine Survey.

INSTRUMENT NAME: IRS_ShortLo_1st_Ord_Center_Pos **NF: 28**

PIX2RADW: 4.84813681E-006[rad/pixel] = 1.0000E+000[arcsec/pixel]

PIX2RADV: 4.84813681E-006[rad/pixel] = 1.0000E+000[arcsec/pixel]

| FRAME | DESCRIPTION | IPF ¹ | SF ² | TOTAL | REQ |
|--------|--------------------------------|------------------|-----------------|--------|------|
| 028(P) | IRS_ShortLo_1st_Ord_Center_Pos | 0.0791 | 0.0855 | 0.1165 | 0.14 |
| 026(I) | IRS_ShortLo_1st_Ord_1st_Pos | 0.0821 | 0.0855 | 0.1186 | N/A |
| 027(I) | IRS_ShortLo_1st_Ord_2nd_Pos | 0.0772 | 0.0855 | 0.1152 | N/A |
| 029(I) | IRS_ShortLo_Module_Center | 0.0809 | 0.0855 | 0.1177 | N/A |

Table 9.9: IPF calibration error summary ([arcsec], 1-sigma, radial)

| RMS METRIC | A PRIORI ³ | A POSTERIORI ³ | ATT. CORRECTED ⁴ | UNITS |
|------------|-----------------------|---------------------------|-----------------------------|--------|
| Radial | 1.5786 | 0.6289 | 0.5543 | arcsec |
| W-Axis | 1.3875 | 0.5477 | 0.5429 | arcsec |
| V-Axis | 0.7528 | 0.3092 | 0.1115 | arcsec |
| Radial | 1.5786 | 0.6289 | 0.5543 | pixels |
| W-Axis | 1.3875 | 0.5477 | 0.5429 | pixels |
| V-Axis | 0.7528 | 0.3092 | 0.1115 | pixels |

Table 9.10: Science measurement prediction error summary (1-sigma)

¹IPF filter removes systematic pointing errors due to: thermomechanical alignment drift (Body to TPF), gyro bias and bias drift, centroiding error, attitude error, and optical distortion. IPF SIGMA presented here is "Scaled" by the Least Squares Scale factor. The Least Squares Scale Factor was: 3.485288. It is assumed that the gyro Angle Random Walk contribution is captured with the Least Squares scaling. The gyro ARW contribution can be approximately calculated as 0.0387 arcseconds, given that $ARW = 100 \mu deg/\sqrt{hr}$, with 6.872852e+002 second Maneuver time (max), and 33 independent Maneuvers.

²Gyro Scale Factor(GSF) assumes 95 ppm error over 0.250 degree maneuver.

³This can be interpreted as estimate of "pixel to sky" pointing reconstruction error if no science data is used.

⁴This can be interpreted as estimate of achieved S/I centroiding error

9.6 IPF EXECUTION SUMMARY OF ID502034

FOCAL PLANE SURVEY ANALYSIS: IOC Fine Survey.

INSTRUMENT NAME: IRS_ShortLo_2nd_Ord_Center_Pos NF: 34

PIX2RADW: 4.84813681E-006[rad/pixel] = 1.0000E+000[arcsec/pixel]

PIX2RADV: 4.84813681E-006[rad/pixel] = 1.0000E+000[arcsec/pixel]

| FRAME | DESCRIPTION | IPF ¹ | SF ² | TOTAL | REQ |
|--------|--------------------------------|------------------|-----------------|--------|------|
| 034(P) | IRS_ShortLo_2nd_Ord_Center_Pos | 0.0308 | 0.0855 | 0.0909 | 0.14 |
| 032(I) | IRS_ShortLo_2nd_Ord_1st_Pos | 0.0346 | 0.0855 | 0.0922 | N/A |
| 033(I) | IRS_ShortLo_2nd_Ord_2nd_Pos | 0.0280 | 0.0855 | 0.0900 | N/A |

Table 9.11: IPF calibration error summary ([arcsec], 1-sigma, radial)

| RMS METRIC | A PRIORI ³ | A POSTERIORI ³ | ATT. CORRECTED ⁴ | UNITS |
|------------|-----------------------|---------------------------|-----------------------------|--------|
| Radial | 1.3822 | 0.9586 | 0.8421 | arcsec |
| W-Axis | 1.2627 | 0.9165 | 0.8131 | arcsec |
| V-Axis | 0.5623 | 0.2809 | 0.2192 | arcsec |
| Radial | 1.3822 | 0.9586 | 0.8421 | pixels |
| W-Axis | 1.2627 | 0.9165 | 0.8131 | pixels |
| V-Axis | 0.5623 | 0.2809 | 0.2192 | pixels |

Table 9.12: Science measurement prediction error summary (1-sigma)

¹IPF filter removes systematic pointing errors due to: thermomechanical alignment drift (Body to TPF), gyro bias and bias drift, centroiding error, attitude error, and optical distortion. IPF SIGMA presented here is "Scaled" by the Least Squares Scale factor. The Least Squares Scale Factor was: 2.459662. It is assumed that the gyro Angle Random Walk contribution is captured with the Least Squares scaling. The gyro ARW contribution can be approximately calculated as 0.0361 arcseconds, given that $ARW = 100 \mu deg/\sqrt{hr}$, with 6.864286e+002 second Maneuver time (max), and 38 independent Maneuvers.

²Gyro Scale Factor(GSF) assumes 95 ppm error over 0.250 degree maneuver.

³This can be interpreted as estimate of "pixel to sky" pointing reconstruction error if no science data is used.

⁴This can be interpreted as estimate of achieved S/I centroiding error

9.7 IPF EXECUTION SUMMARY OF ID502040

FOCAL PLANE SURVEY ANALYSIS: IOC Fine Survey.

INSTRUMENT NAME: IRS_LongLo_1st_Ord_Center_Pos NF: 40

PIX2RADW: 4.84813681E-006[rad/pixel] = 1.0000E+000[arcsec/pixel]

PIX2RADV: 4.84813681E-006[rad/pixel] = 1.0000E+000[arcsec/pixel]

| FRAME | DESCRIPTION | IPF ¹ | SF ² | TOTAL | REQ |
|--------|-------------------------------|------------------|-----------------|--------|------|
| 040(P) | IRS_LongLo_1st_Ord_Center_Pos | 0.0973 | 0.0855 | 0.1295 | 0.28 |
| 038(I) | IRS_LongLo_1st_Ord_1st_Pos | 0.1013 | 0.0855 | 0.1326 | N/A |
| 039(I) | IRS_LongLo_1st_Ord_2nd_Pos | 0.1025 | 0.0855 | 0.1335 | N/A |
| 041(I) | IRS_LongLo_Module_Center | 0.1548 | 0.0855 | 0.1769 | N/A |

Table 9.13: IPF calibration error summary ([arcsec], 1-sigma, radial)

| RMS METRIC | A PRIORI ³ | A POSTERIORI ³ | ATT. CORRECTED ⁴ | UNITS |
|------------|-----------------------|---------------------------|-----------------------------|--------|
| Radial | 4.7663 | 2.2009 | 2.1718 | arcsec |
| W-Axis | 4.7183 | 2.1235 | 2.0956 | arcsec |
| V-Axis | 0.6744 | 0.5784 | 0.5703 | arcsec |
| Radial | 4.7663 | 2.2009 | 2.1718 | pixels |
| W-Axis | 4.7183 | 2.1235 | 2.0956 | pixels |
| V-Axis | 0.6744 | 0.5784 | 0.5703 | pixels |

Table 9.14: Science measurement prediction error summary (1-sigma)

¹IPF filter removes systematic pointing errors due to: thermomechanical alignment drift (Body to TPF), gyro bias and bias drift, centroiding error, attitude error, and optical distortion. IPF SIGMA presented here is "Scaled" by the Least Squares Scale factor. The Least Squares Scale Factor was: 1.481732. It is assumed that the gyro Angle Random Walk contribution is captured with the Least Squares scaling. The gyro ARW contribution can be approximately calculated as 0.0844 arcseconds, given that $ARW = 100 \mu deg/\sqrt{hr}$, with 6.929620e+002 second Maneuver time (max), and 7 independent Maneuvers.

²Gyro Scale Factor(GSF) assumes 95 ppm error over 0.250 degree maneuver.

³This can be interpreted as estimate of "pixel to sky" pointing reconstruction error if no science data is used.

⁴This can be interpreted as estimate of achieved S/I centroiding error

9.8 IPF EXECUTION SUMMARY OF ID501046

FOCAL PLANE SURVEY ANALYSIS: IOC Fine Survey.

INSTRUMENT NAME: IRS_LongLo_2nd_Ord_Center_Pos NF: 46

PIX2RADW: 4.84813681E-06[rad/pixel] = 1.0000E+00[arcsec/pixel]

PIX2RADV: 4.84813681E-06[rad/pixel] = 1.0000E+00[arcsec/pixel]

| FRAME | DESCRIPTION | IPF ¹ | SF ² | TOTAL | REQ |
|--------|-------------------------------|------------------|-----------------|--------|------|
| 046(P) | IRS_LongLo_2nd_Ord_Center_Pos | 0.2542 | 0.0855 | 0.2682 | 0.28 |
| 044(I) | IRS_LongLo_2nd_Ord_1st_Pos | 0.2534 | 0.0855 | 0.2675 | N/A |
| 045(I) | IRS_LongLo_2nd_Ord_2nd_Pos | 0.2599 | 0.0855 | 0.2736 | N/A |

Table 9.15: IPF calibration error summary ([arcsec], 1-sigma, radial)

| RMS METRIC | A PRIORI ³ | A POSTERIORI ³ | ATT. CORRECTED ⁴ | UNITS |
|------------|-----------------------|---------------------------|-----------------------------|--------|
| Radial | 3.5160 | 1.1167 | 1.1052 | arcsec |
| W-Axis | 3.4550 | 1.0373 | 1.0357 | arcsec |
| V-Axis | 0.6521 | 0.4137 | 0.3858 | arcsec |
| Radial | 3.5160 | 1.1167 | 1.1052 | pixels |
| W-Axis | 3.4550 | 1.0373 | 1.0357 | pixels |
| V-Axis | 0.6521 | 0.4137 | 0.3858 | pixels |

Table 9.16: Science measurement prediction error summary (1-sigma)

¹IPF filter removes systematic pointing errors due to: thermomechanical alignment drift (Body to TPF), gyro bias and bias drift, centroiding error, attitude error, and optical distortion. IPF SIGMA presented here is “Scaled” by the Least Squares Scale factor. The Least Squares Scale Factor was: 7.598404. It is assumed that the gyro Angle Random Walk contribution is captured with the Least Squares scaling. The gyro ARW contribution can be approximately calculated as 0.0846 arcseconds, given that $ARW = 100 \mu deg / \sqrt{hr}$, with 6.955400e+02 second Maneuver time (max), and 7 independent Maneuvers.

²Gyro Scale Factor(GSF) assumes 95 ppm error over 0.250 degree maneuver.

³This can be interpreted as estimate of ”pixel to sky” pointing reconstruction error if no science data is used.

⁴This can be interpreted as estimate of achieved S/I centroiding error

9.9 IPF EXECUTION SUMMARY OF ID502052

FOCAL PLANE SURVEY ANALYSIS: IOC Fine Survey.

INSTRUMENT NAME: IRS_ShortHi_Center_Position NF: 52

PIX2RADW: 4.84813681E-006[rad/pixel] = 1.0000E+000[arcsec/pixel]

PIX2RADV: 4.84813681E-006[rad/pixel] = 1.0000E+000[arcsec/pixel]

| FRAME | DESCRIPTION | IPF ¹ | SF ² | TOTAL | REQ |
|--------|-----------------------------|------------------|-----------------|--------|------|
| 052(P) | IRS_ShortHi_Center_Position | 0.0230 | 0.0855 | 0.0885 | 0.14 |
| 050(I) | IRS_ShortHi_1st_Position | 0.0231 | 0.0855 | 0.0886 | N/A |
| 051(I) | IRS_ShortHi_2nd_Position | 0.0230 | 0.0855 | 0.0885 | N/A |

Table 9.17: IPF calibration error summary ([arcsec], 1-sigma, radial)

| RMS METRIC | A PRIORI ³ | A POSTERIORI ³ | ATT. CORRECTED ⁴ | UNITS |
|------------|-----------------------|---------------------------|-----------------------------|--------|
| Radial | 1.1312 | 1.0241 | 0.9296 | arcsec |
| W-Axis | 0.7205 | 0.7654 | 0.6604 | arcsec |
| V-Axis | 0.8720 | 0.6804 | 0.6542 | arcsec |
| Radial | 1.1312 | 1.0241 | 0.9296 | pixels |
| W-Axis | 0.7205 | 0.7654 | 0.6604 | pixels |
| V-Axis | 0.8720 | 0.6804 | 0.6542 | pixels |

Table 9.18: Science measurement prediction error summary (1-sigma)

¹IPF filter removes systematic pointing errors due to: thermomechanical alignment drift (Body to TPF), gyro bias and bias drift, centroiding error, attitude error, and optical distortion. IPF SIGMA presented here is "Scaled" by the Least Squares Scale factor. The Least Squares Scale Factor was: 1.644587. It is assumed that the gyro Angle Random Walk contribution is captured with the Least Squares scaling. The gyro ARW contribution can be approximately calculated as 0.0403 arcseconds, given that $ARW = 100 \mu deg/\sqrt{hr}$, with $7.455714e+002$ second Maneuver time (max), and 33 independent Maneuvers.

²Gyro Scale Factor(GSF) assumes 95 ppm error over 0.250 degree maneuver.

³This can be interpreted as estimate of "pixel to sky" pointing reconstruction error if no science data is used.

⁴This can be interpreted as estimate of achieved S/I centroiding error

9.10 IPF EXECUTION SUMMARY OF ID501058

FOCAL PLANE SURVEY ANALYSIS: IOC Fine Survey.

INSTRUMENT NAME: IRS_LongHi_Center_Position NF: 58

PIX2RADW: 4.84813681E-006[rad/pixel] = 1.0000E+000[arcsec/pixel]

PIX2RADV: 4.84813681E-006[rad/pixel] = 1.0000E+000[arcsec/pixel]

| FRAME | DESCRIPTION | IPF ¹ | SF ² | TOTAL | REQ |
|--------|----------------------------|------------------|-----------------|--------|------|
| 058(P) | IRS_LongHi_Center_Position | 0.0569 | 0.0855 | 0.1027 | 0.28 |
| 056(I) | IRS_LongHi_1st_Position | 0.0578 | 0.0855 | 0.1032 | N/A |
| 057(I) | IRS_LongHi_2nd_Position | 0.0568 | 0.0855 | 0.1027 | N/A |

Table 9.19: IPF calibration error summary ([arcsec], 1-sigma, radial)

| RMS METRIC | A PRIORI ³ | A POSTERIORI ³ | ATT. CORRECTED ⁴ | UNITS |
|------------|-----------------------|---------------------------|-----------------------------|--------|
| Radial | 0.9716 | 0.9682 | 0.9335 | arcsec |
| W-Axis | 0.8113 | 0.9346 | 0.9247 | arcsec |
| V-Axis | 0.5345 | 0.2527 | 0.1279 | arcsec |
| Radial | 0.9716 | 0.9682 | 0.9335 | pixels |
| W-Axis | 0.8113 | 0.9346 | 0.9247 | pixels |
| V-Axis | 0.5345 | 0.2527 | 0.1279 | pixels |

Table 9.20: Science measurement prediction error summary (1-sigma)

¹IPF filter removes systematic pointing errors due to: thermomechanical alignment drift (Body to TPF), gyro bias and bias drift, centroiding error, attitude error, and optical distortion. IPF SIGMA presented here is "Scaled" by the Least Squares Scale factor. The Least Squares Scale Factor was: 1.741864. It is assumed that the gyro Angle Random Walk contribution is captured with the Least Squares scaling. The gyro ARW contribution can be approximately calculated as 0.0877 arcseconds, given that $ARW = 100 \mu deg/\sqrt{hr}$, with $7.477653e+002$ second Maneuver time (max), and 7 independent Maneuvers.

²Gyro Scale Factor(GSF) assumes 95 ppm error over 0.250 degree maneuver.

³This can be interpreted as estimate of "pixel to sky" pointing reconstruction error if no science data is used.

⁴This can be interpreted as estimate of achieved S/I centroiding error

9.11 IPF EXECUTION SUMMARY OF ID502068

FOCAL PLANE SURVEY ANALYSIS: IOC Fine Survey.

INSTRUMENT NAME: IRAC_Center_of_3.6umArray NF: 68

PIX2RADW: 5.86625000E-006[rad/pixel] = 1.2100E+000[arcsec/pixel]

PIX2RADV: 5.86625000E-006[rad/pixel] = 1.2100E+000[arcsec/pixel]

| FRAME | DESCRIPTION | IPF ¹ | SF ² | TOTAL | REQ |
|--------|-------------------------------|------------------|-----------------|--------|------|
| 068(P) | IRAC_Center_of_3.6umArray | 0.0212 | 0.0855 | 0.0881 | 0.14 |
| 070(I) | IRAC_Center_of_3.6umSub-array | 0.0325 | 0.0855 | 0.0915 | N/A |

Table 9.21: IPF calibration error summary ([arcsec], 1-sigma, radial)

| RMS METRIC | A PRIORI ³ | A POSTERIORI ³ | ATT. CORRECTED ⁴ | UNITS |
|------------|-----------------------|---------------------------|-----------------------------|--------|
| Radial | 1.2942 | 0.3671 | 0.3099 | arcsec |
| W-Axis | 1.0238 | 0.2994 | 0.2408 | arcsec |
| V-Axis | 0.7917 | 0.2124 | 0.1951 | arcsec |
| Radial | 1.0696 | 0.3034 | 0.2561 | pixels |
| W-Axis | 0.8461 | 0.2474 | 0.1990 | pixels |
| V-Axis | 0.6543 | 0.1756 | 0.1613 | pixels |

Table 9.22: Science measurement prediction error summary (1-sigma)

¹IPF filter removes systematic pointing errors due to: thermomechanical alignment drift (Body to TPF), gyro bias and bias drift, centroiding error, attitude error, and optical distortion. IPF SIGMA presented here is "Scaled" by the Least Squares Scale factor. The Least Squares Scale Factor was: 0.777790. It is assumed that the gyro Angle Random Walk contribution is captured with the Least Squares scaling. The gyro ARW contribution can be approximately calculated as 0.1390 arcseconds, given that $ARW = 100 \mu deg/\sqrt{hr}$, with 1.073400e+003 second maneuver time (max), and 4 independent Maneuvers.

²Gyro Scale Factor(GSF) assumes 95 ppm error over 0.250 degree maneuver.

³This can be interpreted as estimate of "pixel to sky" pointing reconstruction error if no science data is used.

⁴This can be interpreted as estimate of achieved S/I centroiding error

9.12 IPF EXECUTION SUMMARY OF ID502069

FOCAL PLANE SURVEY ANALYSIS: IOC Fine Survey.

INSTRUMENT NAME: IRAC_Center_of_5.8umArray NF: 69

PIX2RADW: 5.86625000E-06[rad/pixel] = 1.2100E+00[arcsec/pixel]

PIX2RADV: 5.86625000E-06[rad/pixel] = 1.2100E+00[arcsec/pixel]

| FRAME | DESCRIPTION | IPF ¹ | SF ² | TOTAL | REQ |
|--------|-------------------------------|------------------|-----------------|--------|------|
| 069(P) | IRAC_Center_of_5.8umArray | 0.0243 | 0.0855 | 0.0889 | 0.14 |
| 072(I) | IRAC_Center_of_5.8umSub-array | 0.0361 | 0.0855 | 0.0928 | N/A |

Table 9.23: IPF calibration error summary ([arcsec], 1-sigma, radial)

| RMS METRIC | A PRIORI ³ | A POSTERIORI ³ | ATT. CORRECTED ⁴ | UNITS |
|------------|-----------------------|---------------------------|-----------------------------|--------|
| Radial | 1.4185 | 0.3374 | 0.2784 | arcsec |
| W-Axis | 0.9584 | 0.2620 | 0.1956 | arcsec |
| V-Axis | 1.0458 | 0.2126 | 0.1981 | arcsec |
| Radial | 1.1723 | 0.2788 | 0.2301 | pixels |
| W-Axis | 0.7920 | 0.2165 | 0.1616 | pixels |
| V-Axis | 0.8643 | 0.1757 | 0.1637 | pixels |

Table 9.24: Science measurement prediction error summary (1-sigma)

¹IPF filter removes systematic pointing errors due to: thermomechanical alignment drift (Body to TPF), gyro bias and bias drift, centroiding error, attitude error, and optical distortion. IPF SIGMA presented here is “Scaled” by the Least Squares Scale factor. The Least Squares Scale Factor was: 0.747743. It is assumed that the gyro Angle Random Walk contribution is captured with the Least Squares scaling. The gyro ARW contribution can be approximately calculated as 0.1390 arcseconds, given that $ARW = 100 \mu deg / \sqrt{hr}$, with 1.073400e+03 second Maneuver time (max), and 4 independent Maneuvers.

²Gyro Scale Factor(GSF) assumes 95 ppm error over 0.250 degree maneuver.

³This can be interpreted as estimate of ”pixel to sky” pointing reconstruction error if no science data is used.

⁴This can be interpreted as estimate of achieved S/I centroiding error

9.13 IPF EXECUTION SUMMARY OF ID502075

FOCAL PLANE SURVEY ANALYSIS: IOC Fine Survey.

INSTRUMENT NAME: IRAC_Center_of_4.5umArray NF: 75

PIX2RADW: 5.86625000E-006[rad/pixel] = 1.2100E+000[arcsec/pixel]

PIX2RADV: 5.86625000E-006[rad/pixel] = 1.2100E+000[arcsec/pixel]

| FRAME | DESCRIPTION | IPF ¹ | SF ² | TOTAL | REQ |
|--------|-------------------------------|------------------|-----------------|--------|------|
| 075(P) | IRAC_Center_of_4.5umArray | 0.0200 | 0.0855 | 0.0878 | 0.14 |
| 077(I) | IRAC_Center_of_4.5umSub-Array | 0.0392 | 0.0855 | 0.0941 | N/A |

Table 9.25: IPF calibration error summary ([arcsec], 1-sigma, radial)

| RMS METRIC | A PRIORI ³ | A POSTERIORI ³ | ATT. CORRECTED ⁴ | UNITS |
|------------|-----------------------|---------------------------|-----------------------------|--------|
| Radial | 0.9849 | 0.4045 | 0.3437 | arcsec |
| W-Axis | 0.8324 | 0.3242 | 0.2633 | arcsec |
| V-Axis | 0.5264 | 0.2419 | 0.2209 | arcsec |
| Radial | 0.8139 | 0.3343 | 0.2841 | pixels |
| W-Axis | 0.6879 | 0.2679 | 0.2176 | pixels |
| V-Axis | 0.4350 | 0.1999 | 0.1826 | pixels |

Table 9.26: Science measurement prediction error summary (1-sigma)

¹IPF filter removes systematic pointing errors due to: thermomechanical alignment drift (Body to TPF), gyro bias and bias drift, centroiding error, attitude error, and optical distortion. IPF SIGMA presented here is "Scaled" by the Least Squares Scale factor. The Least Squares Scale Factor was: 0.841437. It is assumed that the gyro Angle Random Walk contribution is captured with the Least Squares scaling. The gyro ARW contribution can be approximately calculated as 0.1390 arcseconds, given that $ARW = 100 \mu deg/\sqrt{hr}$, with 1.073400e+003 second maneuver time (max), and 4 independent Maneuvers.

²Gyro Scale Factor(GSF) assumes 95 ppm error over 0.250 degree maneuver.

³This can be interpreted as estimate of "pixel to sky" pointing reconstruction error if no science data is used.

⁴This can be interpreted as estimate of achieved S/I centroiding error

9.14 IPF EXECUTION SUMMARY OF ID502076

FOCAL PLANE SURVEY ANALYSIS: IOC Fine Survey.

INSTRUMENT NAME: IRAC_Center_of_8.0umArray NF: 76

PIX2RADW: 5.86625000E-006[rad/pixel] = 1.2100E+000[arcsec/pixel]

PIX2RADV: 5.86625000E-006[rad/pixel] = 1.2100E+000[arcsec/pixel]

| FRAME | DESCRIPTION | IPF ¹ | SF ² | TOTAL | REQ |
|--------|-------------------------------|------------------|-----------------|--------|------|
| 076(P) | IRAC_Center_of_8.0umArray | 0.0264 | 0.0855 | 0.0895 | 0.14 |
| 079(I) | IRAC_Center_of_8.0umSub-Array | 0.0563 | 0.0855 | 0.1024 | N/A |

Table 9.27: IPF calibration error summary ([arcsec], 1-sigma, radial)

| RMS METRIC | A PRIORI ³ | A POSTERIORI ³ | ATT. CORRECTED ⁴ | UNITS |
|------------|-----------------------|---------------------------|-----------------------------|--------|
| Radial | 1.1567 | 0.3622 | 0.2972 | arcsec |
| W-Axis | 0.7453 | 0.2877 | 0.2240 | arcsec |
| V-Axis | 0.8845 | 0.2200 | 0.1953 | arcsec |
| Radial | 0.9559 | 0.2993 | 0.2456 | pixels |
| W-Axis | 0.6160 | 0.2378 | 0.1851 | pixels |
| V-Axis | 0.7310 | 0.1818 | 0.1614 | pixels |

Table 9.28: Science measurement prediction error summary (1-sigma)

¹IPF filter removes systematic pointing errors due to: thermomechanical alignment drift (Body to TPF), gyro bias and bias drift, centroiding error, attitude error, and optical distortion. IPF SIGMA presented here is “Scaled” by the Least Squares Scale factor. The Least Squares Scale Factor was: 0.808031. It is assumed that the gyro Angle Random Walk contribution is captured with the Least Squares scaling. The gyro ARW contribution can be approximately calculated as 0.1390 arcseconds, given that $ARW = 100 \mu deg/\sqrt{hr}$, with 1.073400e+003 second maneuver time (max), and 4 independent Maneuvers.

²Gyro Scale Factor(GSF) assumes 95 ppm error over 0.250 degree maneuver.

³This can be interpreted as estimate of ”pixel to sky” pointing reconstruction error if no science data is used.

⁴This can be interpreted as estimate of achieved S/I centroiding error

9.15 IPF EXECUTION SUMMARY OF ID703087

FOCAL PLANE SURVEY ANALYSIS: IOC Fine Survey.

INSTRUMENT NAME: MIPS_160um_center_large_FOV NF: 87

PIX2RADW: 7.85398200E-05 [rad/pixel] = 1.6200E+01 [arcsec/pixel]

PIX2RADV: 8.43575790E-05 [rad/pixel] = 1.7400E+01 [arcsec/pixel]

| FRAME | DESCRIPTION | IPF ¹ | SF ² | TOTAL | REQ |
|--------|-----------------------------|------------------|-----------------|--------|------|
| 087(P) | MIPS_160um_center_large_FOV | 1.2025 | 0.0855 | 1.2056 | 3.70 |
| 088(I) | MIPS_160um_plusY_edge | 1.2041 | 0.0855 | 1.2071 | N/A |
| 089(I) | MIPS_160um_large_only | 1.2025 | 0.0855 | 1.2056 | N/A |
| 091(I) | MIPS_160um_small_FOV1 | 1.2147 | 0.0855 | 1.2177 | N/A |
| 092(I) | MIPS_160um_small_FOV2 | 1.2001 | 0.0855 | 1.2031 | N/A |

Table 9.29: IPF calibration error summary ([arcsec], 1-sigma, radial)

| RMS METRIC | A PRIORI ³ | A POSTERIORI ³ | ATT. CORRECTED ⁴ | UNITS |
|------------|-----------------------|---------------------------|-----------------------------|--------|
| Radial | 11.9662 | 6.6786 | 6.6641 | arcsec |
| W-Axis | 8.7924 | 5.4242 | 5.4210 | arcsec |
| V-Axis | 8.1169 | 3.8964 | 3.8760 | arcsec |
| Radial | 0.7157 | 0.4028 | 0.4020 | pixels |
| W-Axis | 0.5427 | 0.3348 | 0.3346 | pixels |
| V-Axis | 0.4665 | 0.2239 | 0.2228 | pixels |

Table 9.30: Science measurement prediction error summary (1-sigma)

¹IPF filter removes systematic pointing errors due to: thermomechanical alignment drift (Body to TPF), gyro bias and bias drift, centroiding error, attitude error, and optical distortion. IPF SIGMA presented here is "Scaled" by the Least Squares Scale factor. The Least Squares Scale Factor was: 1.118672. It is assumed that the gyro Angle Random Walk contribution is captured with the Least Squares scaling. The gyro ARW contribution can be approximately calculated as 0.6934 arcseconds, given that $ARW = 100 \mu deg / \sqrt{hr}$, with 1.335622e+04 second Maneuver time (max), and 2 independent Maneuvers.

²Gyro Scale Factor(GSF) assumes 95 ppm error over 0.250 degree maneuver.

³This can be interpreted as estimate of "pixel to sky" pointing reconstruction error if no science data is used.

⁴This can be interpreted as estimate of achieved S/I centroiding error

9.16 IPF EXECUTION SUMMARY OF ID602095

FOCAL PLANE SURVEY ANALYSIS: IOC Fine Survey.

INSTRUMENT NAME: MIPS_24um_center NF: 95

PIX2RADW: 1.20874169E-005 [rad/pixel] = 2.4932E+000 [arcsec/pixel]

PIX2RADV: 1.25959084E-005 [rad/pixel] = 2.5981E+000 [arcsec/pixel]

| FRAME | DESCRIPTION | IPF ¹ | SF ² | TOTAL | REQ |
|--------|----------------------|------------------|-----------------|--------|------|
| 095(P) | MIPS_24um_center | 0.0224 | 0.0855 | 0.0884 | 0.14 |
| 096(I) | MIPS_24um_plusY_edge | 0.0328 | 0.0855 | 0.0916 | N/A |
| 099(I) | MIPS_24um_small_FOV1 | 0.0214 | 0.0855 | 0.0881 | N/A |
| 100(I) | MIPS_24um_small_FOV2 | 0.0214 | 0.0855 | 0.0881 | N/A |
| 103(I) | MIPS_24um_large_FOV1 | 0.0224 | 0.0855 | 0.0884 | N/A |
| 104(I) | MIPS_24um_large_FOV2 | 0.0224 | 0.0855 | 0.0884 | N/A |

Table 9.31: IPF calibration error summary ([arcsec], 1-sigma, radial)

| RMS METRIC | A PRIORI ³ | A POSTERIORI ³ | ATT. CORRECTED ⁴ | UNITS |
|------------|-----------------------|---------------------------|-----------------------------|--------|
| Radial | 2.4059 | 0.1785 | 0.1634 | arcsec |
| W-Axis | 1.4388 | 0.1059 | 0.0892 | arcsec |
| V-Axis | 1.9283 | 0.1437 | 0.1369 | arcsec |
| Radial | 0.9401 | 0.0697 | 0.0637 | pixels |
| W-Axis | 0.5771 | 0.0425 | 0.0358 | pixels |
| V-Axis | 0.7422 | 0.0553 | 0.0527 | pixels |

Table 9.32: Science measurement prediction error summary (1-sigma)

¹IPF filter removes systematic pointing errors due to: thermomechanical alignment drift (Body to TPF), gyro bias and bias drift, centroiding error, attitude error, and optical distortion. IPF SIGMA presented here is "Scaled" by the Least Squares Scale factor. The Least Squares Scale Factor was: 0.945293. It is assumed that the gyro Angle Random Walk contribution is captured with the Least Squares scaling. The gyro ARW contribution can be approximately calculated as 0.0517 arcseconds, given that $ARW = 100 \mu deg/\sqrt{hr}$, with 5.567000e+002 second Maneuver time (max), and 15 independent Maneuvers.

²Gyro Scale Factor(GSF) assumes 95 ppm error over 0.250 degree maneuver.

³This can be interpreted as estimate of "pixel to sky" pointing reconstruction error if no science data is used.

⁴This can be interpreted as estimate of achieved S/I centroiding error

9.17 IPF EXECUTION SUMMARY OF ID704107

FOCAL PLANE SURVEY ANALYSIS: IOC Fine Survey.

INSTRUMENT NAME: MIPS_70um_center NF: 107

PIX2RADW: 4.79044679E-005[rad/pixel] = 9.8810E+000[arcsec/pixel]

PIX2RADV: 4.87929385E-005[rad/pixel] = 1.0064E+001[arcsec/pixel]

| FRAME | DESCRIPTION | IPF ¹ | SF ² | TOTAL | REQ |
|--------|------------------------------|------------------|-----------------|--------|------|
| 107(P) | MIPS_70um_center | 0.2716 | 0.0855 | 0.2847 | 2.60 |
| 108(I) | MIPS_70um_minusY_edge | 0.3610 | 0.0855 | 0.3710 | N/A |
| 111(I) | MIPS_70um_default_small_FOV1 | 0.1181 | 0.0855 | 0.1458 | N/A |
| 112(I) | MIPS_70um_default_small_FOV2 | 0.1259 | 0.0855 | 0.1522 | N/A |
| 115(I) | MIPS_70um_default_large_FOV1 | 0.1181 | 0.0855 | 0.1458 | N/A |
| 116(I) | MIPS_70um_default_sideA | 0.1192 | 0.0855 | 0.1467 | N/A |

Table 9.33: IPF calibration error summary ([arcsec], 1-sigma, radial)

| RMS METRIC | A PRIORI ³ | A POSTERIORI ³ | ATT. CORRECTED ⁴ | UNITS |
|------------|-----------------------|---------------------------|-----------------------------|--------|
| Radial | 3.1372 | 1.2935 | 1.2896 | arcsec |
| W-Axis | 2.2758 | 1.0617 | 1.0561 | arcsec |
| V-Axis | 2.1594 | 0.7389 | 0.7401 | arcsec |
| Radial | 0.3148 | 0.1301 | 0.1297 | pixels |
| W-Axis | 0.2303 | 0.1074 | 0.1069 | pixels |
| V-Axis | 0.2146 | 0.0734 | 0.0735 | pixels |

Table 9.34: Science measurement prediction error summary (1-sigma)

¹IPF filter removes systematic pointing errors due to: thermomechanical alignment drift (Body to TPF), gyro bias and bias drift, centroiding error, attitude error, and optical distortion. IPF SIGMA presented here is "Scaled" by the Least Squares Scale factor. The Least Squares Scale Factor was: 0.466845. It is assumed that the gyro Angle Random Walk contribution is captured with the Least Squares scaling. The gyro ARW contribution can be approximately calculated as 0.0884 arcseconds, given that $ARW = 100 \mu deg/\sqrt{hr}$, with 7.604000e+002 second Maneuver time (max), and 7 independent Maneuvers.

²Gyro Scale Factor(GSF) assumes 95 ppm error over 0.250 degree maneuver.

³This can be interpreted as estimate of "pixel to sky" pointing reconstruction error if no science data is used.

⁴This can be interpreted as estimate of achieved S/I centroiding error

9.18 IPF EXECUTION SUMMARY OF ID702118

FOCAL PLANE SURVEY ANALYSIS: IOC Fine Survey.

INSTRUMENT NAME: MIPS_70um_fine_center NF: 118

PIX2RADW: 2.47365083E-005[rad/pixel] = 5.1023E+000[arcsec/pixel]

PIX2RADV: 2.54648081E-005[rad/pixel] = 5.2525E+000[arcsec/pixel]

| FRAME | DESCRIPTION | IPF ¹ | SF ² | TOTAL | REQ |
|--------|-----------------------|------------------|-----------------|--------|------|
| 118(P) | MIPS_70um_fine_center | 0.2915 | 0.0855 | 0.3038 | 1.10 |
| 119(I) | MIPS_70um_fine_FOV1 | 0.1528 | 0.0855 | 0.1751 | N/A |
| 124(I) | MIPS_70um_fine_FOV3 | 0.1664 | 0.0855 | 0.1871 | N/A |
| 127(I) | MIPS_70um_fine_FOV4 | 0.1607 | 0.0855 | 0.1820 | N/A |
| 117(I) | MIPS_70um_fine_sideA | 0.1563 | 0.0855 | 0.1782 | N/A |

Table 9.35: IPF calibration error summary ([arcsec], 1-sigma, radial)

| RMS METRIC | A PRIORI ³ | A POSTERIORI ³ | ATT. CORRECTED ⁴ | UNITS |
|------------|-----------------------|---------------------------|-----------------------------|--------|
| Radial | 3.7710 | 1.0000 | 0.9734 | arcsec |
| W-Axis | 3.0524 | 0.7239 | 0.7148 | arcsec |
| V-Axis | 2.2143 | 0.6899 | 0.6607 | arcsec |
| Radial | 0.7319 | 0.1933 | 0.1883 | pixels |
| W-Axis | 0.5982 | 0.1419 | 0.1401 | pixels |
| V-Axis | 0.4216 | 0.1313 | 0.1258 | pixels |

Table 9.36: Science measurement prediction error summary (1-sigma)

¹IPF filter removes systematic pointing errors due to: thermomechanical alignment drift (Body to TPF), gyro bias and bias drift, centroiding error, attitude error, and optical distortion. IPF SIGMA presented here is "Scaled" by the Least Squares Scale factor. The Least Squares Scale Factor was: 1.276359. It is assumed that the gyro Angle Random Walk contribution is captured with the Least Squares scaling. The gyro ARW contribution can be approximately calculated as 0.0723 arcseconds, given that $ARW = 100 \mu deg/\sqrt{hr}$, with 7.987000e+002 second Maneuver time (max), and 11 independent Maneuvers.

²Gyro Scale Factor(GSF) assumes 95 ppm error over 0.250 degree maneuver.

³This can be interpreted as estimate of "pixel to sky" pointing reconstruction error if no science data is used.

⁴This can be interpreted as estimate of achieved S/I centroiding error

9.19 IPF EXECUTION SUMMARY OF ID703121

FOCAL PLANE SURVEY ANALYSIS: IOC Fine Survey.

INSTRUMENT NAME: MIPS_SED_center NF: 121

PIX2RADW: 4.54794500E-005[rad/pixel] = 9.3808E+000[arcsec/pixel]

PIX2RADV: 4.54794500E-005[rad/pixel] = 9.3808E+000[arcsec/pixel]

| FRAME | DESCRIPTION | IPF ¹ | SF ² | TOTAL | REQ |
|--------|-----------------|------------------|-----------------|--------|------|
| 121(P) | MIPS_SED_center | 0.9962 | 0.0855 | 0.9998 | 1.10 |
| 105(I) | MIPS_SED_9 | 0.6511 | 0.0855 | 0.6567 | N/A |
| 106(I) | MIPS_SED_10 | 0.5454 | 0.0855 | 0.5521 | N/A |

Table 9.37: IPF calibration error summary ([arcsec], 1-sigma, radial)

| RMS METRIC | A PRIORI ³ | A POSTERIORI ³ | ATT. CORRECTED ⁴ | UNITS |
|------------|-----------------------|---------------------------|-----------------------------|--------|
| Radial | 3.1314 | 2.7126 | 2.6884 | arcsec |
| W-Axis | 2.9085 | 2.6280 | 2.6067 | arcsec |
| V-Axis | 1.1601 | 0.6723 | 0.6577 | arcsec |
| Radial | 0.3338 | 0.2892 | 0.2866 | pixels |
| W-Axis | 0.3101 | 0.2801 | 0.2779 | pixels |
| V-Axis | 0.1237 | 0.0717 | 0.0701 | pixels |

Table 9.38: Science measurement prediction error summary (1-sigma)

¹IPF filter removes systematic pointing errors due to: thermomechanical alignment drift (Body to TPF), gyro bias and bias drift, centroiding error, attitude error, and optical distortion. IPF SIGMA presented here is "Scaled" by the Least Squares Scale factor. The Least Squares Scale Factor was: 1.144291. It is assumed that the gyro Angle Random Walk contribution is captured with the Least Squares scaling. The gyro ARW contribution can be approximately calculated as 0.0434 arcseconds, given that $ARW = 100 \mu deg/\sqrt{hr}$, with 6.023000e+002 second Maneuver time (max), and 23 independent Maneuvers.

²Gyro Scale Factor(GSF) assumes 95 ppm error over 0.250 degree maneuver.

³This can be interpreted as estimate of "pixel to sky" pointing reconstruction error if no science data is used.

⁴This can be interpreted as estimate of achieved S/I centroiding error

10 LESSONS LEARNED

10.1 General

1. *Integrated Estimation Approach*

All focal plane calibration data sets were analyzed using a high-order 37-state Instrument Pointing Frame (IPF) Kalman filter. This novel high-order estimation approach allowed the estimation of engineering and science parameters simultaneously in the same filter formulation [3][6][4]. For example, pointing alignments, thermomechanical drift, and gyro drifts were estimated simultaneously with plate sales, optical distortion parameters, scan mirror misalignment and scale factors, etc. This contrasts with previous approaches to focal plane survey (e.g., Hubble) where the science and engineering parameters were found in separate steps requiring iteration between different teams of analysts.

The integrated approach was very successful and proved to be both efficient and accurate [7]. It was efficient in the sense that a small team of 4 analysts (i.e., the IPF Team) was able to support and complete the analysis of the entire focal plane survey data set over a 3 month period. This involved the analysis of 76 official calibration data sets, with 4-6 hours nominally allocated to analyze each data set, and any additional runs required to help sort out optimal weightings, filter settings, bad data points, etc. The results were also more accurate in the sense that the estimation problem was solved optimally without artificially dividing it into separate engineering and science sub-problems.

An unanticipated but extremely useful benefit of this integrated approach was for diagnostic purposes, i.e., the ability to monitor the Kalman filter residuals and assess the health of the entire end-to-end telescope pointing system. Artifacts seen in the filter residuals were traced back to detect and diagnose errors entering into the science centroids, telescope pointing, PCRS performance, attitude observers, PCRS-to-PCRS spacing, and any other unwanted systematic errors entering into the end-to-end pointing and data acquisition processes. Bad centroids (not caught by the science teams) could easily be distinguished from bad attitude data and systematically removed using the integrated approach. Polarity errors could also be quickly diagnosed as a consequence of having the engineering and science data integrated together in the same estimator.

2. *Polarity*

Polarity corrections were required on numerous occasions. Polarities for the IRAC and IRS Peak-Up arrays were always correct. However, polarities for the IRS spectroscopy slits and the MIPS scanning arrays often needed correction, probably due to their more complex geometries. These corrections were applied by flipping signs in a designated D matrix (provided in the CS-files). Values were changed based on observing gross anomalous behaviors, inspecting the Kalman filter residuals, and then consulting with the instrument teams. Despite the extra time needed to identify and correct polarities, this overall approach seemed to work satisfactorily.

3. *PCRS Errors*

The calibration runs indicate that the PCRS sensors were meeting their centroiding requirement of 0.14 arcsecond radial (1-sigma). Interesting though, the PCRS centroiding error appears to be mostly due to systematic bias error rather than random error. Accordingly, the sandwich maneuvers did not benefit from acquiring multiple observations (i.e., “dwelling”) on each PCRS array as much as was originally expected.

4. *Large Initial Uncertainty in MIPS Scan Mirror*

There was a large initial uncertainty in the scan mirror position for most of the MIPS arrays. The largest error was 2 arcminutes for the MIPS 70 μm fine (frame 118). Although large, such offsets were considered nominal by the designers of the instrument. However, the fact that such large corrections were nominal was apparently not communicated well to the users of the MIPS instrument who were surprised by the need for such large corrections and did not anticipate it correctly in the planning. For example, the large initial errors caused difficulties in getting sources onto many of the MIPS arrays in early focal plane survey attempts.

5. *Stray Light on MIPS 160 μm*

In early attempts, stray light issues made it difficult to obtain reliable centroids on the 160 μm array using the step-and-stare approach. The MIPS team eventually solved the problem by using a Seyfert galaxy as the calibration source.

6. *Non-Repeatability in the MIPS Scan Mirror*

The commanded scan mirror angle was used in the calibration process rather than the measured scan mirror angle (i.e., using the angle encoder), because the latter was not available on telemetry. This was unfortunate, because it caused the calibration process to be limited by the non-repeatability in the controlled scan-mirror position (i.e., the controller was not perfect). In all other respects, the calibration process was limited by knowledge type errors rather than control type errors. Future missions should make sure that actual scan mirror encoder values are available for calibration purposes, rather than trying to infer them from commanded values.

7. *Gyro Bias Units from MIPL*

A units problem was encountered during IOC in the gyro bias estimates. Specifically, the units expected by the IPF filter for the gyro bias is rad/sec while the units provided originally by MIPL was arcsec/sec. This was traced to an unexpected conversion to engineering units that was being made by the telemetry system upstream of MIPL in the pipeline. It is not clear exactly how this occurred. Fortunately, this units discrepancy had no effect on the focal plane survey accuracy because the gyro mode was needed primarily to support the Fine Surveys, and the problem was detected and corrected before any of the Fine Survey calibrations were performed.

8. *IPF Auto-Documentation Approach*

A novel automatic documentation system was used for generating IPF reports. This auto-documentation capability automatically generates ID reports that summarize the IPF calibration runs for the benefit of the various science and engineering teams. The approach used to auto-generate documents was based on programming MATLAB to write LATEX files having the appropriate tables, calibration information, and data plots. This overall approach turned out to work extremely well and save an enormous amount of time and energy. We highly recommend it for future missions. The customers (science and engineering teams and the project) were very happy with these reports. They served to summarize the runs, for discussing and visualizing the runs, and remain as part of the permanent Spitzer mission archive to document the focal plane survey activities. The construction of this final report was also significantly simplified due to the availability of these ID reports.

10.2 Model Fidelity

Overall, the models used by the IPF filter were adequate to the required accuracies. However, the best level of model fidelity is not always clear before actual mission data is available. The IPF Kalman filter addresses this issue by retaining extra parameters (e.g., higher-order terms), but allows them to be arbitrarily masked out if not justified. Overall, this approach to the calibration problem worked very well. Some issues relevant to this approach are worth mentioning.

1. Γ^2 *Dependent Scale Factors*

The Γ -dependent scale factors were found useful, e.g., for calibrating the MIPS 24 μm array. However, the next higher-order term, the Γ^2 dependent scale factors, were extremely difficult to estimate reliably. They were ultimately masked out and not used for any official runs.

2. *MIPS Scan Mirror Scale Factor*

The IPF filter parametrization of the MIPS scan mirror model uses a linear scale factor model of the form

$$\text{scan mirror angle} = \beta\Gamma \tag{10.1}$$

where Γ denotes the commanded scan mirror angle (in radians) and β represents a multiplicative correction (close to unity) which corrects for scale factor error. There are indications from a separate ground calibration study that a third-order polynomial,

$$\text{scan mirror angle} = \beta_1\Gamma + \beta_2\Gamma^2 + \beta_3\Gamma^3 \tag{10.2}$$

might be warranted, where the extra parameters β_2, β_3 capture the higher-order scan mirror nonlinearities. Because the IPF filter calibrates the scan mirror over much smaller ranges than the third-order model was intended for, a second-order model of the form,

$$\text{scan mirror angle} = \beta_1\Gamma + \beta_2\Gamma^2 \tag{10.3}$$

might strike a reasonable compromise. Of course, despite its higher fidelity, there may be a practical issue of being able to estimate the extra parameter reliably.

3. *IRAC Optical Distortion Model*

The IPF filter calibrated IRAC optical distortion by fitting a second-order (quadratic) moment expansion (associated with the linear scale factor matrices). Post-flight analysis indicates that certain terms from a third-order (cubic) model might have been warranted to help capture the high-order optical distortions. Again, there is still a practical issue of being able to estimate the extra parameters reliably.

11 CONCLUSIONS

This report provides an error analysis of the final focal plane calibration accuracies for the Spitzer Space Telescope. The main conclusion is that all focal plane calibration requirements have been met with the survey strategy as implemented. Margins range from 4 percent for the IRS Long-Lo slit, to 89 percent for the MIPS 70 μm array. These results closely match pre-flight predictions of expected focal survey accuracies.

ACKNOWLEDGEMENTS

This work was performed at the Jet Propulsion Laboratory, California Institute of Technology, under contract with the National Aeronautics and Space Administration.

References

- [1] D.S. Bayard, "Advances in Precision Pointing Control for the NASA Spitzer Space Telescope," Paper AAS 04-071, 27th Annual AAS Guidance and Control Conference, Breckenridge, Colorado, February 4-8, 2004. Publisher: AAS Publications Office, P.O. Box 28130, San Diego, CA 92198.
- [2] D.S. Bayard, P.B. Brugarolas, D. Boussalis, and B.H. Kang, *SIRTF Focal Plane Survey: A Pre-Flight Error Analysis*. JPL D-26678, September 1, 2003; (Appendix A: IRS, D-26678A; Appendix B: IRAC, D-26678B; Appendix C: MIPS, D-26678C).
- [3] D.S. Bayard and B.H. Kang, *SIRTF Instrument Pointing Frame (IPF) Kalman Filter Algorithm*. JPL D-Document D-24809, September 30, 2003.
- [4] D.S. Bayard and B.H. Kang, "A High-Order Kalman Filter for Focal Plane Calibration of NASA's Space Infrared Telescope Facility (SIRTF)," AIAA Guidance, Navigation and Control Conference and Exhibit, Paper # AIAA-2003-5824, Austin, TX, August 11-14, 2003.
- [5] D.S. Bayard, B.H. Kang, *SIRTF Instrument Pointing Frame (IPF) Kalman Filter Unit Test Report*. JPL D-Document D-24810, September 30, 2003.
- [6] D.S. Bayard and B.H. Kang, *An Overview of the SIRTF Instrument Pointing Frame (IPF) Kalman Filter for Focal Plane Calibration*. Jet Propulsion Laboratory, Internal Document, JPL D-26417, December 9, 2003.
- [7] D.S. Bayard, B.H. Kang, P.B. Brugarolas and D. Boussalis, "An Integrated Optimal Estimation Approach to Spitzer Space Telescope Focal Plane Survey," SPIE Conference on Astronomical Telescopes and Instrumentation, Paper # 5487-84, Glasgow, Scotland United Kingdom, June 21-25, 2004.
- [8] R.J. Brown, *Focal Surface to Object Space Field of View Conversion*. Systems Engineering Report SER No. S20447-OPT-051, Ball Aerospace & Technologies Corp., November 23, 1999.
- [9] B.H. Kang, D.S. Bayard, *SIRTF Instrument Pointing Frame (IPF) Software Description Document and User's Guide*. JPL D-Document D-24808, September 30, 2003.
- [10] J.P. Schwenker, B.R. Brandl, W. Burmester, J. Hora, A.K. Mainzer, P.C. Quigley, J. Van Cleve, "SIRTF-CTA optical performance test," IR Space Telescopes and Instruments. Edited by John C. Mather. Proceedings of the SPIE, Volume 4850. pp. 304-317, 2003.
- [11] P.K. Seidelmann, *Explanatory Supplement to the Astronomical Almanac*. University Science Books, Sausalito, California, 1992.
- [12] J.P. Schwenker, B.R. Brandl, W.F. Hoffman, J. Hora, A.K. Mainzer, J.E. Mentzell, J. Van Cleve, "SIRTF-CTA optical performance test results," IR Space Telescopes and Instruments. Edited by John C. Mather. Proceedings of the SPIE, Volume 4850. pp. 30-41, 2003.
- [13] M.D. Shuster and R.V.F. Lopes, "Parameter interference in distortion and alignment calibration, AAS Paper AAS 94-186, Feb. 1994.
- [14] *Space Infrared Telescope Facility In-Orbit Checkout and Science Verification Mission Plan*, JPL D-Document D-22622, 674-FE-301 Version 1.4, February 8, 2002.
- [15] *Space Infrared Telescope Facility Observatory Description Document*, Lockheed Martin LMMS/P458569, 674-SEIT-300 Version 1.2, November 1, 2002.

- [16] *SIRTF Software Interface Specification for Science Centroid INPUT Files (CAFILE, CS-FILE)*, JPL SOS-SIS-2002, November 18, 2002.
- [17] *SIRTF Software Interface Specification for Inferred Frames Offset INPUT Files (OFILE)*, JPL SOS-SIS-2003, November 18, 2002.
- [18] *SIRTF Software Interface Specification for PCRS Centroid INPUT Files (CBFILE)*, JPL SIS-FES-015, November 18, 2002.
- [19] *SIRTF Software Interface Specification for Attitude INPUT Files (AFILE, ASFILE)*, JPL SIS-FES-014, January 7, 2002.
- [20] *SIRTF Software Interface Specification for IPF Filter Output Files (IFFILE, LGFILE, TARFILE)*, JPL SOS-SIS-2005, November 18, 2002.
- [21] E. Wong, W. Breckenridge, D. Boussalis, P. Brugarolas, D.S. Bayard, J. Spanos, G. Singh, "Post-Flight Attitude Reconstruction for the Shuttle Radar Topography Mission," Proc. AAS/AIAA Astrodynamics Specialists Conference, Paper AAS 01-314, Quebec City, Quebec, Canada, July 30, 2001.